1-1-2002

Active feedback control of acoustic noise in 3 - D enclosures

Feng Liu
Iowa State University

Active feedback control of acoustic noise in $3-D$ enclosures

by

Feng Liu

A thesis submitted to the graduate faculty

in partial fulfillment of the requirements for the degree of

MASTER OF SCIENCE

Major: Mechanical Engineering

Program of Study Committee:
Atul G. Kelkar, Major Professor
Greg R. Luecke
J. Adin Mann III

Iowa State University

Ames, Iowa

2002

Graduate College
Iowa State University

This is to certify that the Master's thesis of

Feng Liu

has met the thesis requirements of Iowa State University

Signatures have been redacted for privacy

TABLE OF CONTENTS

LIST OF TABLES

LIST OF FIGURES

ACKNOWLEDGEMENTS

I would like to express my sincere thanks to my major professor Dr. Atul G. Kelkar for his help, support and guidance. I thank Dr. Greg R. Luecke and Dr. J. Adin Mann III for being on my program of study committee and taking their valuable time to read through my thesis. I am grateful to my father and mother who encouraged me to pursue higher studies. This thesis is dedicated to Yan for her love and support. Finally, I would like to acknowledge the financial support of NSF through No. CMS 0196198 and NASA through No. NCC 101039.

1 INTRODUCTION

Excessive noise can affect the working and living of people, harming their hearing ability, decreasing the efficiency of their working, and it can even cause very serious injury. With the development of modern industry, transportation and defense application, noise and vibration control has attracted more and more attention. Engineers have been working hard to to control the noise levels in the environment. Some example approaches include: reducing the radiating ability of sound source, blocking the propagation path of sound energy, and absorbing sound energy using special materials. Generally speaking, the acoustic control methods can be divided into "passive" control and "active" control. The passive noise control methods mainly include: noise absorption and noise isolation. These two methods use similar mechanism to reduce the noise, i.e. to reduce the sound energy via the interaction between sound waves and sound absorbing material or absorbing sound energy into structural vibrations which are damped using damping materials. Although these passive methods are very effective in high frequency region, they are not satisfactory in low frequency regions (especially below $200 - 300Hz$). As a result, to achieve acceptable broadband noise suppression, the passive techniques will require messy and high-volume of acoustic materials, which is impractical.

Over the last few decades, the active control of sound and vibration (at audio frequencies) has emerged as a viable and effective technology to address this problem. Recent advances in active control have been propelled by the rapid technology growth in affordable and practical digital signal processing chips, improvements in transducer technology and emerging of robust control theory. The range of frequencies that is im-

portant in the control of acoustic noise and associated vibrations lie in the audible range of 20 to $20,000Hz$. Disturbances above $1,000Hz$ can usually be handled by passive techniques. The active control has its use in low frequency range $(50 - 1000Hz)$ [1].

1.1 Historical Perspective

The beginnings of active noise control (ANC) date back to early 1930s when Paul Lueg filed his patent on noise control technique [2], since then, there are have been considerable advances in theory and practice of ANC methodology.

In 1933, German scientist Paul Lueg applied for his patent on "Process of Silencing Sound Oscillation" and got his patent in 1934. The principle idea behind Leug's patent was: two overlapping sound waves cause interference which can reduce or enhance the acoustic energy. This patent is considered to be the first design of ANC system [3]. Fig. 1.1 shows a schematic of Leug's patent. The disturbance source located upstream (at location A) produces a longitudinal propagating wave S_1, the sensing microphone, M, located downstream senses the sound pressure due to sound wave S_1 and produces an electrical signal. This signal is passed through an amplifier V before sending it to speaker L, which is spatially separated from microphone such that the sinusoidal wave form S_2 produced by speaker L has 180^o phase shift but same amplitude as S_1. That is the sound wave from the speaker is the "mirror image" of the original sinusoid and the overlapping of the waves produces cancelling effect. It is to be noted that only the sound wave at a specified frequency can be cancelled by this technique, whereas sound waves at other frequencies can in fact be magnified. Lueg had a very good understanding of the basic mechanism of active noise control. The sound wave travels at a lower speed in the air compared to the electronic signal in the cable, which enables the electric circuit and controller transducer to process the signal from microphone in timely manner to produce the counteracting wave at the control speaker. The performance of ANC system depends

on noise frequency, noise bandwidth, and the physical characteristics of the system [2]. To get good noise reduction two conditions needs to be satisfied: the time delay for the sound wave to travel from the microphone to the speaker can be accurately determined and the electronic circuit must have a linear transfer function. The second condition was hard to satisfy as the technology was not much advanced in 1930s, and as a result, Lueg's idea didn't gain much attention for almost two decades.

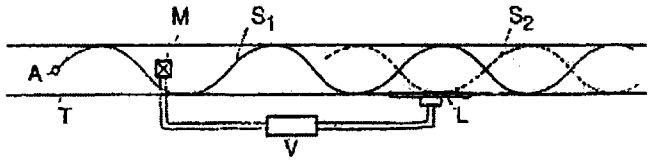

Figure 1.1 Leug's patent

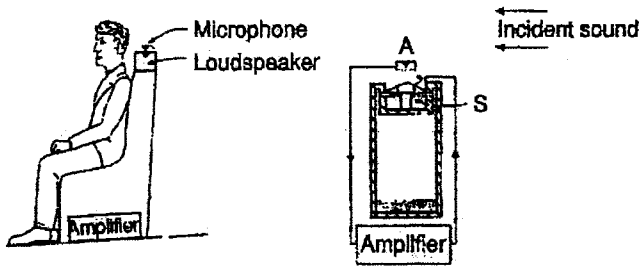

Figure 1.2 Olson's electronic sound absorber

In 1953, Olson and May developed another active noise control system shown in Fig. 1.2 [4]. Olson's electronic sound absorber includes a cavity with sound-absorbing material attached at the end, a microphone, an amplifier and a speaker. The cone-surface of the speaker can be controlled to move in such a pattern that the sound pressure at the microphone can be controlled to approach zero. Olson's method to create the "quiet zone" is pretty similar to Lueg but Olson's method was very ingenious for: Olson used sound-absorbing materials to deal with the feedback of the sound wave from the speaker, and the good linearity of the electronic units and the collocation of the speaker and the microphone, which reduced the phase shift significantly. The drawback of this approach

was its efficiency was not satisfactory over a relatively wider frequency band and the noise reduction was limited to a very samll area, which limited the applicability of Olson's electronic sound absorber. However, Olson proposed many possible applications of his design, In [5], Olson suggested that his sound absorber can be used for creating silencing zone near drivers of automobiles and aircrafts, electronic earmuffs, electronic helmets, and noise control in ducts. In Leug's approach, theoretically, if the frequency is limited to below the cut-on frequency of the first cross mode of the duct, the sound can be completely cancelled downstream from the speaker, whereas in the system of Olson and May, when arranged for free-field radiation control as Fig. 1.2, can only cancel the sound locally [1].

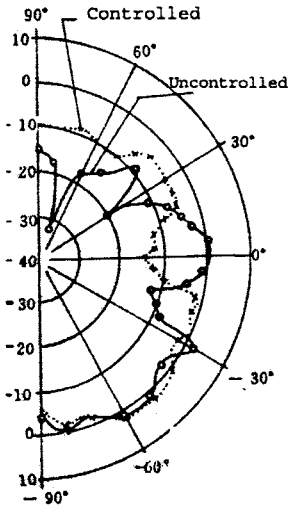

Figure 1.3 Conover's experiment result

Another parallel effort at that time was pussued by W. B. Conover [6]. Conovor's experiment used a $15,000KV$ electrical transformer and several speakers placed very close to the surface of the transformer. The experiments showed that a 10 dB reduction can be achieved at the front end of the electrical transformer, however, the sound pressure became worse for the pole angles bigger than 30 degrees. Nevertheless, Conover induced the concepts of reference signal and error sensor. Since the noise from the electrical

transformer was dominated by sinusoid tones, which were multiples of the electrical line frequency, a reference signal obtained from the electrical line could be used in the controller to generate the control signal. Also in Conover's experiments, a detective microphone was used to monitor the sound field to tune the controller's output. Although some good strides were made in ANC techniques during this period, its practical application was still limited due to the limitations of analog electronic techniques, which could not provide precise control, temporal stability , and reliability.

A real boost to ANC came through with with the development of digital signal processing techniques [7, 8, 9], where the whole process of signal sampling and processing are done in digital domain with high-speed DSP (digital signal processing) board and digital signal processing techniques. With the development of DSP techniques and the adaptive control theory, ANC became easier to realize. However, the real progress in ANC was still largely limited due to lack of physical understanding of the acoustic wave dynamics to a great depth. Since then, leading researches spent considerable time in understanding of physics behind ANC. One example of such effort is the work by Nelson and Elliott [10]. This work in ANC was also based on destructive interference of sound field. Nelson and Elliott have studied the minimum acoustic power output of arrays of point sources: when the secondary sources are close to the primary source (in term of wavelength), large attenuations of sound are achieved. In this case the primary and secondary sources in effect are combined together to achieve a compact high-order sound source (dipole, quadrapole, etc.) with a lower overall radiation efficiency and the sound level are thus controlled globally. When the second source is far from the primary source (in term of wave length) the reduction is poor and the resultant radiated sound will be an interference with local minima and maxima. Thus for good performance, the second source should be close to the primary source and the required spacing decreases with frequency. The mechanism of control in this case is that the secondary source radiates sound toward the primary and lowers the radiation resistance

that the primary source "sees". In another approach, if the secondary sources were constructed from sources which only radiate sound outwards (such as cardioidal sources) then the reduction of the sound in the far-field could be achieved without generating a control field which propagates towards the primary source. In this case, the primary source must radiate sound which propagate to and is absorbed by the secondary sources. Jessel and Mangiante's control strategies were based on this principle [11]. In summary, there were three main approach to ANC: (1) local minimization, where an interference field is created with local minima and maxima; (2) global minimization, in which the power output of the noise source reduced through a reduction of the radiation resistance; and (3) power absorption, in which the active sources absorb power from the primary source.

ANC has two primary approaches: *feedforward* and *feedback*. The Leug's approach can be regarded as a *feedforward* control while Olson's approach can be considered as a *feedback* approach. In the ensuing sections, we will briefly compare the history of *feedforward* and *feedback* control methods.

1.1.1 Era of Feedforward Control

For several years feedforward methods were very popular as it was argued that since feedforward scheme doesn't alter the system dynamics, there was no risk of destabilizing the system (or making it any worse). These schemes required (or assumed) that the disturbance measuring microphone (located upstream) does not sense the output from the control speaker (located downstream); if it did, then it would be a feedback scenario with a danger of the closed-loop instabilities. This meant that the schemes could be successfully implemented only with unidirectional microphones and speakers. In general, these conditions are very stringent. Nevertheless, researchers came up with ingenious arrangements and obtained impressive results. Most well-known are the experiments based on feedforward control by Ross [9, 12] and Roure [13] wherein the controller was

designed to perfectly cancel the acoustic noise. This involves exact knowledge of several system transfer functions, i.e., the design needs to calculate differences of transfer functions and invert them leading to high sensitivity of the controllers to uncertainty in the system model. Owing to high sensitivity, the model information had to be obtained experimentally. This remedy, however, did not alleviate the problems as the controllers were very sensitive to the implementation and finite digit arithmetics and had to be implemented with on-line adaptation schemes. In spite of these hurdles, their success was a big inspiration for much of the work in active control of acoustic noise [1] [14]. Roure [13] was successful in obtaining a 40 dB attenuation over the 200–600Hz bandwidth in industrial application - a very impressive result. However, one important drawback of the feedforward strategies that were used was the necessity of an on-line adaptation, not due to the nature of the system (acoustic duct) but due to the nature of the controller itself. Adaptive control comes at a price, both conceptual and practical [15]. On the practical side, for a large bandwidth systems such as a 3-D acoustic duct, support of a fast digital signal processor with significant memory is essential. Therefore, the implementation of feedforward controller really got boost only after the arrival of cheap, high performance DSP chips [1]. Another difficulty with feedforward schemes is to ensure that the adaptive control algorithm will always converge. Most algorithms guarantee convergence with known model, known controller order, and known persistency of excitation but, in general, such ideal conditions are very hard to meet.

1.1.2 Feedback Methods

The major hurdles in successful implementation of feedforward methods included availability of reference signal having strong correlation to noise source, necessity of online adaptation, and lack of robustness. For example, for structure-borne sound in aircraft it is difficult to obtain a reference signal which is strongly correlated with the noise producing mechanism. This makes feedforward control very ineffective. With the

advances in robust control methodologies coupled with knowledge gained in feedforward control schemes made it possible to develop closed-loop stable feedback control methods. Moreover, feedback methods have natural robustness compared to feedforward methods which is inherent in the architecture.

A considerable amount of research has been done in feedback control of acoustic noise in reverberant enclosures. A comparison of LQG, rate feedback, and filtered-x LMS algorithm was presented in [16] for SISO feedback control of structure-acoustic dynamics. This work showed that there is a definite rationale to work with feedback methods. Other Literature on feedback include [17, 18, 19, 20, 21, 22]. All this literature warrants thorough investigation of feedback control for ANC. However, the literature addressing control of acoustic-structure interaction problems is very limited. Most of the work in 3-D acoustic modelling and control has focused on the basic wave equation with possibly discrete point sources of acoustic disturbances. Besides [10], Dr. Pota and Kelkar's paper [23] presents closed-form mathematical models for an acoustic duct with general boundary conditions, also in [23], based on the basic wave equation, finite dimensional approximations of infinite dimensional models using quartic functions is provided, with which passive-based controller are used to achieve broadband noise reduction in 1-D duct where noise and control coming from the same channel. In [24, 25] and [26], the acoustic-structure interaction control for 2-D and 3-D enclosures is discussed to reduce the sound pressure levels using a PDE-based modelling technique. The experimental results on control of acoustic radiation from a plate were given in [27]. An alternate derivation of 3-D rectangular acoustic enclosure is given in [28], which is easy to understand from controls perspective. The $\mathcal{H}_\infty$ design was used in [29] to control the unwanted noise in a cylindrical acoustic cavity. In [30] and [31] *LQG/* $\mathcal{H}_\infty$ method and *minimax LQG* approach were used for active noise control in acoustic duct, respectively. Recently, in [32], results on analytical modelling, system identification, and feedback control of acoustic-structure interaction dynamics in 3-D enclosure was presented.

Among the feedback control strategies, LQG controller can not only be tuned to penalize each modes, it also overcomes the need to measure the entire state by estimating the state using a Kalman filter [33]; passivity-based controller can guarantee the stability after passification, $\mathcal{H}_\infty$ controller can both shape the closed-loop bode plot for nominal plant, and also guarantee the stability if the uncertainty bound is considered in $\mathcal{H}_\infty$ design [34]. Furthermore, LQG and $\mathcal{H}_\infty$ controllers design can be easily obtained with MATLAB software [35, 36], so these three kinds of control methods are used in this thesis.

1.2 Applications of Active Noise Control

Applications of ANC are numerous. ANC techniques are primarily useful in low frequency region where passive methods are not effective and are cumbersome to use. Also, high frequency acoustic modes are well damped and do not pose great difficulty compared to low frequency modes. The success of ANC in casting low frequency noise can benefit various sections of society. Given Below is the list of some examples which has motivated this research: [37]:

- *Transportation:* noise attenuation inside automobiles, aircraft cabins, ship engine rooms, heavy equipment operator cabins, active engine mounts, snowmobiles, helicoper cabins, diesel locomotives, electronic mufflers for exhaust systems, etc.

- *Household Appliances:* Air-conditioning ducts, window air-conditioners, refrigerators, washing machines, driers, furnaces, dehumidifiers, lawn mowers, vacuum cleaners, etc.

- *Industrial:* Fans, air ducts, chimneys, transformers, blowers, compressors, pumps, chain saws, wind tunnels, noisy machinery, debarring tools, high pressure air and coolant hoses, etc.

1.3 Objectives and Organization of Thesis

The rest of the thesis is organized as follows: Chapter 2 gives analytical development of dynamic model for a $3-D$ enclosure followed by the system identification process and experimental results. The dynamic models are derived both in time as well as frequency domain. This chapter also deals with the uncertainty modelling. Chapter 3 presents control design formulation for linear quadratic Gaussian (LQG) design. Control system analysis and synthesis are provided along with robustness formulation. Simulation as well as experimental results are given to demonstrate control effectiveness. Chapter 4 presents robust control design based on passivity theory. Both, constant-gain as well as dynamic, controllers are designed and implemented. Simulation as well as experimental results are provided. Chapter 5 gives another robust control design method using $\mathcal{H}_\infty$ theory. Finally, chapter 6 compares various controllers results and provides direction for future research.

2 MODELLING OF $3-D$ ACOUSTIC ENCLOSURE

In this chapter, a general mathematical model is derived for a $3-D$ acoustic enclosure with hard boundaries. The mathematical model, in differential equation form, is converted into frequency as well as time domain finite dimensional approximate models suitable for control design. Mathematical model also accounts for the structure-acoustic interaction dynamics as a result of one of the boundary being a vibrating boundary surface. Analytical model is compared to the system identification-based model using laboratory test article built to conduct experimental verification of the theoretical results. Section 2.1 gives development of analytical model followed by the experimental setup and system identification presented in Sections 2.6 and 2.3, respectively. Finally, Section 2.4 presents uncertainty characterization and modelling, which will be used later in robust control design.

2.1 Mathematical Model of $3-D$ Acoustic Enclosure

Consider a $3-D$ acoustic enclosure (shown in Fig. 2.1) with a part of one boundary surface representing a vibrating plant (denoted by S_1). The boundary surface denoted by S_1 consists of a vibrating plate which can be set into vibrations to generate acoustic disturbance using the piezo-actuator attached at the center of the plate. Consider a coordinate system xyz with the xy plane coinciding with the plane of the vibrating plate. The variables $\vec{v}(t,x,y,z)$, $p(t,x,y,z)$, $\rho(t,x,y,z)$ and $w(t,x,y)$ represent fluid velocity, acoustic pressure fluctuation from equilibrium, fluid density fluctuation from

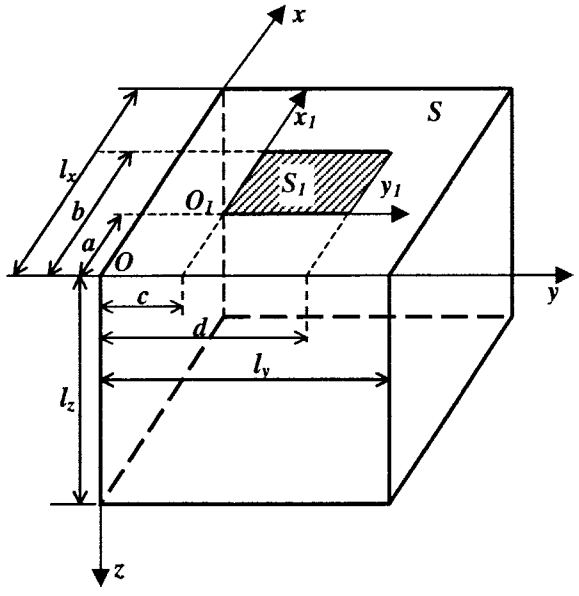

Figure 2.1 Schematic of $3-D$ acoustic enclosure

equilibrium, and transverse displacement of the plate, respectively. p_0 and ρ_0 are acoustic pressure and fluid density at equilibrium, respectively. $f(t,x,y)$ and $F(t)$ represent externally applied force on the plate due to acoustic pressure from an exterior noise field and the force from the piezo-actuator acting at the point (x_0, y_0) on the plate and normal to the plate, respectively. The development that follows is taken from [32] for completeness.

2.1.1 Dynamics of Acoustic-Structure Interaction

The governing equation of the vibrating boundary S_1 can be expressed as

$$D\nabla^4 w + h\rho_p \frac{\partial^2 w}{\partial t^2} = F(t)\delta(x-x_0)\delta(y-y_0) + f(t,x,y) \tag{2.1}$$

with boundary conditions:

$$\begin{aligned} w(t,0,y) &= 0, \quad \frac{\partial w(t,0,y)}{\partial x} = 0 \\ w(t,l_x,y) &= 0, \quad \frac{\partial w(t,l_x,y)}{\partial x} = 0 \\ w(t,x,0) &= 0, \quad \frac{\partial w(t,x,0)}{\partial y} = 0 \end{aligned} \tag{2.2}$$

$$w(t,x,l_y) = 0, \quad \frac{\partial w(t,x,l_y)}{\partial y} = 0$$

In Eqs. (2.1) and (2.2), h and ρ_p are the thickness and density of the plate, respectively. E is the Young's modulus, ν is the Poisson's ratio, $D = \frac{Eh^3}{12(1-\nu^2)}$ is the flexural rigidity of the plate, and l_x and l_y are the measures of the plate.

Using assumed modes method, the solution for $w(\cdot)$ can be given by

$$w(t,x,y) = \sum_i q_i^p(t)\psi_i(x,y) \tag{2.3}$$

where, $q_i^p(t)$ are the modal coordinates and $\psi_i(x,y)$ are the corresponding normal mode shapes obtained from solving the homogeneous part of Eq. (2.1). After introducing the modal damping ζ_i^p for all modes, we obtain the governing dynamics for the vibrating plate as follows

$$\ddot{q}_i^p(t) + 2\zeta_i^p\omega_i\dot{q}_i^p(t) + \omega_i^2 q_i^p(t) = \frac{1}{h\rho_p}[\frac{1}{S}F(t)\psi_i(x_0,y_0) + f_i(t)] \tag{2.4}$$

where, ω_i are the natural frequencies of the plate and forcing functions $f_i(t)$ are given by

$$f_i(t) = \frac{1}{S}\int\int_S f(t,x,y)\psi_i(x,y)dS \tag{2.5}$$

For the closed $3-D$ enclosure under consideration, the dynamics of acoustic system can be given by the non-homogeneous wave equation as follows

$$\nabla^2 p(t,x,y,z) - \frac{1}{c_0^2}\frac{\partial^2 p(t,x,y,z)}{\partial t^2} = -\rho_0 w_{tt}(t,x,y)\delta(z) + \rho_0 u(t)\delta(x-x_1)\delta(y-y_1)\delta(z-z_1)$$

with boundary condition:

$$\vec{\nabla}p(t,x,y,z)\cdot\vec{n} = 0 \quad \text{on all boundary surfaces} \tag{2.6}$$

where, $u(t)$ is the baffle acceleration of the speaker located at (x_1,y_1,z_1) and is considered as the control input, $w_{tt}(t,x,y)$ is the accelerate of the plate. Again using assumed modes approach, we assume the solution of Eq. (2.6) as

$$p(x,y,z,t) = \sum_j q_j^a(t)\phi_j(x,y,z) \tag{2.7}$$

where, $q_j^a(t)$ are the modal coordinates and $\phi_j(x,y,z)$ are the corresponding normal mode shapes of the acoustic system. Following similar steps as in the derivation of the plate, we obtain

$$\ddot{q}_j^a(t) + 2\zeta_j^a \Omega_j \dot{q}_j^a(t) + \Omega_j^2 q_j^a(t) = \frac{c_0^2 \rho_0}{V} \sum_i \alpha_{ij} \ddot{q}_i^p(t) - \frac{c_0^2 \rho_0}{V} \phi_j(x_1, y_1, z_1) u(t) \tag{2.8}$$

where, ζ_j^a are modal damping ratios, Ω_j are the natural frequencies of the enclosed acoustic media, V is the enclosure volume, and α_{ij} are the coefficients given by

$$\alpha_{ij} = \int\int_S \phi_j(x,y,0)\psi_i(x,y)dS \tag{2.9}$$

Let the state variable vector be defined as $X = \{(q_i^p, \dot{q}_i^p, i = 1, \cdots, n_p), (q_j^a, \dot{q}_j^a, j = 1, \cdots, n_a)\}$, where n_p and n_a are the number of structural and acoustic modes, respectively, of the system after truncating the high frequency modes. For the configuration where sensing microphone is located at (x_2, y_2, z_2), the state equation of the acoustic-structure interaction dynamics with piezo voltage as input can be written from Eqs. (2.4) and Eq. (2.8) as follows

$$X(t) = E^{-1} A_F X(t) + E^{-1} B_F u(t) + E^{-1} D_F f(t) \tag{2.10}$$

Matrices E, A_F, B_F, and D_F are given by

$$E = \begin{bmatrix} E_{11} & 0 \\ E_{21} & E_{22} \end{bmatrix} \qquad A_F = \begin{bmatrix} A_{11} & 0 \\ 0 & A_{22} \end{bmatrix}$$
$$B = \frac{1}{h\rho_0 S_1} \begin{bmatrix} B_{11} \\ 0 \end{bmatrix} \qquad D = \frac{1}{h\rho_0} \begin{bmatrix} D_{11} \\ 0 \end{bmatrix} \tag{2.11}$$

where, $E_{11} = I$ and $A_{11} = \text{diag}(A_{11}^i)$ are square matrices of order n_p, $E_{22} = I$ and $A_{22} = \text{diag}(A_{22}^j)$ are block-wise square matrices, B_{11} is a $n_p \times r$ matrix, and D_{11} is a

$n_p \times 1$ matrix. Moreover, matrices E_{21}, A_{11}, A_{22}, B_{11}, and D_{11} are given as follows

$$E_{21} = -\frac{c_0^2 \rho_0}{V} \begin{bmatrix} 0 & 0 & \cdots & 0 & 0 \\ 0 & \alpha_{11} & \cdots & 0 & \alpha_1 n_p \\ \cdots & \cdots & \cdots & \cdots & \cdots \\ 0 & 0 & \cdots & 0 & 0 \\ 0 & \alpha_{n_a 1} & \cdots & 0 & \alpha_{n_a n_p} \end{bmatrix} \tag{2.12}$$

$$A_{11}^i = \begin{bmatrix} 0 & 1 \\ -\omega_i^2 & -2\zeta_i \omega_i \end{bmatrix} \tag{2.13}$$

$$A_{22}^j = \begin{bmatrix} 0 & 1 \\ -\omega_j^2 & -2\zeta_j \omega_j \end{bmatrix} \tag{2.14}$$

$$B_{11} = \begin{bmatrix} 0 & \cdots & 0 \\ \phi_{11}(x_{11}, y_{11}) & \cdots & \phi_{11}(x_{1r}, y_{1r}) \\ \cdots & \cdots & \cdots \\ 0 & \cdots & 0 \\ \phi_{n_p n_a}(x_{11}, y_{11}) & \cdots & \phi_{n_p n_a}(x_{1r}, y_{1r}) \end{bmatrix} \tag{2.15}$$

$$D_{11} = \begin{bmatrix} 0 \\ \gamma_{11} \\ \cdots \\ 0 \\ \gamma_{n_p} \end{bmatrix} \tag{2.16}$$

If we place k microphones in the position of $(x_i, y_i, z_i), i = 1, \cdots, k$, the outputs of the system can be written as $P(t) = (p(t, x_1, y_1, z_1), \cdots, p(t, x_k, y_k, z_k))^T$. Since matrix E is

invertible, the state-space model can be re-written as

$$\begin{aligned} \dot{x}(t) &= E^{-1}A_F x(t) + E^{-1}B_F u(t) + E^{-1}D_F f(t) \\ p(t) &= Cx(t) \end{aligned} \tag{2.17}$$

where

$$C = [C_1' \quad C_2' \quad \cdots \quad C_k']^T \tag{2.18}$$

C matrix has k rows, and each C_i has the form

$$C_i = [0, \cdots, 0;\ \psi_1(x_i, y_i, z_i),\ 0,\ \psi_2(x_i, y_i, z_i),\ 0, \cdots,\ \psi_{n_a}(x_i, y_i, z_i), 0] \qquad i = 1, \cdots, k \tag{2.19}$$

For single-input-single-output ($SISO$) system, if we let $f(t, x_1, y_1) = 0$ and take Laplace transform of Eqs. (2.4) and (2.8), we get

$$(s^2 + 2\zeta_i\omega_i s + \omega_i^2)\ Q_i(s) = \frac{1}{h\rho_p S_1}\phi_i(x_{11}, y_{11})\ F(s) \tag{2.20}$$

$$(s^2 + 2\zeta_j\omega_j s + \omega_j^2)\ Q_j(s) = \frac{c_0^2\rho_0}{V}\sum_{i=1}^{n_p}\alpha_{ij}s^2\ Q_i(s) \tag{2.21}$$

that is

$$Q_j(s) = \frac{Js^2}{s^2 + 2\zeta_j\omega_j s + \omega_j^2}\sum_{i=1}^{n_p}\frac{\alpha_{ij}\phi_i(x_{11}, y_{11})}{s^2 + 2\zeta_i\omega_i s + \omega_i^2} \cdot F(s) \tag{2.22}$$

where, $J = \frac{c_0^2\rho_0}{Vh\rho_p S_1}$. Taking the Laplace transform of Eq. (2.7), we can obtain a $SISO$ transfer function for the output being the acoustic pressure measured at the microphone located at (x_0, y_0, z_0) and input being the force applied by the piezo as

$$G(s) = \frac{P(s)}{F(s)} = Js^2\sum_{j=0}^{n_a}\frac{\psi_j(x_0, y_0, z_0)}{s^2 + 2\zeta_j\omega_j s + \omega_j^2}[\sum_{i=1}^{n_p}\frac{\alpha_{ij}\phi_i(x_{11}, y_{11})}{s^2 + 2\zeta_i\omega_i s + \omega_i^2}] \tag{2.23}$$

Although in configuration of interest, there is only one control input, one disturbance input and one measurement output, one can expand the analysis to multi-input multi-output ($MIMO$) case, easily with state-space model.

2.1.2 Total Energy of the System

For active noise control, the control law is obtained by minimization of some appropriate cost function. For acoustic noise control application an appropriate cost function would be the total acoustic energy of the system. Since minimization of such cost function would result in a control law that will cause extraction of total energy of the system in the closed-loop. This Section is devoted to the derivation of acoustic energy expression for the $3-D$ enclosure under consideration [32]. The energy function is then expressed as the quadratic function of the state vector, which can naturally fit into the cost function used in many optimal control formulations.

2.1.2.1 Energy of the vibrating boundary

The kinetic energy, K_p, and the potential energy, U_p, of the vibrating boundary (plate) can be expressed as follows

$$K_p = \frac{h}{2}\int\int_S \rho_p(\frac{\partial w}{\partial t})^2 dS \tag{2.24}$$

$$U_p = \frac{D}{2}\int\int_S \left\{(\frac{\partial^2 w}{\partial x^2}+\frac{\partial^2 w}{\partial y^2})^2 - 2(1-\nu)[\frac{\partial^2 w}{\partial x^2}\frac{\partial^2 w}{\partial y^2} - (\frac{\partial^2 w}{\partial x \partial y})^2]\right\} dS \tag{2.25}$$

Using Eq. (2.3), the kinetic energy and potential energy of the plate at any time instant can be calculated as

$$K_p(t) = \frac{h\rho_p}{2}\sum_i (\dot{q}_i^p)^2 \tag{2.26}$$

$$U_p(t) = \frac{D}{2}\sum_i (q_i^p)^2\omega_i^4 \tag{2.27}$$

The total vibrational energy of the plate at any time instance is then given by

$$E_p(t) = K_p(t) + U_p(t) \tag{2.28}$$

2.1.2.2 Energy in the acoustic field of the enclosure

The kinetic and potential energy densities of the acoustic field are given by [38]

$$E_a^k(x,y,z,t) = \frac{1}{2}\rho_0|\vec{v}(x,y,z,t)|^2 \tag{2.29}$$

$$E_a^p(x,y,z,t) = \frac{1}{2\rho_0 c_0^2}p^2(x,y,z,t) \tag{2.30}$$

The acoustic dynamics inside the enclosure can be given by the following wave equation

$$\frac{1}{c_0^2}\frac{\partial p(x,y,z,t)}{\partial t} + \rho_0\vec{\nabla}\cdot\vec{v}(x,y,z,t) = 0 \tag{2.31}$$

$$\rho_0\frac{\partial \vec{v}(x,y,z,t)}{\partial t} + \nabla p(x,y,z,t) = 0 \tag{2.32}$$

Now using Eq. (2.7), we can write

$$\nabla p(x,y,z,t) = \sum_i q_i^a(t)\nabla\phi_i(x,y,z)$$

Similarly, from Eq. (2.32), we can get

$$\vec{v}(x,y,z,t) = \sum_j v_j(t)\vec{\nabla}\phi_j(x,y,z) \tag{2.33}$$

Substituting Eq. (2.33) into Eq. (2.31), we get

$$\rho_0\sum_j v_j(t)\nabla^2\phi_j(x,y,z) + \frac{1}{c_0^2}\sum_j \dot{q}_j^a(t)\phi_j(x,y,z) = 0 \tag{2.34}$$

It can be easily proved that $\nabla^2\phi_j(x,y,z)$ form a set of orthogonal functions and $\nabla^2\phi_j(x,y,z)$ and $\phi_j(x,y,z)$ are orthogonal to each other, i.e.,

$$\int_V [\nabla^2\phi_i(x,y,z)][\nabla^2\phi_j(x,y,z)]dV = \delta_{ij}\beta_j \tag{2.35}$$

$$\int_V [\phi_i(x,y,z)\nabla^2\phi_j(x,y,z)]dV = \delta_{ij}\gamma_j \tag{2.36}$$

where, δ_{ij} is Kronecker delta function. Multiplying Eq. (2.34) by $\nabla^2\phi_j(x,y,z)$ and then integrating over V, we get

$$v_j(t) = -\frac{1}{\rho_0 c_0^2}\frac{\gamma_j}{\beta_j}\dot{q}_j^a(t) \tag{2.37}$$

$\vec{v}$ is now given by

$$\vec{v}(x,y,z,t) = -\frac{1}{\rho_0 c_0^2}\sum_j \frac{\gamma_j}{\beta_j}\dot{q}_j^a(t)\nabla\phi_j(x,y,z) \tag{2.38}$$

The total energy of the acoustic field at any time instant can be given by

$$\begin{aligned} E_a(t) &= \int_V [E_a^k(x,y,z,t) + E_a^p(x,y,z,t)]dV \\ &= \frac{1}{2\rho_0 c_0^2}\sum_j [(q_j^a)^2 + \frac{\gamma_j^2}{\beta_j c_0^2}(\dot{q}_j^a)^2] \end{aligned} \tag{2.39}$$

2.1.2.3 Total energy of the enclosure

From Eqs. (2.28) and (2.39), the total energy of the acoustic-structure interaction system (enclosure) at any time instant can be written as

$$\begin{aligned} E(t) &= E_p(t) + E_a(t) \\ &= \frac{1}{2}[\sum_i (D\omega_i^4 (q_i^p)^2 + h\rho_p(\dot{q}_i^p)^2) \\ &\quad + \sum_j ((q_j^a)^2 + \frac{1}{\rho_0^2}(\dot{q}_j^a)^2)] \\ &= \frac{1}{2}X^T Q_0 X \end{aligned} \tag{2.40}$$

Equation 2.40 gives the total energy of the system in the form of the quadratic function of the states of the system which can be used in the cost function for control design.

2.2 Experimental Set-up

To verify the mathematical model derived in Section 2.1, an experimental setup was built in our laboratory. The $3-D$ enclosure in Fig. 2.2 is a representative of the acoustic-structure dynamics observed in real life situation such as in aircraft cabins, where the vibrations of the fuselage walls cause excitation of interior noise. The test article consists of a $3-D$ rectangular wooden box with one of the boundary surface made of aluminum plate. The aluminum plate can be excited by a piezo-actuator (external

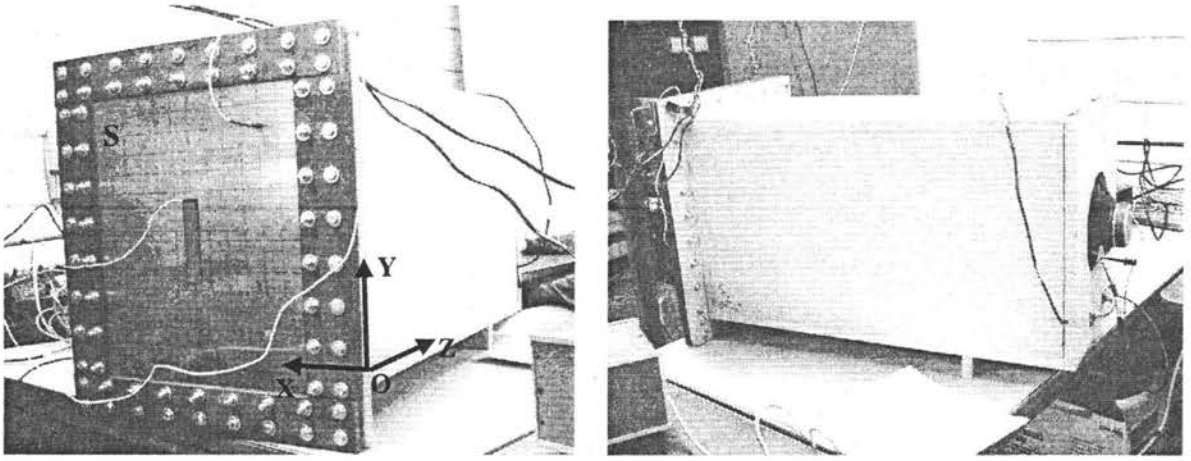

Figure 2.2 Front and rear view of lab apparatus

input), located at the center of the plate. Vibrating plate can excite acoustic noise inside the enclosure. Another external input can be provided by the speaker mounted at the center of the opposite boundary surface. Both of these external inputs can be treated as either as disturbance or control input. In the work presented here, piezo is used as the disturbance input and speaker is used as the control input. The feedback sensor is the microphone located inside of the enclosure at (6.75",7", 11.25"), as shown in Fig. 2.5. One problem with the boundary condition for the clamped-clamped plate is that it poses difficulty in obtaining closed-form analytical model of the system. As it will be seen later analytical model obtained using approximations to overcome this problem doesn't fit the experimental response as good as the identified model.

The data acquisition system used is *dSpace* 1103 board with associated user friendly software which allows real-time data capture, display, and on-line tuning of controller gains. The control system is integrated using $REALTIME\ WORKSHOP$ and $SIMULINK$ toolbox in $MATLAB$. The sine sweep excitation is generated using $SRT785$ Spectrum Analyzer from Stanford Research. Signal conditioning units from PCB Piezotronics and Krohn-Hite are used to process the sensed output. Inputs to piezo and speaker are generated using piezo-amplifier built in house and RCA PA system amplifier, respectively.

Figure 2.3 Picture of $3-D$ enclosure with instruments and control computer

Details of main instruments are given as follows:

- ACP 12-channel signal conditioner: model $483B21$;
- Stanford Research dynamic signal analyzer (spectrum analyzer): model $SRT785$;
- Amplifier for piezo-actuator: model MEC 005;
- RCA amplifier for speaker: model $STAV$ 3880;
- Low pass filter: model $KROHN-HITE$ 3202;
- Data acquisition system: dSpace 1103 board with ACE kit,
- Computer: PII 400MHz process with $MATLAB$ 5.3 with $SIMULINK$ and $REALTIME\ WORKSHOP$.

The speaker's frequency response is shown in Fig. 2.4 , and it is modelled together with the amplifier in our research [23]. The physical parameters of the test-article are given in Table 2.1.

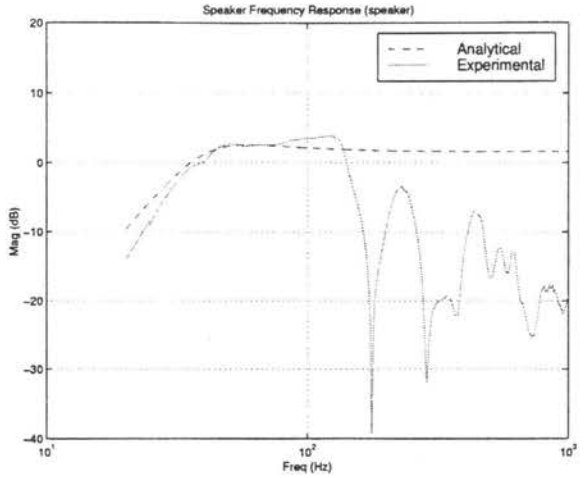

Figure 2.4 Experimental speaker frequency response

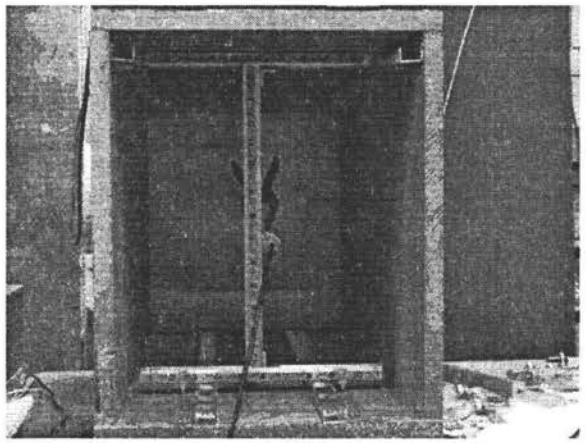

Figure 2.5 Rear view showing microphone location

The analytical model derived in Section 2.1 was used with the parameters given in Table 2.1 to obtain natural frequencies of the system. The estimate of the damping for different modes is extremely difficult to obtain. Also the natural frequncies of the clamped plate can not be obtained accurately. Table 2.2 gives first 28 natural frequncies of the system obtained from analytical model. In this table, $*$ indicates frequency missing in analytical model and $\sharp$ indicates frequency missing in experimental data. These will be compared later with the experimental data. As mentioned prevously, a more accurate model of the system can be obtained using system identification methods based on frequency response data. Next section presents system identification process

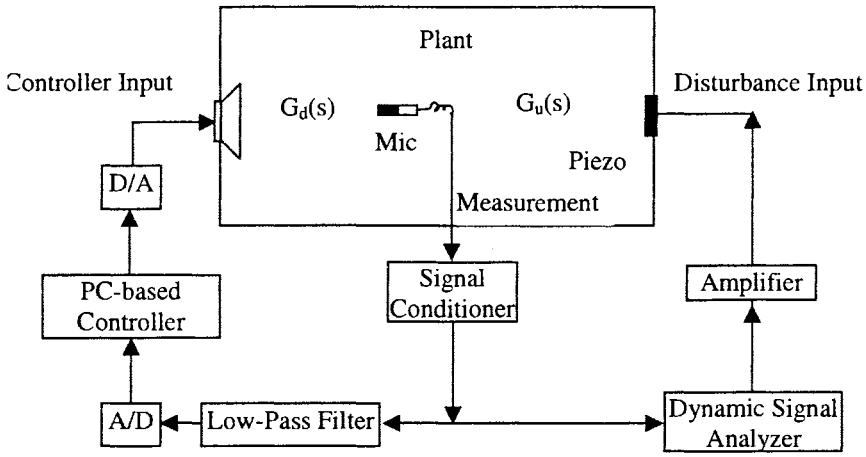

Figure 2.6 Schematic of experimental set-up for control

Table 2.1 Parameters for $3-D$ lab apparatus

Parameter	value	Parameter	Value
l_x	0.3048 m	l_y	0.3810 m
l_z	0.7874 m	a	0.0063 m
b	0.2985 m	c	0.0063 m
d	0.3747 m	h	0.000813 m
E	$71*10^9$ N/m^2	μ	0.33
ρ	2810 kg/m^3	c_0	343 m/s
ρ_0	1.13 kg/m^3	x_0	0.1270 m
y_0	0.1524 m	z_0	0.3112 m
x_1	0.1524 m	y_1	0.1905 m

and control design models obtained with these techniques.

2.3 System Identification

System identification is the process of deriving a mathematical model of a physical system using experimental data. System identification is a very important tool in control design since more accurate the model is, more effective the controller is based on this design model. Analytical methods seldom give highly accurate models for intricate real life systems and has to rely on system identification models. Here Eigensystem

Table 2.2 Comparison of analytical and experimental frequencies

Mode no.	Frequency (Hz)	
	Analytical	Experimental
1	37.5	32.0
2	*	62.4
3	80.8	73.0
4	80.8	83.6
5	*	97.7
6	*	99.8
7	106.4	111.1
8	149.8	♯
9	153.2	143.7
10	217.8	♯
11	221.4	♯
12	222.1	224.5
13	*	236.0
14	254.4	254.5
15	264.8	264.8
16	*	272.3
17	*	280.3
18	323.4	311.6
18	337.1	319.1
19	382.3	381.0
20	384.6	♯
21	425.7	416.7
22	*	423.5
23	435.6	♯
24	438.4	♯
25	450.1	454.5
26	453.6	♯
27	453.6	♯
28	498.0	479.0

Realization Algorithm (ERA) based system identification method is used.

2.3.1 System Identification with ERA Method

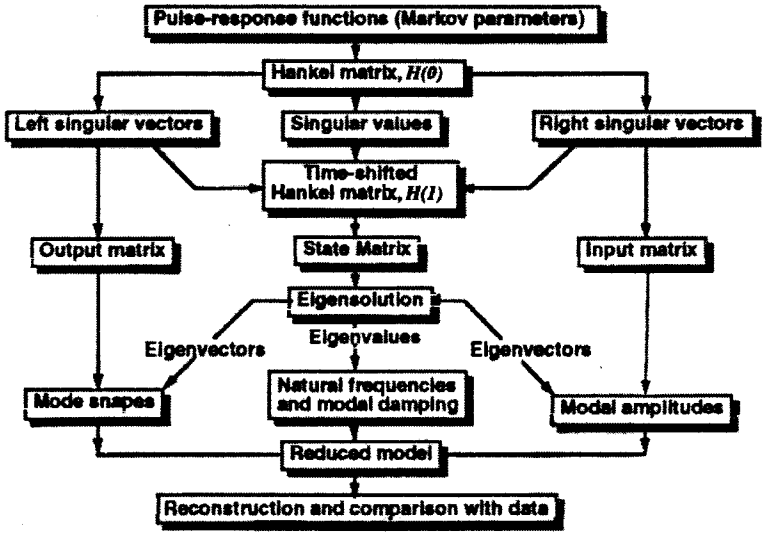

Figure 2.7 Flowchart for the ERA

ERA method is a very effective system identification method used in discrete domain. If we apply an impulse sequence to a system, then the output sequence directly yields Markov parameters of the system. ERA algorithm uses these Markov parameters to generate system model. The computational steps for system identification with ERA method are below and depicted in flow chart given in Fig. 2.7 [39].

1) Construct a block Hankel matrix $H(0)$ by arranging the Markov parameters (pulse response samples) into blocks.

2) Decompose $H(0)$ using singular value decomposition.

3) Determine the order of the system by examining the singular values of the Hankel matrix $H(0)$.

4) Construct a minimum order realization, using a shifted block Hankel Matrix $H(1)$.

5) Find the eigensolution of the realized state matrix and transform the realized model to modal coordinates to calculate the system damping and frequencies.

6) Calculate the modal amplitude coherence and mode singular values to quantify the system and noise modes.

7) Determine the reduced system model based on the accuracy indicators computed in step 6, reconstruct Markov parameters and compare with the measured Markov parameters.

Table 2.3 First 20 modes of the $3-D$ acoustic enclosure

No	Freq(Hz)	Damp,%,	msv,%	mci,%	moi,%
1	99.759	1.620	100.0	7.6	50.7
2	264.826	0.976	96.5	5.8	97.8
3	62.355	23.704	89.5	84.9	31.1
4	224.522	1.757	71.1	6.1	76.8
5	236.012	1.572	61.6	4.0	83.2
6	290.117	0.640	59.1	1.9	81.7
7	41.290	33.921	57.7	50.7	20.6
8	143.684	100.0	47.9	100.0	42.9
9	254.532	0.369	47.0	0.5	93.2
10	97.728	2.186	46.6	2.2	49.8
11	44.801	8.499	45.6	8.0	23.3
12	31.991	25.086	44.1	22.5	16.0
13	272.282	2.437	39.4	2.4	97.4
14	280.281	3.053	30.5	1.9	96.4
15	311.633	0.241	29.2	0.2	86.5
16	242.454	6.628	25.8	2.7	88.0
17	111.129	2.454	19.7	0.5	53.3
18	83.552	2.154	19.3	0.4	43.2
19	319.101	0.678	17.7	0.2	98.5
20	73.047	13.100	16.3	1.6	37.0

The system identification toolbox SOCIT developed at NASA Lanley Research Center [39] based on above *ERA* algorithm was used to obtain transfer functions needed for control design. The frequency range of interest was $20-450$ Hz, since low frequency models are hard to control by passive means. Table 2.3 gives first 20 modes with various indices that are used by SOCIT to rank the the modes. These indices are msv (normalized mode singular values), and the corresponding frequencies, msv (normalized

mode singular values), mci (modal controllability index), and moi (modal controllability index). From Table 2.3 we can easily see that the $1st$ $(99.757Hz)$, $2nd$ $(264.826Hz)$, $4th$ $(224.522Hz)$, $5th$ $(236.012Hz)$, $6th$ $(290.117Hz)$ and $9th$ $(254.532Hz)$ modes have prominent peaks and should be included in the design model. The state-space model of the nominal plant can be given as:

$$\dot{x}(t) = Ax(t) + [B_u \vdots B_d] \begin{bmatrix} u(t) \\ \dots \\ d(t) \end{bmatrix} \tag{2.41}$$

$$m(t) = C_m x(t) + [D_u \vdots D_d] \begin{bmatrix} u(t) \\ \dots \\ d(t) \end{bmatrix} \tag{2.42}$$

where, $u(t)$ is the controller input (speaker input), $d(t)$ is the disturbance input (piezo force), B_u is the input matrix related to the piezo input, B_d is the input matrix related to the disturbance input, D_u is the direct transmission from $u(t)$, and D_d is the direct transmission from $d(t)$. Matrices A, B_u, B_d, C_m, D_u, and D_d can be obtained by ERA method, once we decide how many modes need to be included in the design model.

Figures 2.8 and 2.9 give comparison of the magnitude and phase plots for the experimental data and identified models for control input. From the Figs. 2.8 and 2.9 we can see that the amplitude of the estimated and measured transfer functions match very well under $300Hz$, and difference in the phase plots is within acceptable range.

Also, since ERA method is based on generalized Hankel matrices obtained from the Markov Parameters using pulse response data, the frequency response match is much better in distrete domain compared to continuous domain. This is one limiting factor in obtaining good continuous time models and further research is needed to overcome this problem.

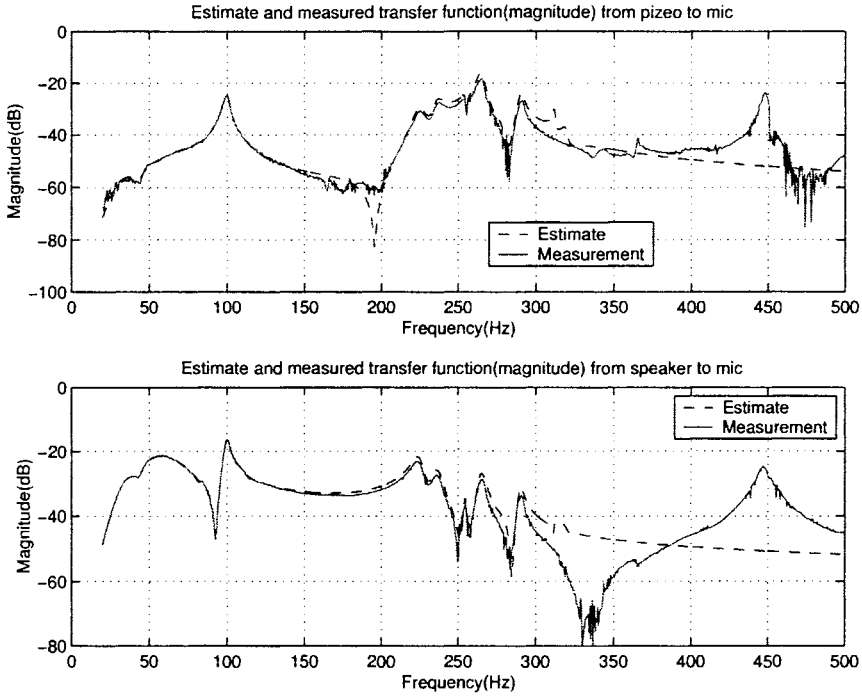

Figure 2.8 Magnitude of the estimated and measured FRF's

2.4 Characterization of System Uncertainty

As discussed in the previous section, the mathematical model of the system derived analytically or through system identification is often approximate and/or erroneous. That means, when such a model is used for control design, stability of control system depends on the robustness of the controller to modelling errors and uncertainties. The design methodologies for robust controller often require some sort of uncertainty characterization in terms of low the uncertainty is modelled and what kind of norm bound it satisfies. This section will present the uncertainty characterization used in the work of this thesis. The main uncertainty to be considered is the uncertainty arising from the spillover (unmodelled high frequency) dynamics. A suitable uncertainty model that describe this type of uncertainty is additive uncertainty as shown in Fig. 2.10. The true plant (transfer function) is assumed to be of the form:

$$P(s) = P_0(s) + \Delta_A(s) \tag{2.43}$$

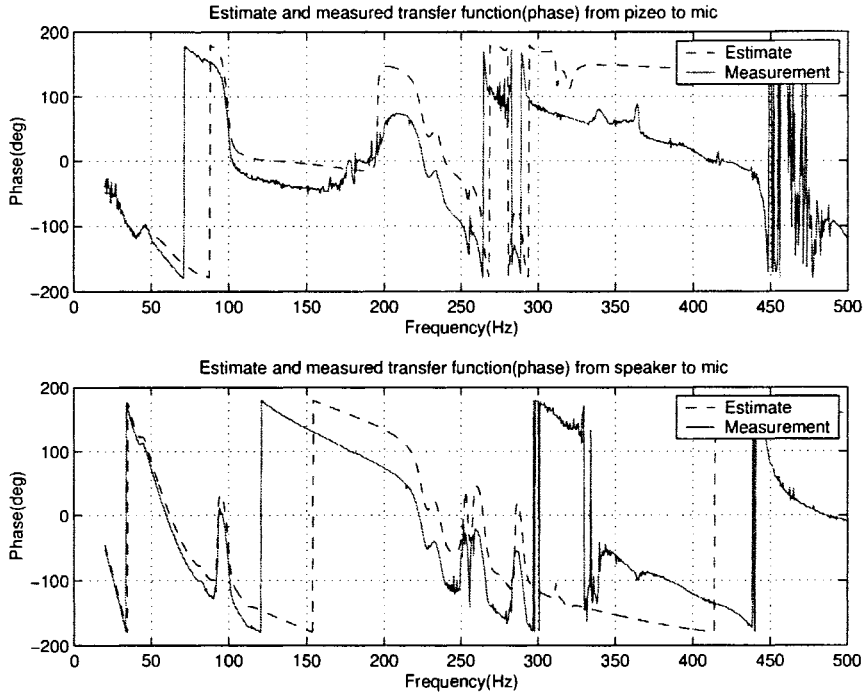

Figure 2.9 Phase of the estimated and measured FRF's

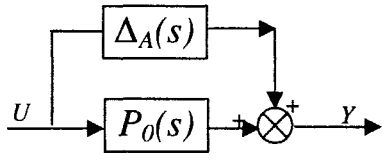

Figure 2.10 Additive uncertainty of the plant

where, $P_0(s)$ represents the nominal transfer function (design model) and $\Delta_A(s)$ represents the additive uncertainty. If $\Delta_A(s)$ is written as, $\Delta_A(s) = \Delta(s)\Delta_{max}(s)$, where $\Delta_{max}(s)$ is a suitable weighting transfer function and $\Delta(s)$ is an uncertain transfer function such that $\|\Delta_A(s)\| \leq \|\Delta_{max}(s)\|$. That is the transfer function $\|\Delta(s)\|$ satisfies the $\mathcal{H}_\infty$ norm bound:

$$\|\Delta(s)\|_\infty \leq 1. \tag{2.44}$$

Figure 2.11 shows uncertainty configuration where $\Delta_{max}(s)$ and $\Delta(s)$ appear in series. The configuration of Fig. 2.11 will be useful in the analysis and design of robust controllers later in the thesis. An augmented plant $\tilde{P}(s)$, in Fig. 2.11 is used as the nominal plant in robust control design process.

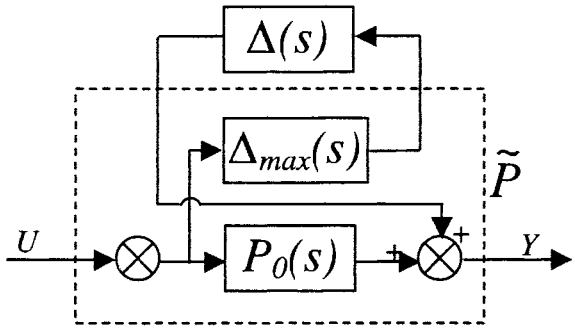

Figure 2.11 Standard form of additive uncertainty

The uncertainty weighting transfer function $\Delta_{max}(s)$ is chosen such that

$$|P(j\omega) - P_0(j\omega)| \leq |\Delta_{max}(j\omega)| \tag{2.45}$$

where, $P(j\omega)$ is the measured frequency response for the entire frequency range and $P_0(j\omega)$ is the frequency response for the approximated model. For example, for the system under consideration, high frequency dynamics above 350 Hz was considered as an additive uncertainty $\Delta_A(s)$, $\Delta_{max}(s)$ was then chosen to bound $\Delta_A(s)$.

Magnitude plots of $\Delta_{max}(j\omega)$ and $|P(j\omega) - P_0(j\omega)|$ are shown in Fig. 2.12. Note that Δ_{max} selected does not satisfy Eq. (2.45) at all frequencies. This is done intentionally to obtain the controller with desired control authority. These are some practical considerations [31] in controller design which will be discussed in detail later.

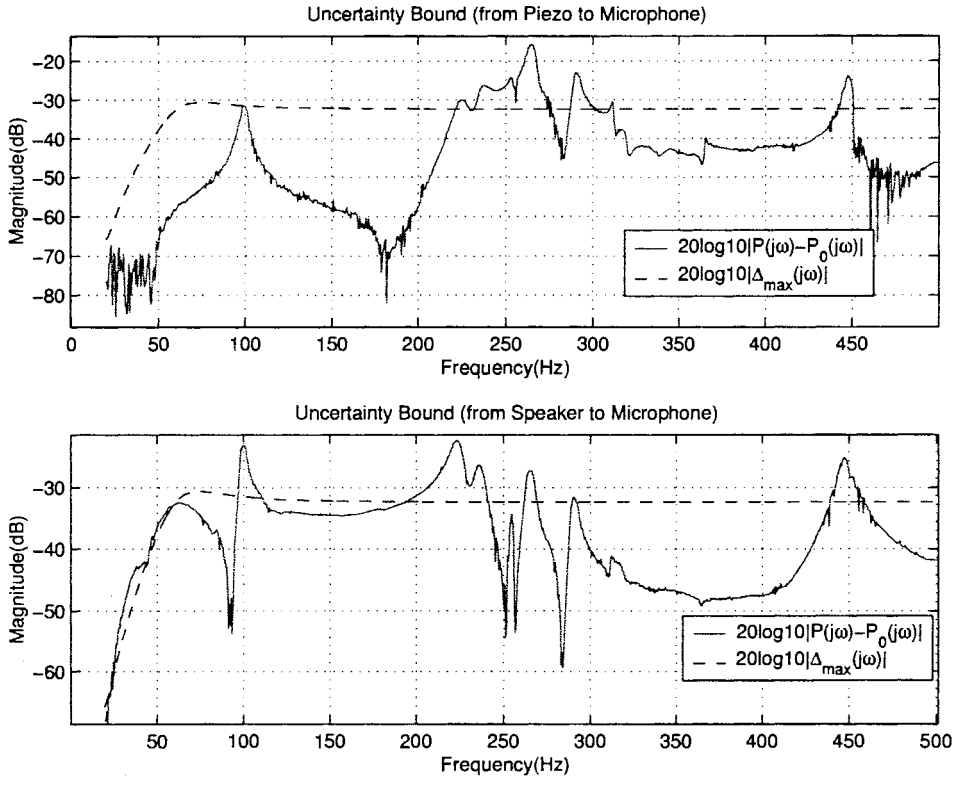

Figure 2.12 Additive uncertainty bounds

3 LQG ROBUST CONTROL

In the previous chapter, we established the mathematical model of $3-D$ acoustic enclosure using both analytical and system identification techniques. In this chapter, we present a robust and optimal controller design based on Linear Quadratic Gaussian (LQG) theory using identified system model. The simulation and experimental results are given to demonstrate the effectiveness of the control design.

3.1 Formulation of LQG Design

The LQG-based control design combines linear quadratic (LQ) with Kalman filter to derive controller. The regulator design is based on full state feedback and is independent of Kalman filter design. Regulator and Kalman Filter can be designed independently based on a well known separation principle [40]. Given below is the formulations of LQG controller design where controller state-space description is obtained in the closed form.

Let the plant be described by the following linear state equations:

$$\begin{aligned} \dot{x}(t) &= Ax(t) + B_u u(t) + B_d d(t) \\ m(t) &= C_m x(t) + D_u u(t) + \zeta(t) \\ y_p(t) &= m(t) \quad \text{(performance output is same as the sensed output)} \end{aligned} \tag{3.1}$$

where $u(t)$ is the control input, $d(t)$ is the disturbance input, $\zeta(t)$ is the measurement noise, $y_p(t)$ is the performance output, and $m(t)$ is the measurement output. $\zeta(t)$ is assumed to be zero-mean white noise process. The model obtained by system identification

toolbox SOCIT can be written in the form given by Eq. (3.1).

The performance function for LQG design is given as:

$$J = E\left\{\frac{1}{2}\int_0^\infty \left[x(t)^T Q x(t) + u^T(t) R u(t)\right] dt\right\} \tag{3.2}$$

where, E is the expectation operator and weighting matrices $Q = Q^T \geq 0$ and $R = R^T > 0$. The LQG feedback gain approaches a constant value far from the final time, and the Kalman Filter Gain approaches a constant value far from the initial time. For long time intervals, both gains are approximately constant over most of the interval. That is, the steady-state solutions of these gains tend to be constant and use of these constant state feedback and Kalman gains simplifies the implementation of the controller. The steady-state control input is given by following state-feedback control law:

$$u(t) = -K\hat{x}(t) = -R^{-1}B_u^T P\hat{x}(t) \tag{3.3}$$

where, $\hat{x}(t)$ is the estimated state and $K = R^{-1}B_u^T P$ is the regulator gain. P in the expression of K is the solution of the following (steady-state) algebraic Riccati equation (ARE):

$$A^T P + PA - PB_u R^{-1} B_u^T P + Q = 0 \tag{3.4}$$

$\hat{x}(t)$ is the solution of the following observer (Kalman filter) dynamics:

$$\begin{aligned}
\dot{\hat{x}}(t) &= A\hat{x}(t) + B_u u(t) + L(m(t) - \hat{m}(t)) \\
&= A\hat{x}(t) + B_u u(t) + L(C_m x(t) + D_u u(t) + \zeta(t) - C_m\hat{x}(t) - D_u u(t)) \\
&= (A - LC_m - B_u K)\hat{x}(t) + LC_m x(t) + L\zeta(t)
\end{aligned} \tag{3.5}$$

where, L is the Kalman gain given by: $L = \Sigma(t) C_m^T V^{-1}$. $V = E\left[\zeta\zeta^T\right]$ and Σ is the solution of the following ARE called the filter Riccati equation.

$$\Sigma A^T + A\Sigma - \Sigma C_m^T V^{-1} C_m \Sigma + B_u W^{-1} B_u^T = 0 \tag{3.6}$$

where, $W = E\left[dd^T\right]$, and it is assumed that:

$$E[\zeta(t) d^T(t+\tau)] = 0 \tag{3.7}$$

$$E[x(0)d(t)] = 0 \quad for\ all\ t \geq 0 \tag{3.8}$$

$$E[x(t)\zeta(t+\tau)] = 0 \quad for\ all\ \tau \tag{3.9}$$

Equation (3.7) comes from the orthogonality of zero mean noise, since they are generally assumed to be generated by different phenomena [41]. Equation (3.8) comes from the assumption that the plant noise and the initial state are uncorrelated and therefore orthogonal. This assumption follows from the fact that the plant noise can only affect future states, and white noise is uncorrelated from one time instant to the next. Equation (3.9) comes for the assumption that the state and the measurement noise are uncorrelated and orthogonal. Thus, the Kalman filter generates the linear estimate of the plant state (3.1) that minimizes the mean squared estimation error:

$$J_K = E[\{x(t) - \hat{x}(t)\}^T\{x(t) - \hat{x}(t)\}] = \sum_{i=1}^{n} E[\{x_i(t) - \hat{x}_i(t)\}^2] \tag{3.10}$$

The data used in generating this estimate are the measurements from time zero to current time. With the assumptions above, we can estimate the state as Eq. (3.5).

The LQG controller is the combination of the Kalman filter and regulator and is given by

$$\begin{aligned} \dot{\hat{x}}(t) &= (A - LC_m - B_uK - LD_uK)\hat{x}(t) + Lm(t) \\ u(t) &= -K\hat{x}(t) \end{aligned} \tag{3.11}$$

The closed-loop equations for the feedback interconnection of the plant and the LQG controller are given by

$$\begin{aligned} \begin{bmatrix} \dot{x} \\ \dot{\hat{x}} \end{bmatrix} &= \begin{bmatrix} A & -B_uK \\ LC_m & A_s - LC_m - B_uK \end{bmatrix} \begin{bmatrix} x \\ \hat{x} \end{bmatrix} + \begin{bmatrix} B_d & 0 \\ 0 & L \end{bmatrix} \begin{bmatrix} d(t) \\ \zeta(t) \end{bmatrix} \\ y_p &= \begin{bmatrix} C_m & -D_uK \end{bmatrix} \begin{bmatrix} x \\ \hat{x} \end{bmatrix} + \zeta(t) \end{aligned} \tag{3.12}$$

A block diagram of the feedback control system is given in Fig. 3.1.

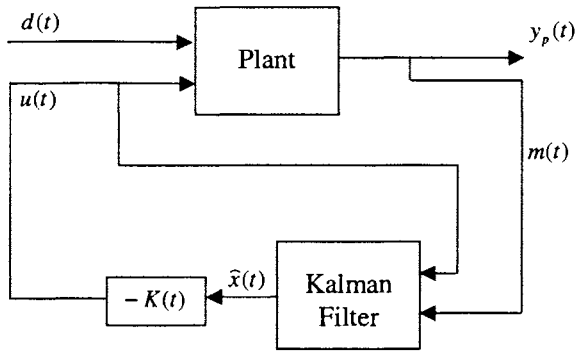

Figure 3.1 A LQG optimal control system

3.2 LQG Controller Design for Acoustic Enclosure

The control design methodology given in section 3.1 is used to obtain LQG controller that can provide robust broadband noise reduction in the frequency range of interest.

The design model for the plant and the controller are given by Eqs. (3.1) and (3.11), respectively. It is to be noted that the state space model obtained analytically (Eq. (2.17)) does not use the same state description as the one used in Eq. (3.1), which is obtained using system identification. However, these two state-space models are related by a similarity transformation $X(t) = Tx(t)$, where T is nonsingular real matrix given as follows. The state variables that we use in obtaining the analytical model are the modal coordinates, q and $\dot{q}$, while in the system identification process, the software gives the model with different state description. Thus, the state matrices, $A_E := E^{-1}A_F$ (from analytical model) and A (from system identification model) are in different forms. The form for A_E is obtained in section 2.1.1 and the form for A is given as:

$$A = \begin{bmatrix} -\zeta_1\omega_1 & \omega_1\sqrt{1-\zeta_1^2} & 0 & \cdots & 0 \\ -\omega_1\sqrt{1-\zeta_1^2} & -\zeta_1\omega_1 & 0 & \cdots & \vdots \\ 0 & \cdots & \ddots & 0 & 0 \\ \vdots & \cdots & 0 & -\zeta_n\omega_n & \omega_n\sqrt{1-\zeta_n^2} \\ 0 & \cdots & 0 & -\omega_n\sqrt{1-\zeta_n^2} & -\zeta_n\omega_n \end{bmatrix} \tag{3.13}$$

where, ζ_i and ω_i represent the damping ratio and the natural frequency of the i-th

mode. Since A_E and A have the same eigenvalues, they are similar, and they can both be transformed to a diagonal matrix Λ. That is, for matrix A_E, we can find a matrix V_{A_E}, composed of the eigenvectors of A_E, such that $AV_{A_E} = \Lambda$. For matrix A_s, we can find a matrix V_A, composed of the eigenvectors of A_s, such that $AV_A = \Lambda$. Thus $A = T^{-1}A_F T$, where $T = V_E V_A^{-1}$. Now, the total energy of the system Eq. (2.40) can be rewritten as:

$$E(t) = \frac{1}{2}x^T Q x \tag{3.14}$$

where

$$Q = T^T Q_0 T \tag{3.15}$$

The matrix Q given by Eq. (3.15) can be used as the state weighting matrix in the LQG performance function (Eq. (3.2)). The choice of the particular Q has great significance, as it causes optimal control input to minimize the total acoustic energy of the enclosure directly. The penalty on control power, which is the weighting matrix R in the performance function is chosen by trial and error. The consideration for choosing R is the minimization of control power while obtaining desirable performance. Other control design parameters are noise covariance matrix V and W.

3.2.1 Controller Parameters and Simulation Results

Two LQG controllers were designed – one which used the weighting matrix from Eq. (3.15) and other where Q was picked manually by iterative design process. Other controller parameters were chosen as: $R = 10$, $V = I$, and $W = 5E-6$ for both designs. For the LQG controller with these parameters, the simulated open- and closed-loop frequency responses are shown in Figs. 3.2 and 3.3. Bode plots of these two controllers are shown in Figs. 3.4 and 3.5. Comparing Figs. 3.2 and 3.3, it can be seen that, for the nominal plant, the LQG controller designed with Q minimizing total energy gives better performance.

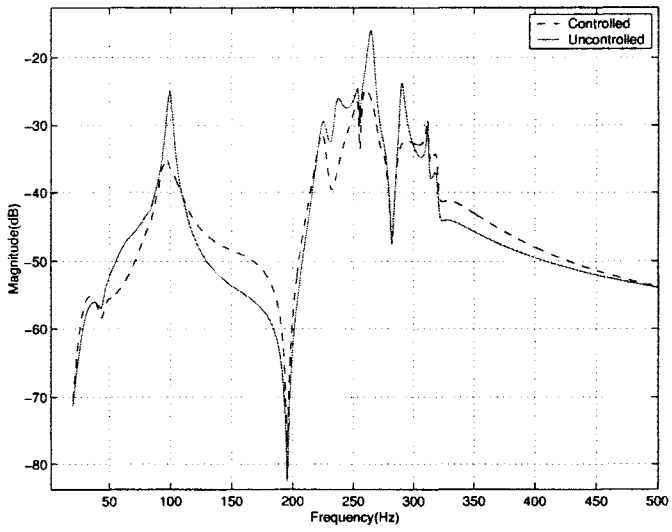

Figure 3.2 Simulated open-loop and closed-loop frequency response with Q designed to minimize total acoustic energy

The LQG designs were also tested in time domain by analyzing response to different disturbance inputs. Figure 3.6 shows implementation diagram in *SIMULINK*. The disturbance inputs selected include single as well as multiple tone harmonics. Figs. 3.7 and 3.8 show open- and closed-loop simulated responses for 100 Hz and 225Hz monotone sinusoids, Figs. 3.9 and 3.10 show open- and closed-loop simulated responses for 290 Hz monotone sinusoid and multi-tone sinusoid consisting of 100 Hz, 225 Hz, and 290 Hz components, respectively. From the simulation results, it can be seen that the monotone as well as multi-tone noise can be effectively reduced.

3.2.2 Experimental Results

To test the LQG controller designed, experiments were carried out with the setup shown in Fig. 2.6. Sweep sinusoid from 20 to 500 Hz was applied to the system via piezo actuator as disturbance, and the speaker's vibration works as control input. Open-loop and closed-loop bode plots are shown in Fig. 3.11. From these results, one can see that the controller performed very well not only in the frequency range where the nominal model was obtained (20-350Hz), but also in the frequency range beyond (i.e.,

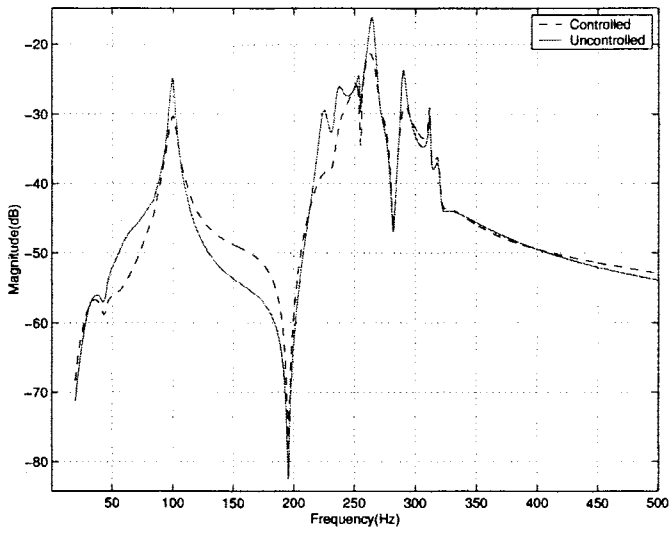

Figure 3.3 Simulated open-loop and closed-loop frequency response with iterative Q design

350-500Hz). There is fairly good agreement between simulation and experimental results. Similar to simulation, 3 monotone sinusoid and multi-tone sinusoids consisting of 100 Hz, 225 Hz, and 290 Hz were used as disturbance signals. The open-loop and closed-loop time responses are shown in Figs. 3.12, 3.13, 3.14, and 3.15. These time responses agree with those in Fig. 3.11 quite well.

Also, to test the global performance of the controller, another microphone located at different location was used. The performance output is now different from the sensed output, The performance microphone was located at (2.75",4", 4.75"), where as the sensing microphone was located at (6.75",7", 11.25"). The results are presented in Fig. 3.16. The figure on the left shows the experimental result for the controller with Q obtained from Eq. (2.40). The figure on the right shows the experimental result for for controller with Q selected by trial and error. From these results, we can see that although in both cases, the response deteriorates for certain frequency, the controller designed to reduce the total energy works better than the other.

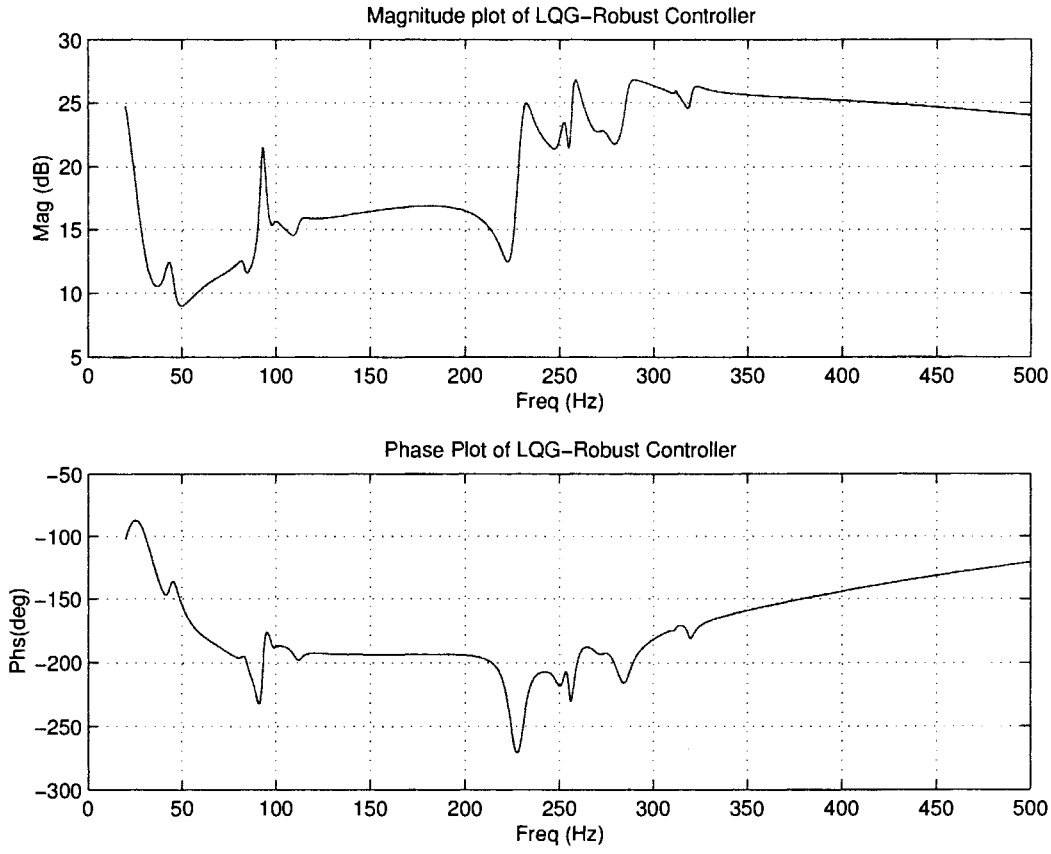

Figure 3.4 Bode plot of LQG controller with Q designed to minimize total acoustic energy

3.3 Robust Stability Analysis

The robustness of the LQG design to modelling uncertainties is guaranteed by ensuring that the controller parameters satisfy the frequency-domain condition for robust stability. The modelling uncertainty, which includes unmodeled dynamics as well as modelling errors, is accounted for by using the additive unstructured uncertainty model. The difference between the true plant model and the nominal design model was modelled as the additive unstructured uncertainty (see Fig. 2.10).

If $P(s)$ denotes the true plant model and $P_0(s)$ denotes the nominal design model, then, in the presence of additive unstructured uncertainty, the true plant model $P(s)$ is

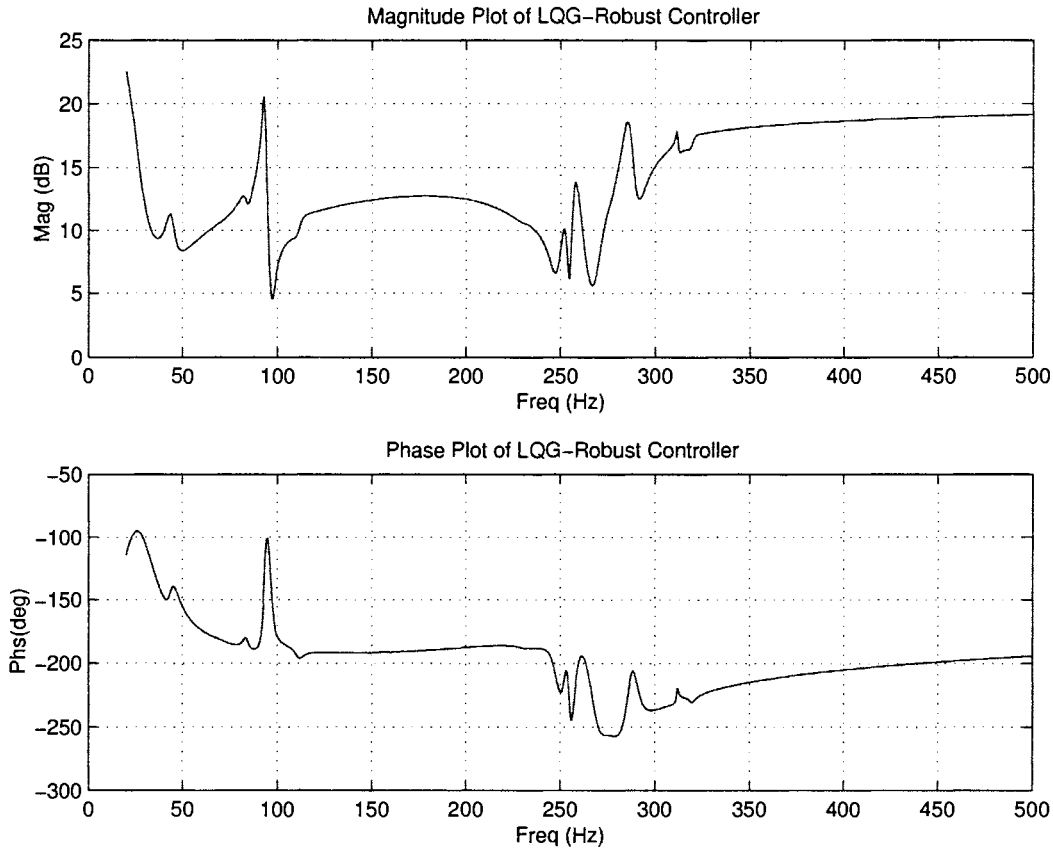

Figure 3.5 Bode plot of LQG controller with iterative Q design

given by (refer to 3.16)

$$P(s) = P_0(s) + \Delta_A(s) \tag{3.16}$$

After closing the loop, rearranging and simplifying, Figure 2.10 can be redrawn into a standard form as shown in Fig. 3.17. This configuration will be used for evaluating the stability robustness of the closed-loop system. The controller $C(s)$ is designed to stabilize the augmented nominal plant $\tilde{P}(s)$ (represented as the dotted box in Fig. 3.17). Fig. 3.18 shows the block diagram with the feedback loop between $\tilde{P}(s)$ and $C(s)$ closed. Uncertainty $\Delta(s)$ is now shown in the feedback interconnection with the nominal closed-loop system $N(s)$. This is known in the robust control literature as $N-\Delta$ configuration.

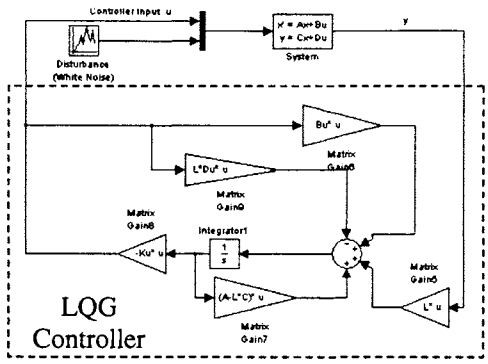

Figure 3.6 Simulink model of LQG controller

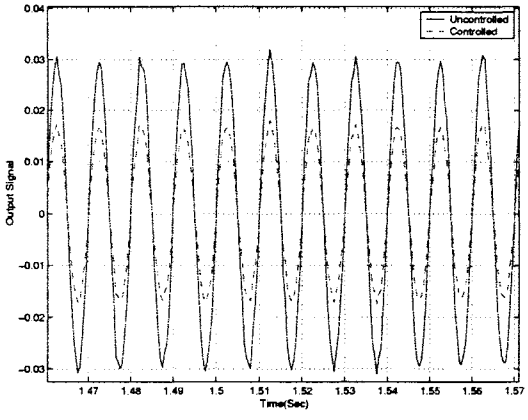

Figure 3.7 Time response (100 Hz)

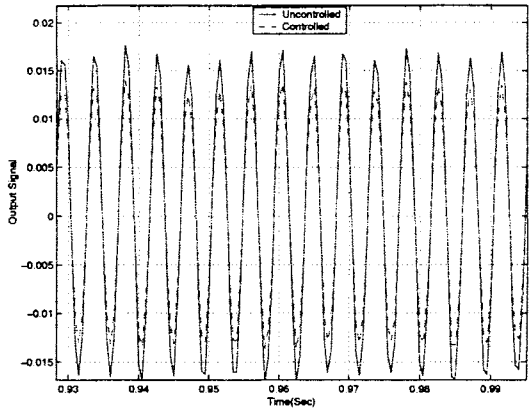

Figure 3.8 Time response (225 Hz)

The $N-\Delta$ system is thus given by

$$\begin{bmatrix} Y_d \\ Y \end{bmatrix} = \begin{bmatrix} N_{Y_dW_d} & N_{Y_dW} \\ N_{YW_d} & N_{YW} \end{bmatrix} \begin{bmatrix} W_d \\ W \end{bmatrix} \tag{3.17}$$

In the $N-\Delta$ configuration, the only source of closed-loop instability is due to feedback interconnection of $N_{Y_dW_d}$ and $\Delta(s)$. Then, for robust stability, one needs to ensure that this interconnection is stable. This is ensured if the following sufficient condition is satisfied:

$$||N_{Y_dW_d}(s)\Delta(s)||_\infty \leq 1 \tag{3.18}$$

Since using the choice of $\Delta_{max}(s)$ we have ensured that $\|\Delta(s)\|_\infty \leq 1$, the interconnection

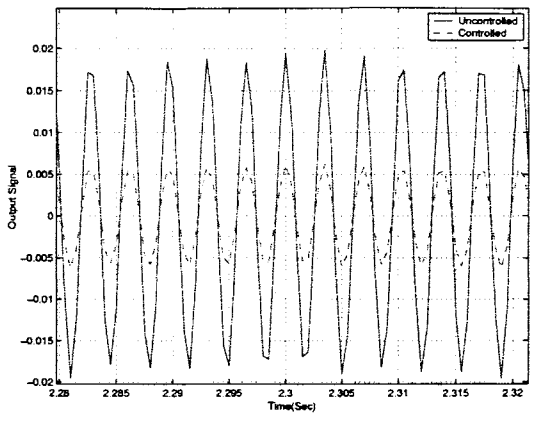

Figure 3.9 Time response (290 Hz)

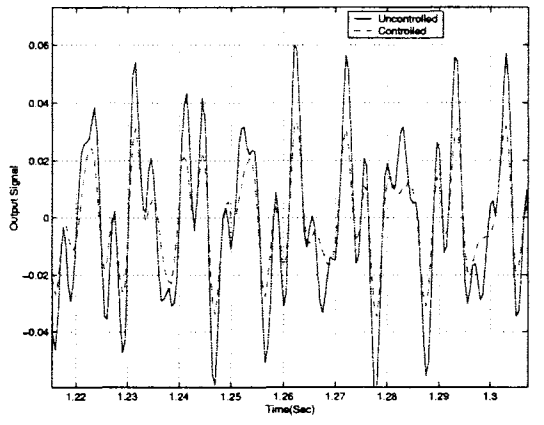

Figure 3.10 Time response (multitone)

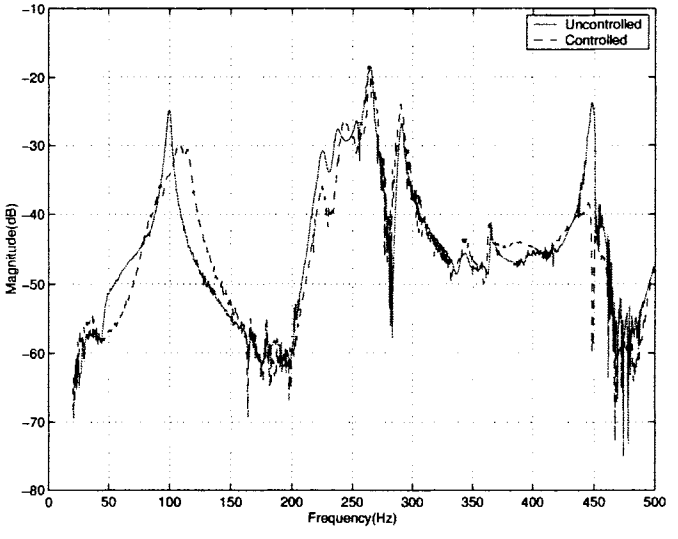

Figure 3.11 Experimental open-loop and closed-loop frequency response

is robustly stable if

$$\|N_{Y_d W_d}(s)\|_\infty \leq 1 \tag{3.19}$$

This is the robust stability condition that will be used to check the robustness of the LQG controller design. In our case,

$$Y_d = \begin{bmatrix} Y_{du} \\ Y_{dd} \end{bmatrix} \quad W_d = \begin{bmatrix} W_{du} \\ W_{dd} \end{bmatrix} \quad Y_d = N_{Y_d W_d} W_d \tag{3.20}$$

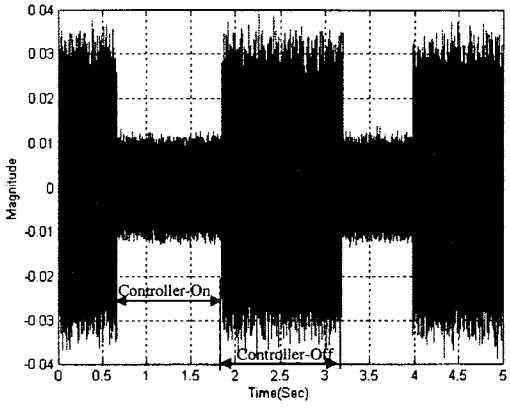

Figure 3.12 Time response (100 Hz)

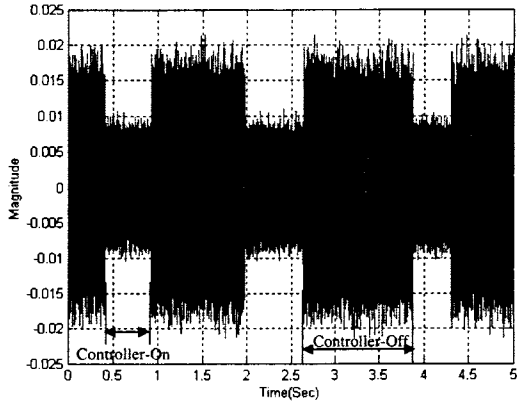

Figure 3.13 Time response (225 Hz)

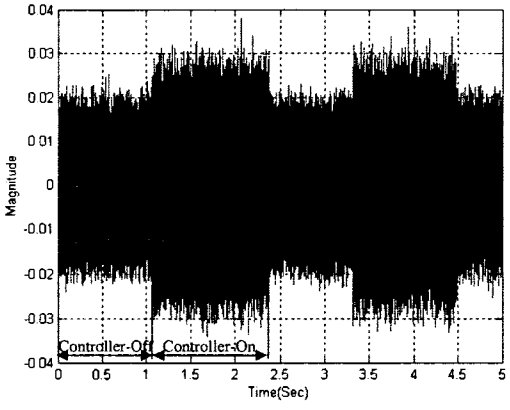

Figure 3.14 Time response (290 Hz)

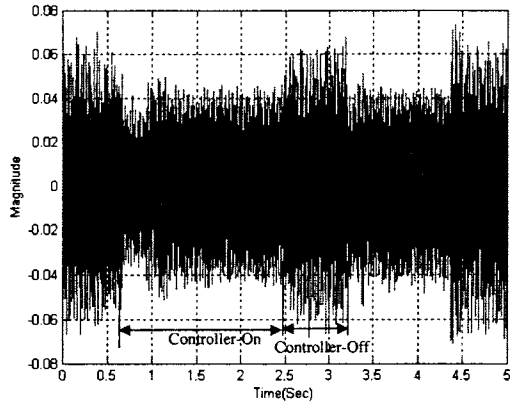

Figure 3.15 Time response (multitone)

Thus, $N_{Y_dW_d}$ turns out to be

$$N_{Y_dW_d} = \begin{bmatrix} N_{Y_dW_d11} & N_{Y_dW_d12} \\ 0 & 0 \end{bmatrix} \tag{3.21}$$

where $N_{Y_dW_d11} = N_{Y_dW_d12} = \Delta_{max}(s)C(s)[1 - C(s)P_{0uy}(s)]^{-1}$. So, the infinity norm of $N_{Y_dW_d}$ is

$$\|N_{Y_dW_d}\|_\infty = 2\|\frac{C(j\omega)}{1 - C(j\omega)P_{0uy}(j\omega)}\Delta_{max}(j\omega)\|^2 \tag{3.22}$$

where $P_{0uy}(j\omega)$ is the open loop transfer function from u to y_p or $m(t)$. $C(s)$ is the controller given by Eq. (3.11) and can be obtained as

$$C(s) = -K[sI - (A_s - LC_m - B_uK + LD_uK)]^{-1}L \tag{3.23}$$

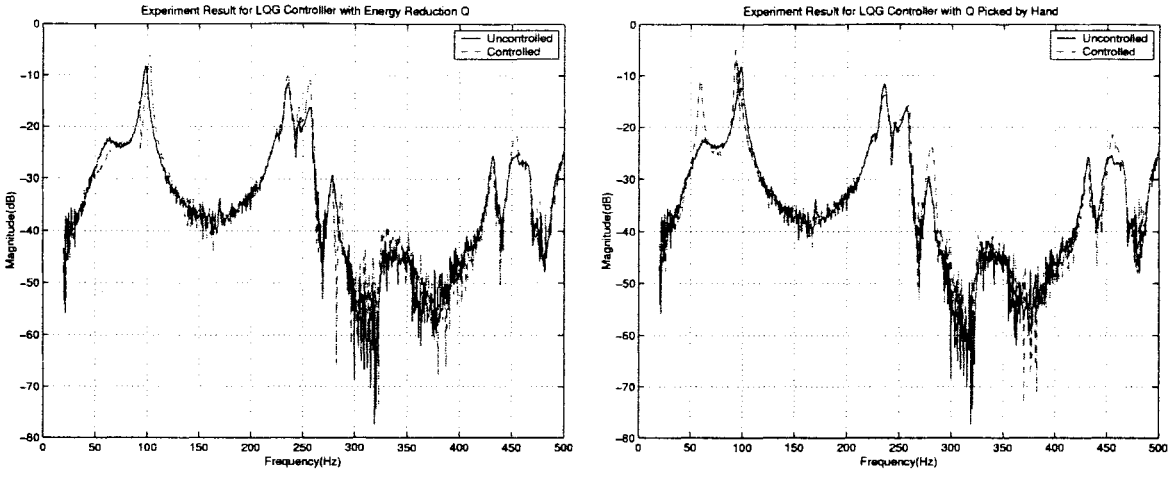

Figure 3.16 Experimental open-loop and closed-loop frequency response at other sensor position

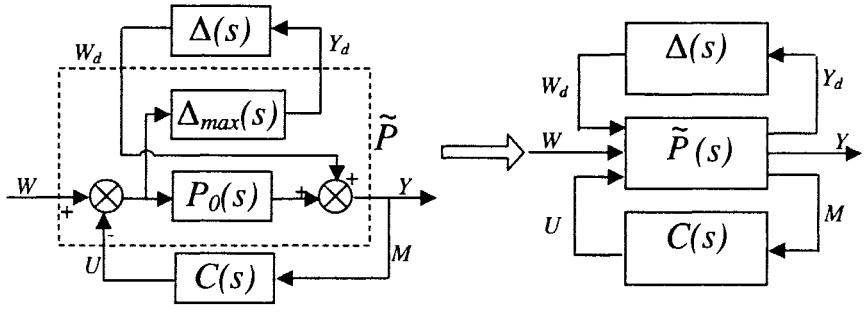

Figure 3.17 Standard form of additive uncertainty

For the LQG controller designed, the infinity norm of $N_{Y_d W_d}$ is plotted as a function of frequency in Fig. 3.19. One can see that the condition of Eq. (3.19) is satisfied and therefore, the system is robustly stable.

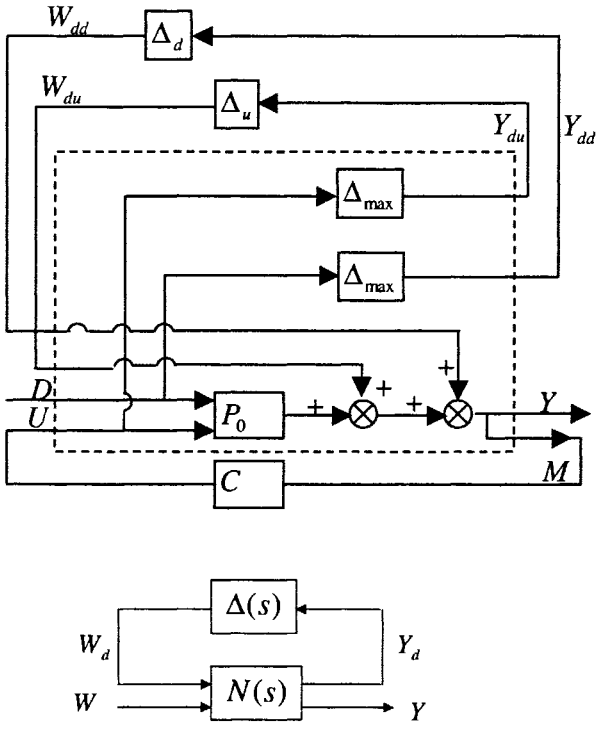

Figure 3.18 $N - \Delta$ configuration

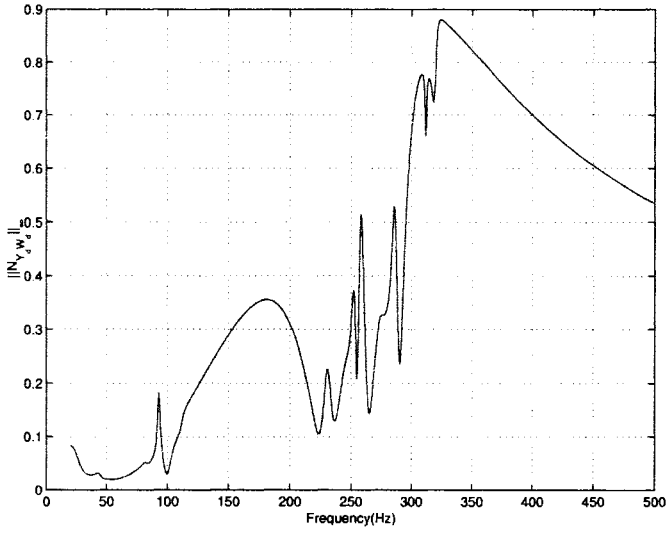

Figure 3.19 $||N_{Y_d W_d}||_\infty$ versus frequency

4 PASSIVITY-BASED CONTROL

Passivity is an important property of dynamic systems. A large class of physical systems (such as flexible structures) can be classified as being naturally passive. A passive system can be robustly stabilized by any strictly passive controller, despite the unmodeled dynamics and parametric uncertainties. It is this robust stabilization property of passivity-based controller that has received considerable attention in the literature [42, 43, 44, 45, 46]. There is a large class of systems that are naturally passive; for example, large flexible structures with collocated actuators and sensors, robots with torque actuators and rate sensors, and many others. There also exist a large class of real-life systems that are not inherently passive. Some examples of such systems include flexible aircraft with non-collocated actuators and sensors, acoustic systems and systems with transportation delay. For non-passive systems such as acoustic systems, passivity-based control deign can be used provided the system is first "passified", i.e., rendered passive via suitable compensation. Methods for such passification are given in [47, 48, 49]. In this chapter, a passivity-based controller design is obtained using the techniques given in [47, 48, 49] for the acoustic system under consideration. Two different types of passivity-based controller are designed: a constant gain controller [50] and dynamic LQG optimal controller [51]. Both simulation and experimental results are provided.

4.1 Passivity of Linear System

Given below is a brief background of passivity. For finite-dimensional linear time-invariant (LTI) systems, passivity is equivalent to "positive realness" of the transfer function. The concept of strict positive realness has also been defined in the literature, and is closely related to strict passivity.

Let $G(s)$ denote an $m \times m$ matrix whose elements are proper rational functions of the complex variable s. $G(s)$ is said to be stable if all of its elements are analytic in $Re(s) \geq 0$. Let the conjugate-transpose of a complex matrix H be denoted by H^*.

Definition 1 [52]: An $m \times m$ rational matrix $G(s)$ is said to be *positive real* (PR), if

(i) all elements of $G(s)$ are analytic in $Re(s) > 0$;

(ii) $G(s) + G^*(s) \geq 0$ in $Re(s) > 0$; or equivalently,

(iia) poles on the imaginary axis are simple and have nonnegative-definite residues, and

(iib) $G(j\omega) + G^*(j\omega) \geq 0$ for $\omega \in (-\infty,\ \infty)$.

There are various definitions of *strictly* positive real (SPR) systems found in the literature. Given below is the definition of a class of SPR systems, namely, marginally strictly positive-real $(MSPR)$ systems.

Definition 2: An $m \times m$ rational matrix $G(s)$ is said to be *marginally strictly positive real* (MSPR) if it is positive real, and

$$G(j\omega) + G^*(j\omega) > 0 \ for \ \omega \in (-\infty, \infty).$$

Definition 2 gives the least restrictive class of SPR systems. If $G(s)$ is $MSPR$, it can be expressed as: $G(s) = G_1(s) + G_2(s)$, where $G_2(s)$ is weak SPR [53]and all the poles of $G_1(s)$ (in the Smith-McMillan sense) are purely imaginary. The stability theorem for feedback interconnection of the PR and $MSPR$ systems is given next without proof.

Stability Theorem [52]: The closed-loop system consisting of negative feedback interconnection of $G_1(s)$ and $G_2(s)$ is globally asymptotically stable if $G_1(s)$ is PR, $G_2(s)$

is $MSPR$, and none of the purely imaginary poles of $G_2(s)$ is a transmission zero of $G_1(s)$.

Note that in the above theorem, systems $G_1(s)$ and $G_2(s)$ can be interchanged. Most physical systems, however, are not inherently passive, and passivity-based control techniques cannot extend directly for such systems. The acoustic system of our research is one such example. One method of making non-passive systems amenable to passivity-based control is to *passify* [47, 48] such systems (i.e., rendering system passive), using suitable compensation. If the compensated system is *robustly passive* despite plant uncertainties, it can be robustly stabilized by any $MSPR$ controller. In [50] various passification techniques, series, feedback, feedforward, and hybrid passifications were presented and some numerical examples were given for demonstrating the use of such techniques. For the acoustic system considered in this thesis, a combination of feedforward and series compensators are used to passify the acoustic system. Once passified, the system can be controlled by any $MSPR$ or weakly SPR ($WSPR$) controller. One important thing to note here is that, in the case of inherently passive systems, the use of an $MSPR$ controller guarantees stability robustness to unmodeled dynamics and parametric uncertainties; however, in the case of non-passive systems, rendered passive using passifying compensation, the stability robustness depends on the robustness of passification. That is, the problem of *robust stability* is transformed into the problem of *robust passification*, i.e., the real plant (and not just the nominal plant) should be passive after passification.

4.1.1 Passification of Non-Passive LTI Systems

As stated previously, the passification method essentially aims at exploiting the stability properties of passivity-based control laws by rendering a non-passive system passive via some passifying compensator and then closing the feedback loop using suitable passive controller. The passifying compensators that have been proposed in [47], [48],

and [49] include: series compensation, output feedback compensation, feedforward compensation, hybrid compensation (i.e., combination of series, feedback, and feedforward), and sensor blending and/or actuator allocation (applicable to systems having redundant sensors and actuators).

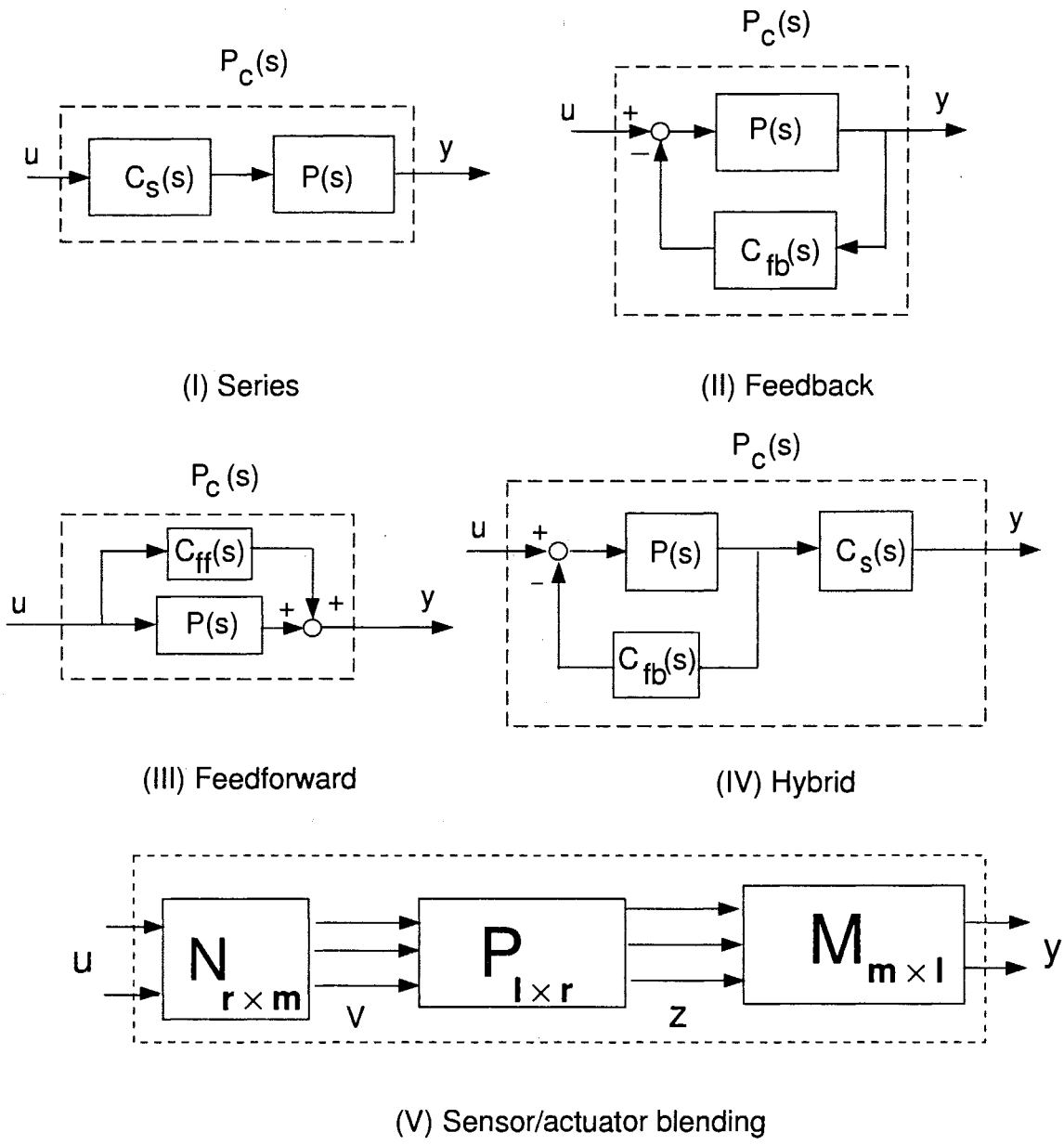

Figure 4.1 Methods of passification

Figure 4.1 shows block diagram of different types of passifications. In each of the cases

(i-v) in Fig. 4.1, $P(s)$ indicates the non-passive plant and $P_c(s)$ indicates the passified plant. Fig. 4.1-(iv) shows one of many possible configurations for hybrid passification. Different types of non-passive system will warrant different types or combination of different types of passification methods. For example, for systems with non-minumum phase zeros passification will require feedforward compensation first to render the system minimum phase. Similarly, open-loop unstable systems will first require inner-loop feedback compensation for rendering system stable. One important consideration in the design of passifying compensator is the robustness of passification. The stability robustness depends on the robustness of passification as the passivity is not inherent to the system, but depends on the compensator. The process of controller design thus involves first rendering the system robustly passive by introducing compensation and then stabilizing the system by any MSPR controller.

4.2 Design of Constant-Gain Positive-Real Controller

For non-passive systems, overall controller is a combination of passifying compensator and strictly passive feedback controller. For the acoustic system under consideration, the passifying compensation is typically a two-step process. The first step will involve design of feedforward compensation to render the system minimum phase (as discussed in previous section) and the second step will involve design of series compensator to passify the system. In some cases, feedforward solely by feedforward alone simultaneously renders the system minimum phase as well as passive. The acoustic system under consideration falls under this category. That is, the passification was accomplished solely by feedforward compensator. The overall control design, however, included series compensator before feedback loop was closed with SPR controller. This series compensator was designed to suppress the resonance mode dynamics of the system to enhance the performance at those resonance frequencies.

Resonant modes are characteristics of frequency response of systems such as flexible structures [54, 55] and acoustic systems. The main idea behind resonant mode control is as follows: Consider a system of Fig. 4.2. Suppose the plant $P(s)$ has a resonant mode at frequency Ω_0. Then, suppose we design a feedback controller, $K_0(s) = N(s)/D(s)$, such that $D(s)$ has a pole at Ω_0, then the closed-loop transfer function will have $D(s)$ in the numerator. That means the closed-loop transfer function will have zeros at the root of $D(s)$. Thus if the system is excited with the disturbance $d(t)$ at frequency Ω_0, it will be blocked by the zero at Ω_0 and will not affect the output $y(t)$.

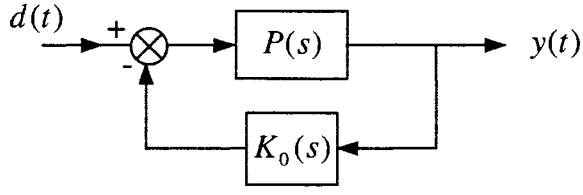

Figure 4.2 Feedback system with resonant-mode controller

4.2.1 Controller Synthesis

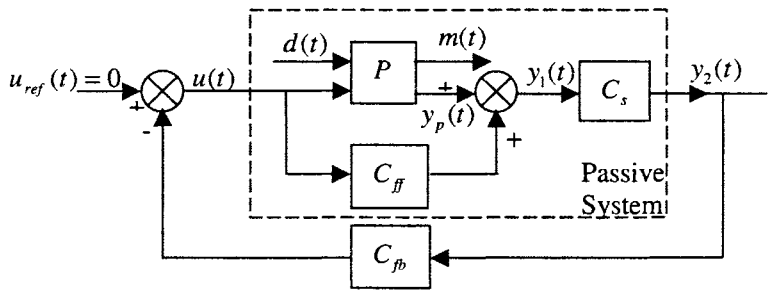

Figure 4.3 Passive constant gain controller

For the $3-D$ acoustic enclosure in Fig. 2.1, the control architecture is given by the block diagram of Fig. 4.3. Various signals and transfer functions in Fig. 4.3 are defined as follows: $P(s)$ is the plant, $C_{ff}(s)$ is the feedforward compensator, $C_s(s)$ is the resonance-mode series compensator, $C_{fb}(s)$ is feedback SPR controller, $d(t)$ is the disturbance signal produced by the piezo, $u(t)$ is the control input from speaker, and $m(t)$

is the measurement signal at the microphone,. The overall controller is the combination of $C_{ff}(s)$, $C_S(s)$, and $C_{fb}(s)$. The stability of the closed-loop system shown in Fig. 4.3 is ensured by the stability theorem given in Section 4.1. The feedforward controller C_{ff} was a simple constant gain controller. As stated previously, C_{ff} was adequate to render system minimum phase as well as passive. The resonant controller $C_s(s)$, was designed to be a parallel combination of several second order controllers, $K_i(s)$ (Fig. 4.4). Each $K_i(s)$ has one resonant mode, which matches with one of the plant's resonant poles. The number of $K_i(s)$ needed equals the number of resonant modes of the system to be damped. The most important aspect in the design of $C_s(s)$ is once poles of the $K_i(s)$ are selected such that the passivity of the system is reserved, i.e., system from input $u(t)$ to output $y_2(t)$ remains passive.

The final step of the design is to choose a feedback controller $C_{fb}(s)$ such that it satisfies wither $WSPR$ or $MSPR$ [53]. The constant gain feedback controller $C_{fb}(s)$ is the simplest SPR controller, namely, a constant-gain controller. The most important thing to note is that the overall controller, a combination of the feedforward, resonant, and compensator, is a low-order, output-feedback controller and therefore easy to implement. The infinite gain margin of this controller is a great advantage over many other controllers presented in the literature. Even better performance can be achieved if the SPR controller can be dynamic and optimized with respect to some desired performance measure.

Given below is the development of the closed-loop state and output equations for the configuration shown in Fig. 4.3.

- Open-loop system:

$$P(s) \sim \begin{cases} \dot{x}(t) = Ax(t) + B_u u(t) + B_d d(t) \\ m(t) = C_m x(t) + D_m u(t) + D_d d(t) \quad \text{(Measurement Output)} \\ y_p(t) = C_p x(t) + D_{pu} u(t) + D_{pd} d(t) \quad \text{(Performance Output)} \end{cases} \tag{4.1}$$

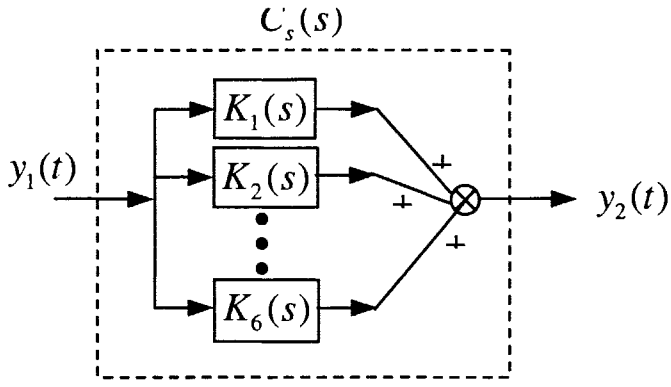

Figure 4.4 Structure of resonance-mode compensator

In our case, $m(t) = y_p(t)$, thus $C_m = C_p$; $D_m = D_{pu}$; and $D_d = D_{pd}$.

- Plant after feedforward compensation:

$P(s) + C_{ff}(s) \sim$

$$\begin{cases} \dot{x}(t) = Ax(t) + B_u u(t) + B_d d(t) \\ y_1(t) = m(t) + C_{ff}u(t) = C_m x(t) + (D_m + C_{ff})u(t) + D_d d(t) \end{cases} \tag{4.2}$$

- Passified plant with resonant mode controller $C_s(s)$: $C_s(s)[P(s) + C_{ff}(s)] \sim$

$$\begin{cases} \dot{x}(t) = Ax(t) + B_u u(t) + B_d d(t) \\ \dot{x}_s(t) = A_s x_s(t) + B_s C_m x(t) + B_s(D_m + C_{ff})u(t) + B_s D_d d(t) \\ y_2(t) = m(t) + C_{ff}u(t) = C_m x(t) + (D_u + C_{ff})u(t) + D_d d(t) \end{cases} \tag{4.3}$$

In the matrix form:

$$\begin{aligned} \begin{bmatrix} \dot{x}(t) \\ \dot{x}_s(t) \end{bmatrix} &= \begin{bmatrix} A & 0 \\ B_s C_m & A_s \end{bmatrix} \begin{bmatrix} x(t) \\ x_s(t) \end{bmatrix} + \begin{bmatrix} B_u \\ B_s(D_m + C_{ff}) \end{bmatrix} u(t) \\ &+ \begin{bmatrix} B_d \\ B_s D_d(t) \end{bmatrix} d(t) \\ y_2(t) &= \begin{bmatrix} D_s C_m & C_s \end{bmatrix} \begin{bmatrix} x(t) \\ x_s(t) \end{bmatrix} + D_s(D_u + C_{ff})u(t) \\ &+ (D_s D_d)d(t) \end{aligned} \tag{4.4}$$

- Finally, the closed-loop system with the feedback loop closed using the constant-gain SPR controller

$$\begin{aligned} u(t) &= -C_{fb}y_2(t) \\ &= -\begin{bmatrix} C_{fb}D_sC_m & C_{fb}C_s \end{bmatrix}\begin{bmatrix} x(t) \\ x_s(t) \end{bmatrix} \\ &- C_{fb}D_s(D_m + C_{ff})u(t) - (C_{fb}D_sD_d)d(t) \\ \Rightarrow u(t) &= \frac{1}{1 + C_{fb}D_s(D_m + C_{ff})}[-\tilde{C}\tilde{x}(t) - \tilde{D}_d d(t)] \end{aligned}$$

where

$$\begin{aligned} \tilde{C} &= \begin{bmatrix} C_{fb}D_sC_m & C_{fb}C_s \end{bmatrix} \\ \tilde{x}(t) &= \begin{bmatrix} x(t) \\ x_s(t) \end{bmatrix} \\ \tilde{D}_d &= C_{fb}D_sD_d \end{aligned} \tag{4.5}$$

Substituting Eq. (4.5) back into Eq. (4.2) and defining $\tilde{g} = 1 + C_{fb}D_s(D_m + C_ff)$, we obtain

$$\begin{aligned} \begin{bmatrix} \dot{x}(t) \\ \dot{x_s}(t) \end{bmatrix} &= A_{cl}\begin{bmatrix} x(t) \\ x_s(t) \end{bmatrix} + B_{cld}d \\ y_p(t) &= C_{cl}\begin{bmatrix} x(t) \\ x_s(t) \end{bmatrix} + D_{cld}d(t) \end{aligned}$$

where

$$A_{cl} = \begin{bmatrix} A - \frac{1}{\tilde{g}}B_uC_{fb}D_sC_m & -\frac{1}{\tilde{g}}B_uC_{fb}C_s \\ B_sC_m - \frac{1}{\tilde{g}}B_s(D_m + C_ff)C_fbD_sC_m & A_s - \frac{1}{\tilde{g}}B_s(D_m + C_ff)C_fbC_s \end{bmatrix}$$

$$B_{cld} = \begin{bmatrix} B_d - \frac{1}{\tilde{g}}B_uC_{fb}D_sD_d \\ B_sD_d - \frac{1}{\tilde{g}}B_s(D_m + C_{ff})C_{fb}D_sD_d \end{bmatrix}$$

$$C_{cl} = \begin{bmatrix} C_p - \frac{1}{\tilde{g}}D_{pu}C_{fb}D_sC_m & -\frac{1}{\tilde{g}}D_{pu}C_{fb}C_s \end{bmatrix}$$

$$D_{cld} = D_{pd} - \frac{1}{\tilde{g}} D_{pu} C_{fb} D_s D_d \tag{4.6}$$

The controller state-space equations can be obtained as follows:

$$\begin{aligned} u(t) &= -C_{fb} y_2(t) \\ &= -C_{fb}(C_s x_s(t) + D_s y_1(t)) \\ &= -C_{fb}(C_s x_s(t) + D_s(y_m + C_{ff} u(t))) \\ \Rightarrow u(t) &= -\frac{1}{\tilde{g}} C_{fb} C_s x_s(t) - \frac{1}{\tilde{g}} C_{fb} D_s y_m(t) \\ &= C_C x_s(t) + D_C y_m(t) \end{aligned}$$

Substituting Eq. (4.7) into Eq. (4.4), we get

$$\begin{aligned} \dot{x_s}(t) &= A_s x_s(t) + B_s y_m(t) + B_s C_{ff} u(t) \\ &= [A_s - \frac{1}{\tilde{g}} B_s C_{ff} C_{fb} C_s] x_s(t) + [B_s - \frac{1}{\tilde{g}} B_s C_{ff} C_{fb} D_s] y_m(t) \\ &= A_C x_s(t) + B_C y_m(t) \end{aligned} \tag{4.7}$$

Thus, the overall controller is given by:

$$C(s) \sim \begin{cases} \dot{x}_s(t) = A_C x_s(t) + B_C m(t) \\ u(t) = C_C x_s(t) + D_C m(t) \end{cases} \tag{4.8}$$

4.2.2 Robustness to Uncertainty

One important design consideration for choosing passifying compensator is that the passification remains robust in the presence of unmodelled dynamics and parameter uncertainties. For the plant under consideration, $C_{ff} = 0.1$ was adequate to robustly passify the plant. Figures 4.5 and 4.5 show that $C_{ff} = 0.05$ passifies the nominal but not the real plant. However, for $C_{ff} = 0.1$, Figs. 4.7 and 4.8 show that the passification is robust. As robustness and performance always have contradicting demand on the plant, boosting one of them causes reduction in other. That is, the choice of $C_{ff} = 0.1$ will limit performance compared to the value of $C_{ff} = 0.05$.

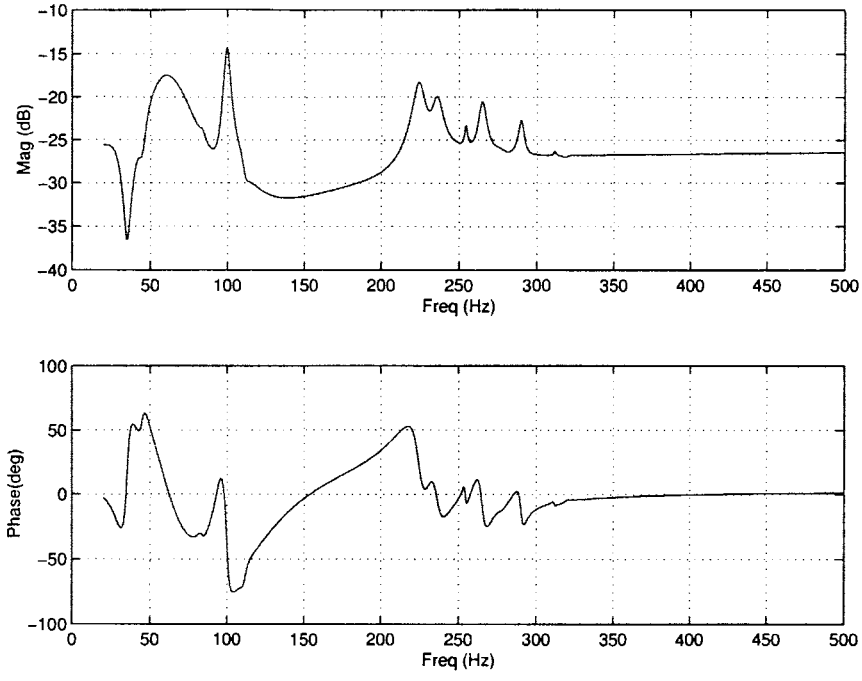

Figure 4.5 Bode plot for $C_{ff} = 0.05$ (nominal plant)

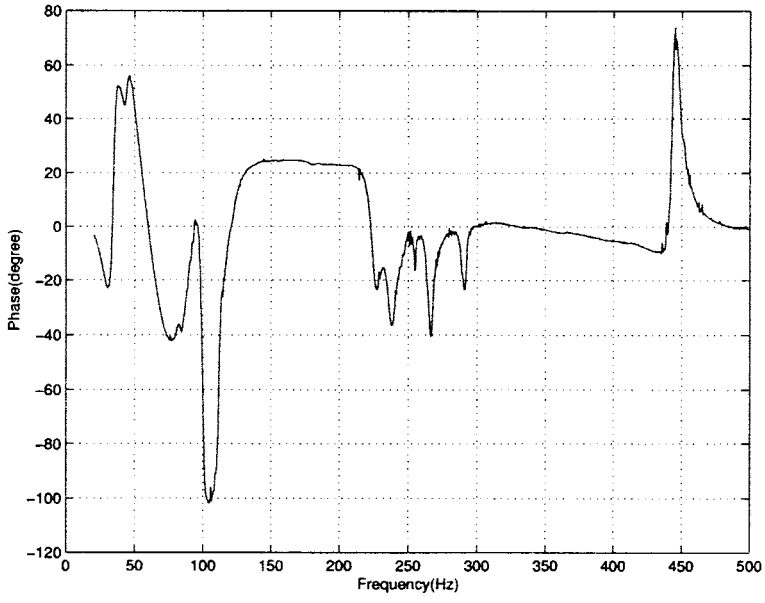

Figure 4.6 Phase plot for $C_{ff} = 0.05$ (real plant)

4.2.3 Design of $C_s(s)$ and $C_{fb}(s)$

The parameters selected for the resonant-mode and feedback controller are given below. The six resonant-mode frequencies (in Hz) that are targeted by controller are given by

$$\Omega = [99.759, 224.522, 236.012, 254.532, 264.826, 290.117]$$

The controller $C_s(s)$ has the form

$$C_s(s) = \Sigma_{i=1}^{6} K_i(s)$$

where

$$\begin{aligned}
K_1(s) &= \frac{(\frac{s}{2\pi\times 95}+1)(\frac{s}{2\pi\times 105}+1)}{\frac{s^2}{\Omega_1^2}+\frac{0.5s}{\Omega_1}+1} \\
K_2(s) &= 1.5\times\frac{(\frac{s}{2\pi\times 220}+1)(\frac{s}{2\pi\times 228}+1)}{\frac{s^2}{\Omega_2^2}+\frac{0.03s}{\Omega_2}+1} \\
K_3(s) &= 5\times\frac{(\frac{s}{2\pi\times 232}+1)(\frac{s}{2\pi\times 240}+1)}{\frac{s^2}{\Omega_3^2}+\frac{0.3s}{\Omega_3}+1} \\
K_4(s) &= 5\times\frac{(\frac{s}{2\pi\times 250}+1)(\frac{s}{2\pi\times 258}+1)}{\frac{s^2}{\Omega_4^2}+\frac{0.3s}{\Omega_4}+1} \\
K_5(s) &= 7\times\frac{(\frac{s}{2\pi\times 260}+1)(\frac{s}{2\pi\times 270}+1)}{\frac{s^2}{\Omega_5^2}+\frac{0.1s}{\Omega_5}+1} \\
K_6(s) &= 20\times\frac{(\frac{s}{2\pi\times 290}+1)(\frac{s}{2\pi\times 295}+1)}{\frac{s^2}{\Omega_6^2}+\frac{0.3s}{\Omega_6}+1}
\end{aligned}$$

The constant-gain SPR controller $C_{fb}(s)$ was chosen to be $C_{fb} = 10.0$. The open- and closed-loop frequency responses from disturbance and control inputs to performance output are given in Figs. 4.9 and 4.10, respectively. If the disturbance enters at the same channel as the control input, the passivity-based controller is very effective as shown in Fig. 4.10, where reduction of up to 25 dB can be achieved at some frequencies. It is to be noted that in both cases, although with varying performance the reductions broadband

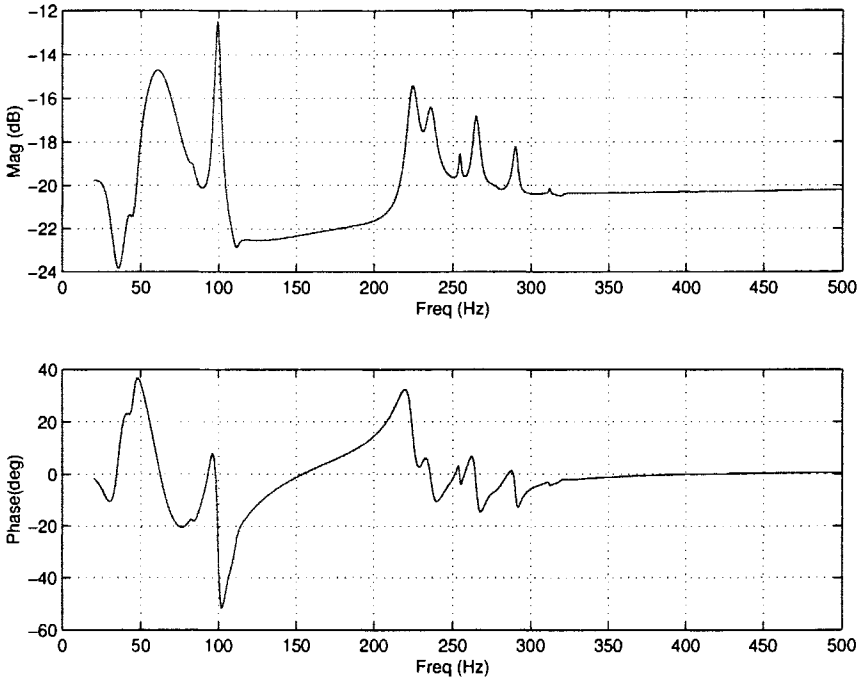

Figure 4.7 Bode plot for nominal plant ($C_{ff} = 0.10$)

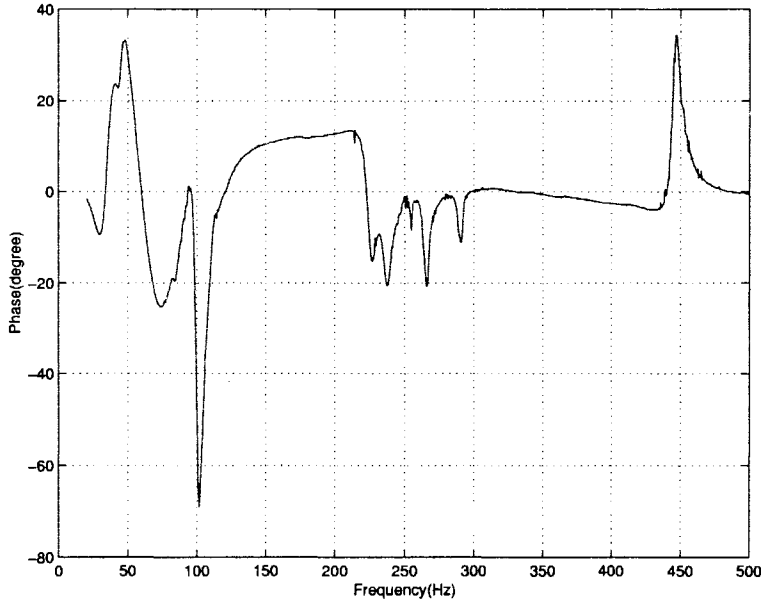

Figure 4.8 Phase plot for real plant ($C_{ff} = 0.10$)

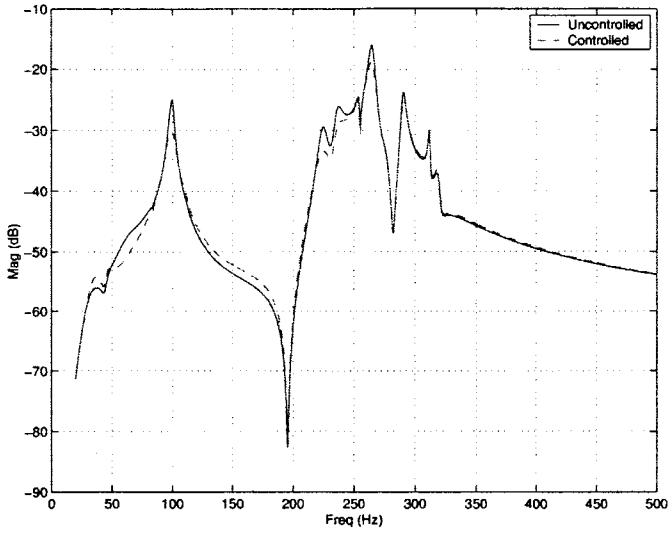

Figure 4.9 Simulated frequency response for constant-gain PR controller for disturbance input

without amplification in any other range. For the case with disturbance entering through different channel, about 5 dB reduction was achieved at 100Hz and about 3 dB deduction was achieved at other peaks. The result is not as good as the other case but it still gives satisfactory noise reduction results. Bode plot of the constant-gain PR controller is shown in Fig. 4.11.

4.2.4 Experiment Results

After simulations, the control design was verified experimentally. Note that in the passivity-based controller, high sampling rate is strongly recommended, since the passivity-based controller is for continuous systems, while the experiment is carried out with discrete controller. In our case, due to the order of the controller and the limitation of dSPACE, the sampling time is 5E-5 seconds. Figure 4.12 shows the experimental results for the case when the disturbance and control input entering through different channel. As seen from Figs. 4.9 to 4.13, the best response is when disturbance is entering through same channels of the control input. The performance degradation occurs when acoustic pressure is measured at the location different from the feedback sensor loca-

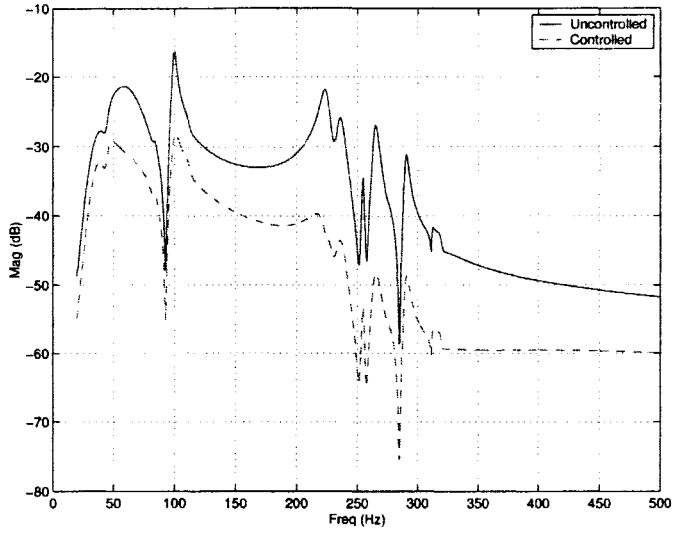

Figure 4.10 Simulated frequency response for constant-gain PR controller for control input

tion. However, there are no instabilities indicating effectiveness of controller in robustly stabilizing the plant.

4.3 Passivity-Based LQG Controller

This section will present the design of LQG optimal dynamic PR controller, which has more design freedom than the constant-gain controller.

4.3.1 Background Theory

The control system configuration for passive LQG controller is depicted in Fig. 4.14. The stability of this design is again ensured by the stability theorem given in Section 4.1.

Consider a Strictly Positive Real (SPR) system as

$$\begin{aligned} \dot{z}(t) &= Dz(t) + Fu(t) + d(t) \\ y_2(t) &= Gz(t) + \zeta(t) \end{aligned} \tag{4.9}$$

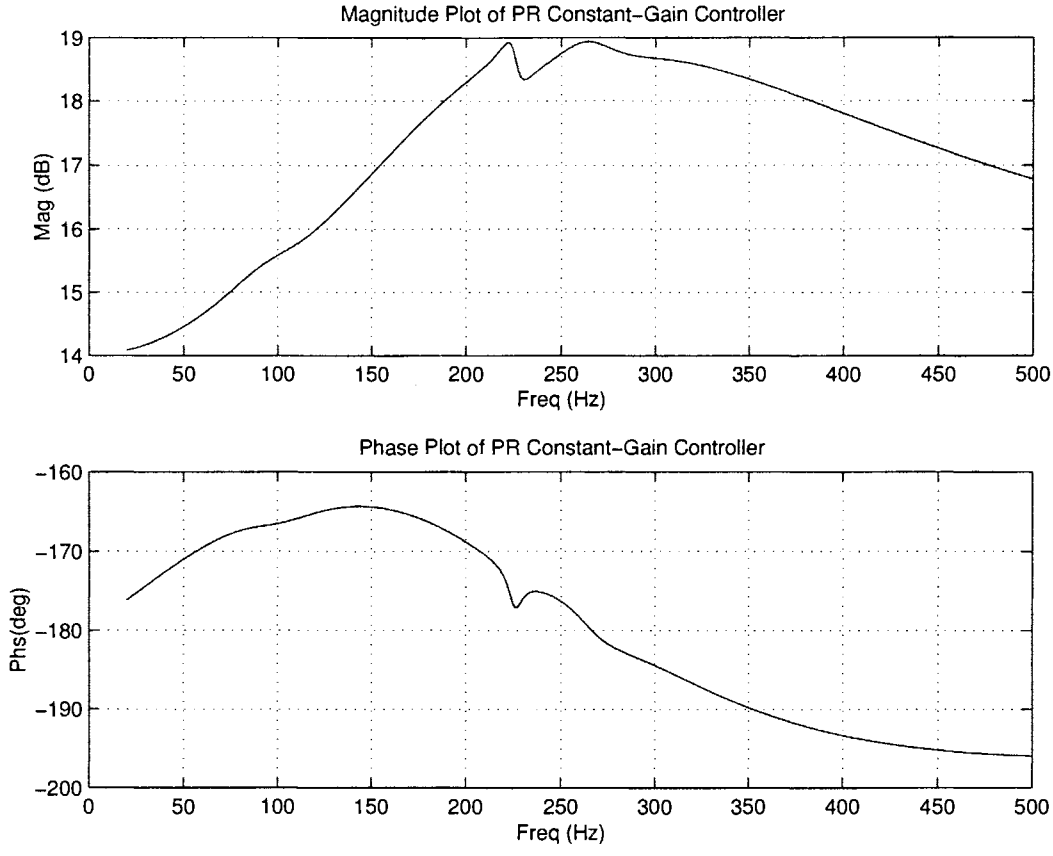

Figure 4.11 Bode plot of constant-gain PR controller

where, $d(t)$ and $\zeta(t)$ are zero-mean white noise process. Then, from the Kalman-Yakubovich-Popov (KYP) lemma [56], there exist matrices $P = P^T > 0$ and L such that

$$\begin{aligned} D^T P + PD &= -LL^T \\ PF &= G^T \end{aligned} \tag{4.10}$$

Now using a transformation with $z(t) = P^{-\frac{1}{2}}\overline{x}(t)$, where $P^{\frac{1}{2}}$ is the symmetric square root of P obtained above, the system given by Eqn. (4.10) can be transformed as follows:

$$\begin{aligned} P^{-\frac{1}{2}}\dot{\overline{x}}(t) &= P^{-\frac{1}{2}}\overline{x}(t) + Fu(t) \\ y_2(t) &= GP^{-\frac{1}{2}}\overline{x}(t) \end{aligned}$$

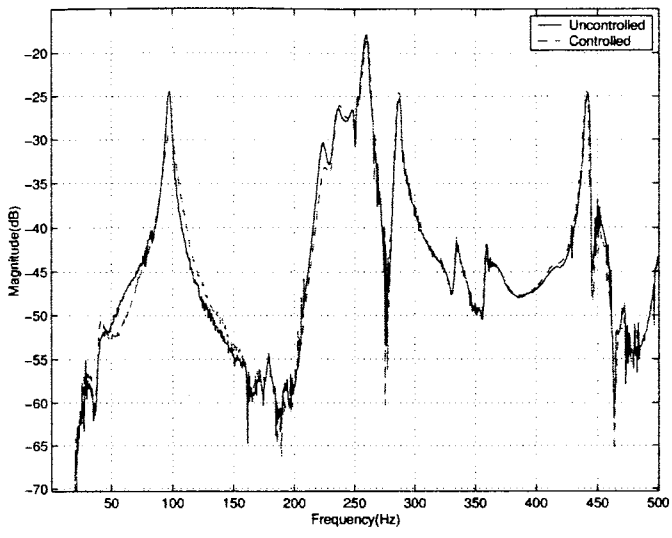

Figure 4.12 Experimental response for constant-gain PR controller with $d(t)$ and $u(t)$ entering through seperate channels

i.e.,

$$\begin{aligned} \dot{\overline{x}}(t) &= \underbrace{P^{\frac{1}{2}}DP^{-\frac{1}{2}}}_{\overline{A}}\overline{x}(t) + \underbrace{P^{\frac{1}{2}}F}_{\overline{B}}u(t) \\ y_2(t) &= \underbrace{GP^{-\frac{1}{2}}}_{\overline{C}}\overline{x}(t) \end{aligned} \tag{4.11}$$

The transformed ("new") system given by Eq. (4.11) (called the dual realization of the original system), is still SPR, and KYP lemma applies to this system, as well. That is,

$$\begin{aligned} \overline{A}^T + \overline{A} &= P^{-\frac{1}{2}}D^TP^{\frac{1}{2}} + P^{\frac{1}{2}}DP^{-\frac{1}{2}} \\ &= -P^{-\frac{1}{2}}LL^TP^{-\frac{1}{2}} \\ &= Q_{\overline{A}} \end{aligned} \tag{4.12}$$

where $Q_{\overline{A}} =: -P^{-\frac{1}{2}}LL^TP^{-\frac{1}{2}}$ and $\overline{B} = \overline{C}^T$. Now we want to find an LQG controller for the plant given by dual realization (Eq. (4.11)) which is also SPR. Let the LQG controller has the following state-space form:

$$\begin{aligned} \dot{x}_c(t) &= A_cx_c(t) + B_cy_2(t) \\ u(t) &= -C_cx_c(t) \end{aligned} \tag{4.13}$$

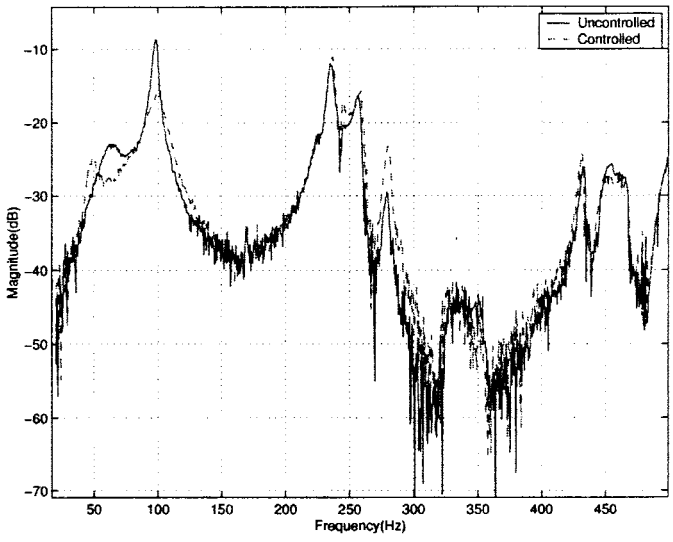

Figure 4.13 Response measured at location other than feedback sensor location

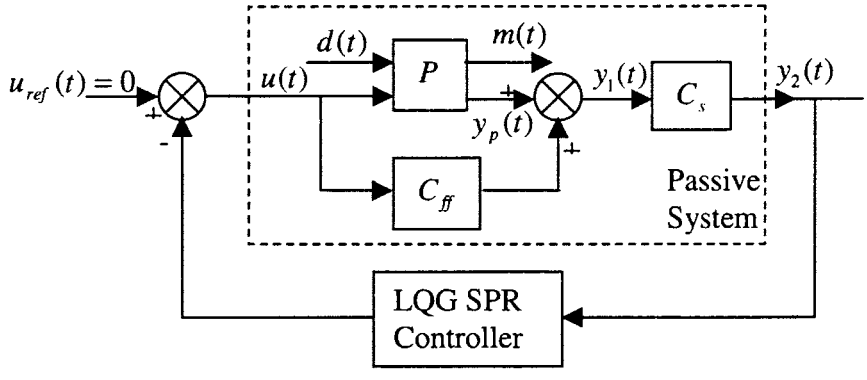

Figure 4.14 Passive LQG controller

where A_c, B_c, C_c are functions of $P_c = P_c^T > 0, P_f = P_f^T > 0$ and P_c, P_f are solutions to the following Riccati Equations:

$$\begin{aligned} P_c\overline{A} + \overline{A}^T P_c - P_c\overline{B}R^{-1}\overline{B}^T P_c + Q &= 0 \\ P_f\overline{A}^T + \overline{A}P_f - P_f - P_f\overline{B}R_\zeta^{-1}\overline{B}^T P_f + Q_d &= 0 \end{aligned} \tag{4.14}$$

where Q is the state weighting function, R is the control weighting function, Q_d is the covariance of $d(t)$, and R_ζ is the covariance of $\zeta(t)$. The controller matrices are given by

$$A_c = \overline{A} - \overline{B}R^{-1}\overline{B}^T P_c - P_f\overline{B}R_\zeta^{-1}\overline{B}^T$$

$$\begin{aligned} B_c &= P_f \overline{B} R_\zeta^{-1} \\ C_c &= R^{-1} \overline{B}^T P_c \end{aligned} \tag{4.15}$$

The proof that controller given by Eq. (4.15) is optimal and also satisfies KYP lemma can be found in [51]. Given below is the part of the proof which show that the controller of Eq. (4.15) satisfies the KYP lemma.

From Eq. (4.14) we obtain:

$$\begin{aligned} &P_c(\overline{A} - \overline{B}R^{-1}\overline{B}^T P_c - P_f \overline{B} R_\zeta^{-1} \overline{B}^T) + (\overline{A} - \overline{B}R^{-1}\overline{B}^T P_c - P_f \overline{B} R_\zeta^{-1} \overline{B}^T)^T P_c \\ &\quad = -Q - P_c P_f \overline{B} R_\zeta^{-1} \overline{B}^T - P_c \overline{B} R^{-1} \overline{B}^T P_c - \overline{B} R_\zeta^{-T} \overline{B}^T P_f^T P_c \\ &\quad = -Q - P_c P_f \overline{B} R_\zeta^{-1} \overline{B}^T - P_c \overline{B} R^{-1} \overline{B}^T P_c - \overline{B} R_\zeta^{-1} \overline{B}^T P_f P_c \end{aligned} \tag{4.16}$$

Note that $P_c = P_c^T$, $P_f = P_f^T$, $R^{-T} = R^{-1}$, and $R_\zeta^{-T} = R_\zeta^{-1}$. Now, if one selects

$$\begin{aligned} R_\zeta &= R \\ Q &= Q_{\overline{B}} + \overline{B} R^{-1} \overline{B}^T \\ Q_d &= Q_{\overline{A}} + \overline{B} R^{-1} \overline{B}^T \end{aligned} \tag{4.17}$$

then, $P_f = I$ becomes the solution of Eq. (4.14). Completing the square of Eq. (4.16) by using Eq. (4.17) gives:

$$\begin{aligned} P_c A_c + A_c^T P_c &= -Q_{\overline{B}}(-\overline{B}R^{-1}\overline{B}^T - P_c \overline{B} R^{-1} \overline{B}^T - \overline{B} R^{-1} \overline{B}^T P_c - P_c \overline{B} R^{-1} \overline{B}^T P_c) \\ &= -Q_{\overline{B}} - (P_c + I)\overline{B} R^{-1} \overline{B}^T (P_c + I) < 0 \end{aligned} \tag{4.18}$$

Also, for $R_\zeta = R$ and $P_f = I$,

$$\begin{aligned} B_c &= P_f \overline{B} R_w^{-1} = \overline{B} R^{-1} \\ C_c &= R^{-1} \overline{B}^T P_c = B_c^T P_c \end{aligned} \tag{4.19}$$

Thus,

$$B_c^T P_c = C_c \tag{4.20}$$

Equations (4.18)-(4.20) show that controller matrices satisfy the KYP lemma.

4.3.2 Development of Controller Equations

Similar to the constant-gain case, the first step in the design is to render the open-loop system passive via suitable passification technique. The acoustic system is passified using a feedforward controller block $C_{ff}(s)$ and the compensator $C_s(s)$ fis used to render the passified plant strictly proper as the LQG design technique discussed in the previous section requires strictly proper plant. The feedback controller $C_{fb}(s)$ is then given by Eq. (4.15). Given below is the step-by-step derivation of closed-loop system equations.

- The open-loop system:

$$P(s) \sim \begin{cases} \dot{x}(t) = Ax(t) + B_u u(t) + B_d d(t) \\ m(t) = C_m x(t) + D_m u(t) + D_d d(t) \quad \text{(Measurement Output)} \\ y_p(t) = C_p x(t) + D_{pu} u(t) + D_{pd} d(t) \quad \text{(Performance Output)} \end{cases} \tag{4.21}$$

  Since in our case, $m(t) = y_p(t)$, $C_m = C_p$; $D_m = D_{pu}$; and $D_d = D_{pd}$.

- The passified plant after feedforward compensator: $P(s) + C_{ff}(s) \sim$

$$\begin{cases} \dot{x}(t) = Ax(t) + B_u u(t) + B_d d(t) \\ y_1(t) = C_m x(t) + (D_m + C_{ff}) u(t) + D_d d(t) \end{cases} \tag{4.22}$$

- Passified plant with series compensator $C_s(s)$:

$$\text{If } C_s(s) \sim \begin{cases} \dot{x}_s(t) = A_s x_s(t) + B_s y_1(t) \\ = A_s x_s(t) + B_s C_m x(t) + B_s (D_m + C_{ff}) u(t) + B_s D_d d(t) \\ y_2(t) = C_s x_s(t) \end{cases}$$

  Then, $C_s(s)[P(s) + C_{ff}(s)]$ is given by

$$\begin{bmatrix} \dot{x}(t) \\ \dot{x}_s(t) \end{bmatrix} = \begin{bmatrix} A & 0 \\ B_s C_m & A_s \end{bmatrix} \begin{bmatrix} x(t) \\ x_s(t) \end{bmatrix} + \begin{bmatrix} B_u \\ B_s (D_m + C_{ff}) \end{bmatrix} u(t) + \begin{bmatrix} B_d \\ B_s D_d \end{bmatrix} d(t)$$

$$y_2(t) = \begin{bmatrix} 0 & C_s \end{bmatrix} \begin{bmatrix} x(t) \\ x_s(t) \end{bmatrix} \tag{4.23}$$

- Consider a feedback controller

$$C_{fb}(s) \sim \begin{cases} \dot{x}_{fb}(t) = A_{fb}x_{fb}(t) + B_{fb}y_2(t) \\ y_{fb}(t) = C_{fb}x_{fb}(t) \\ u(t) = u_{ref}(t) - y_{fb}(t) \end{cases} \tag{4.24}$$

Where A_{fb}, B_{fb}, and C_{fb} are given in Eq. (4.15), the closed-loop system is given by

$$\begin{aligned} \dot{\hat{x}}(t) &= \hat{A}\hat{x}(t) + \hat{B}_u u_{ref}(t) + \hat{B}_d d(t) \\ y_m(t) &= \hat{C_m}\hat{x}(t) + \hat{D_m}u_{ref}(t) + \hat{D}_d d(t) \end{aligned} \tag{4.25}$$

where

$$\dot{\hat{x}}(t) = \begin{bmatrix} x(t) \\ x_s(t) \\ x_{fb}(t) \end{bmatrix}$$

$$\hat{A} = \begin{bmatrix} A & 0 & B_u C_{fb} \\ B_s C_m & A_s & B_s(D_m + C_{ff})C_{fb} \\ 0 & B_{fb}C_s & A_{fb} \end{bmatrix}$$

$$\hat{B}_u = \begin{bmatrix} B_u \\ B_s(D_m + C_{ff}) \\ 0 \end{bmatrix}$$

$$\hat{B}_d = \begin{bmatrix} B_d \\ B_s D_d \\ 0 \end{bmatrix}$$

$$\hat{C_m} = \begin{bmatrix} C_m & 0 & D_m C_{fb} \end{bmatrix}$$

$$\begin{aligned} \hat{D}_m &= D_m \\ \hat{D}_d &= D_d \end{aligned} \tag{4.26}$$

The overall controller is the combination of $C_{ff}(s)$, $C_s(s)$, and $C_{fb}(s)$ and can be obtained as follows:

The input to the controller is the measured output $m(t)$ and the output of the controller is the control input $u(t)$.

$$\begin{aligned} u(t) &= - \; C_{fb}x_{fb}(t) + u_{ref}(t) \;\; u_{ref} = 0 \\ \dot{x}_s(t) &= A_s x_s(t) + B_s y_1(t) \\ &= A_s x_s(t) + B_s(y_m + C_{ff}u(t)) \\ &= A_s x_s(t) + B_s C_{ff} C_{fb} x_{fb}(t) + B_s y_m(t) \\ \text{and } \dot{x}_{fb}(t) &= A_{fb}x_{fb}(t) + B_{fb}y_2(t) \\ &= A_{fb}x_{fb}(t) + B_{fb}C_s x_s(t) \\ \text{Also, } u(t) &= -C_{fb}x_{fb}(t) \\ &= \begin{bmatrix} 0 \vdots C_{fb} \end{bmatrix} \begin{bmatrix} x_s(t) \\ x_{fb}(t) \end{bmatrix} \end{aligned}$$

In a matrix form, we obtain

$$\begin{aligned} \begin{bmatrix} \dot{x}_s(t) \\ \dot{x}_{fb}(t) \end{bmatrix} &= \begin{bmatrix} A_s & B_s C_{ff} C_{fb} \\ B_{fb}C_s & A_{fb} \end{bmatrix} \begin{bmatrix} x_s(t) \\ x_{fb}(t) \end{bmatrix} + \begin{bmatrix} B_s \\ 0 \end{bmatrix} m(t) \\ u &= \begin{bmatrix} 0 \vdots & C_{fb} \end{bmatrix} \begin{bmatrix} x_s(t) \\ x_{fb}(t) \end{bmatrix} \end{aligned} \tag{4.27}$$

4.3.3 Simulation and Experiment Results

The feedforward controller $C_{ff}(s)$ was selected to be the same as constant-gain case, i.e., $C_{ff}(s) = 0.1$. The series compensator $C_s(s)$ chosen to render system strictly proper

was

$$Cs(s) = \frac{1}{\frac{s}{3e3} + 1} \tag{4.28}$$

The Bode plot of the open-loop transfer function from $u(t)$ to $y_2(t)$ is shown in Fig. 4.15.

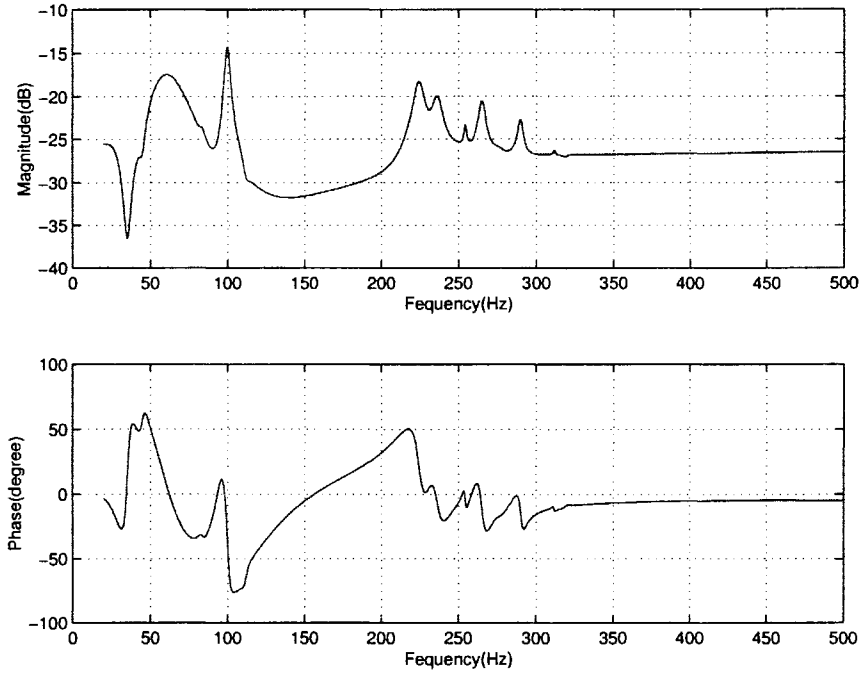

Figure 4.15 Open-loop transfer function from u to y_2

The LQG design parameter Q (state-weight) was selected according to Eq. (3.15), which target reduction of acoustic energy in the enclosure. Other control design parameters consistent with Eq. (4.17) are given as follows: $R = 1e-4$,

$$W = \begin{bmatrix} (P^{-1/2})^T Q P^{-1/2} + \overline{B} R^{-1} \overline{B} & 0 \\ 0 & R \end{bmatrix} \quad V = \begin{bmatrix} I & 0 \\ 0 & R \end{bmatrix} \tag{4.29}$$

The simulated frequency responses for two different cases where $d(t)$ and $u(t)$ enters the system via separate channels and via same channel are given in Figs. 4.16 and 4.17, respectively. Bode plot of the LQG-PR controller is shown in Fig. 4.18, from the figure, we can see that due to the constraints of the positive realness condition, the LQG-PR

controller is very similar to the constant-gain PR controller, which can also be seen from the simulated and experimental results.

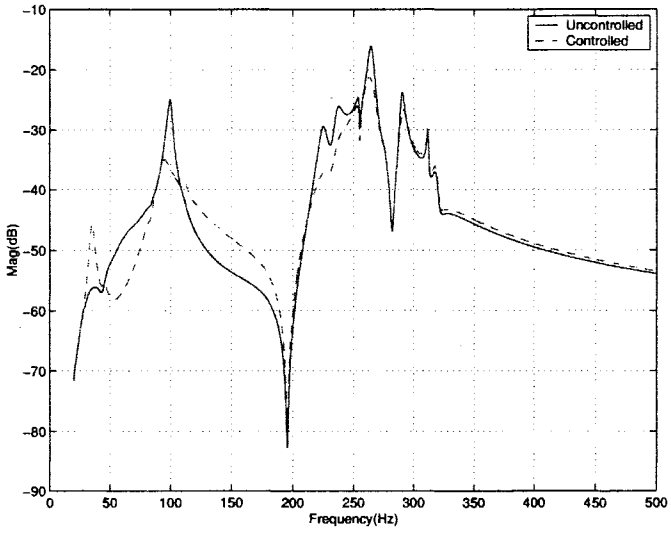

Figure 4.16 Simulated frequency response for LQG PR controller for disturbance input

The experimental frequency responses for the LQG PR controller for cases when disturbance and control input entering from separate channels is given in Fig. 4.19. From Fig. 4.19, it can be seen that the LQG PR controller does not perform satisfactorily. This is because the control design is very conservative due to constraints of Eq. (4.17). Note however that for the case when $d(t)$ and $u(t)$ enter through the same channel the controller is effective. Figure 4.20 shows the controller performance at location other than feedback sensor location. As it is seen from Fig. 4.20, although performance is not as good, the stability is robust.

In a summary, the passivity-based controllers (constant-gain and LQG PR) can provide robust stability for acoustic system. The performance is best when the disturbance and control enter the system through same channel. For the case when disturbance enters the system through separate channel than the control input, the performance is not good over broadband. The deterioration in performance can be attribute to the loss of passivity property due to discretization, conservatism of existing synthesis techniques,

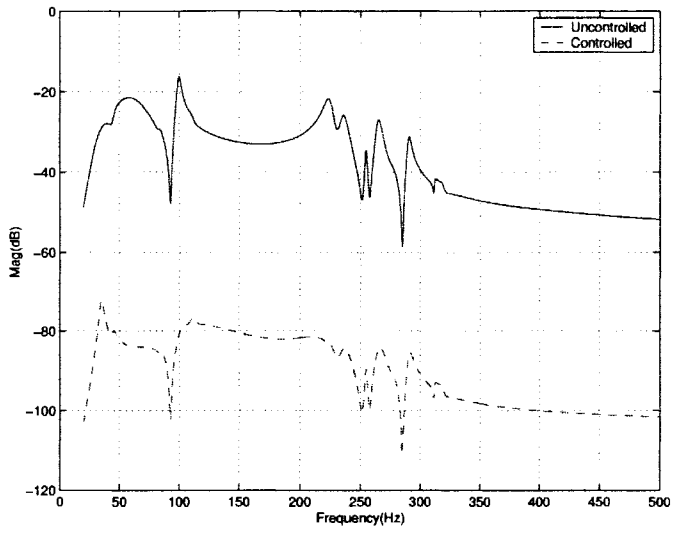

Figure 4.17 Simulated frequency response for LQG PR controller for control input

and inherent limitation of acoustic system.

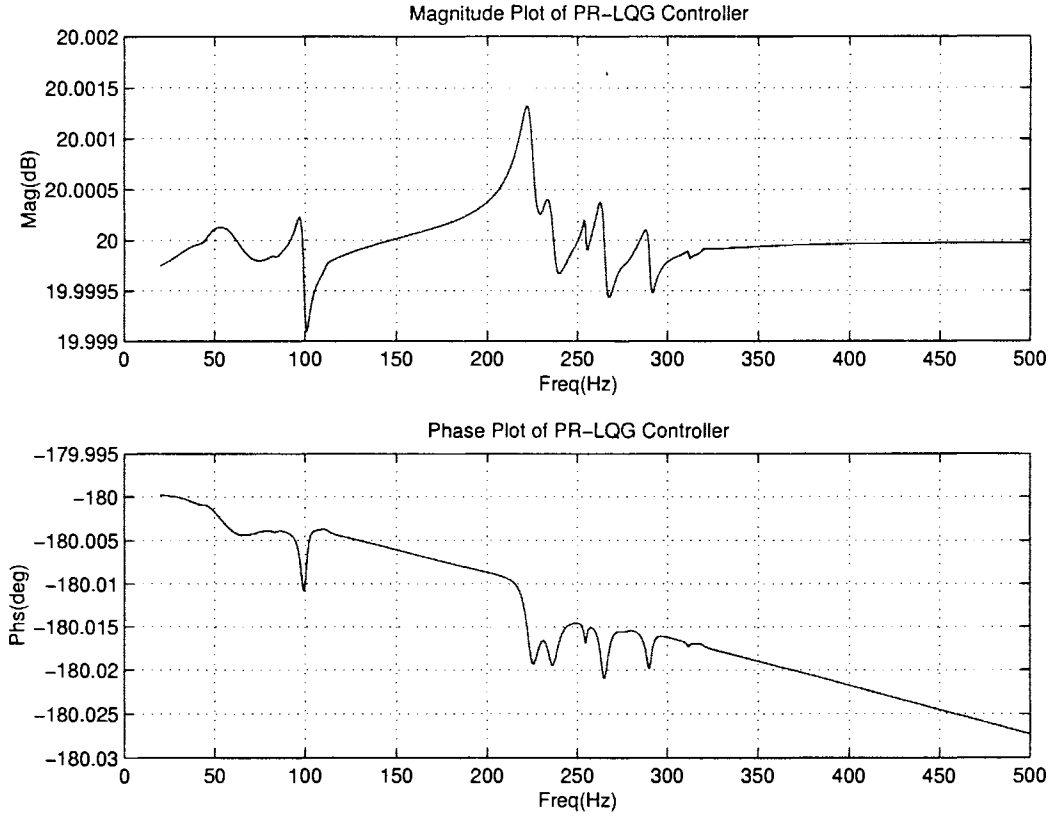

Figure 4.18 Bode plot of LQG-PR controller

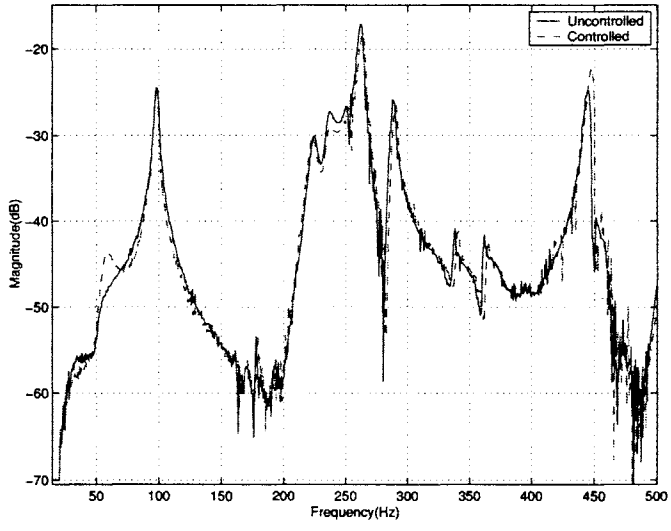

Figure 4.19 Experimental response for LQG PR controller with $d(t)$ and $u(t)$ entering through separate channels

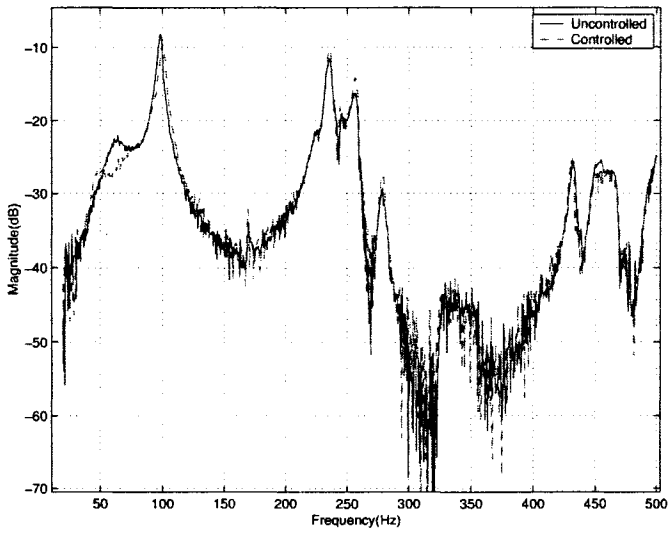

Figure 4.20 Response measured at location other than feedback sensor location

5 $\mathcal{H}_\infty$ CONTROL

This chapter presents controller design based on another control design methodology known as $\mathcal{H}_\infty$ method. $\mathcal{H}_\infty$ method allows systematic design procedure to accommodate uncertainty estimates as well as performance specifications. The robust stability property of the controller hinges on the the small gain theorem. The design model of the system is often inaccurate and "good" controller design should be robust to such inaccuracies. These inaccuracies arise from unmodeled dynamics and parametric uncertainty. Furthermore, there are unknown disturbance that affect the system performance. The $\mathcal{H}_\infty$ design technique, originally developed in frequency domain, has state-space formulation as well. The basic idea was introduced by Zames [57] in the late 1970s. Apart from enabling the design for robust stability, it also allows the loop shaping for closed-loop system to shape performance characteristics. The control law is obtained as a solution to an optimization problem, which incorporates the infinity-based performance objective in its cost function [58]. In this chapter, $\mathcal{H}_\infty$ control designs for nominal performance as well as robust stability will be developed for $3-D$ acoustic enclosure of Fig. 2.1.

5.1 $\mathcal{H}_\infty$ Control Design Framework

Consider a closed-loop configuration shown in Fig. 5.1, where G_u is the open-loop transfer function from the control input $u(t)$ to the performance output (which is also the measurement output) $m(t)$, G_d is the open-loop transfer function from the disturbance input to the performance output $y_m(t)$, $u_{ref}(t) = 0$ is the reference input, and $e(t) =$

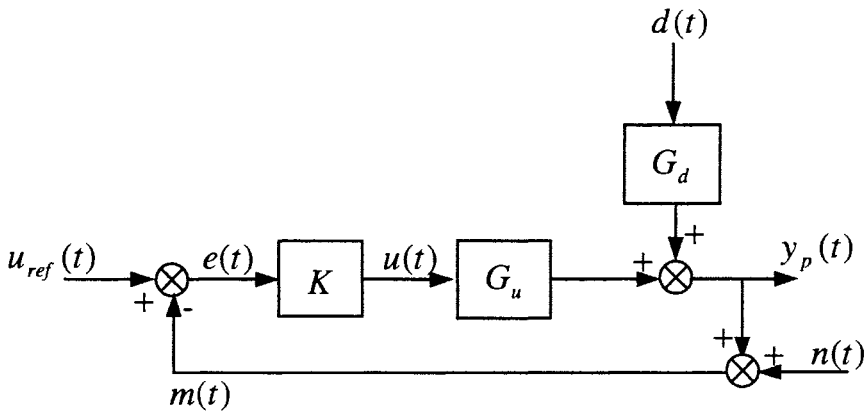

Figure 5.1 Unity feedback configuration

$u_{ref}(t) - m(t)$ is the error signal. From Fig. 5.1, we get the output

$$\begin{aligned} Y_p(s) &= \underbrace{(I + G_u K)^{-1} G_u K}_{T} U_{ref}(s) + \underbrace{(I + G_u K)^{-1}}_{S} G_d D(S) - \underbrace{(I + G_u K)^{-1} G_u K}_{T} N(s) \\ &= TU_{ref}(s) + SG_d D(s) - TN(s) \end{aligned} \tag{5.1}$$

where $S = (I + G_u K)^{-1}$ is the sensitivity transfer function, and $T = (I + G_u K)^{-1} G_u K$ is the complementary sensitivity transfer function. From Eq. (5.1) we can see that the effect of disturbance is minimized if we can make S to be much less than one. But, this is impossible to achieve over entire frequency spectrum as the inherent limitation requires $S + T = 1$ to be satisfied over all frequencies, which means T has to be equal to 1 at all frequencies. But it will cause sensor noise ($N(s)$) to amplify. For filtering effect of noise, we need $T \approx 0$, which implies $S \approx 1$. Thus, the requirements on T and S seem to be contradicting. However, considering the frequency-dependent characteristics of the noise $N(s)$ and dynamic characteristics of $G_u(s)$, the requirement of T and S turn out to be complementary. For example, noise being high frequency phenomena we can impose T to be small in the high frequency region, where S could be high. Similarly, in the low frequency region, T could be high (close to 1) and S could be small (≈ 0). In addition to these constraints, these are constraints on loop gain imposed by robust stability conditions. All these requirement can be put in the systematic mathematical

framework using the block diagram of Fig. 5.2.

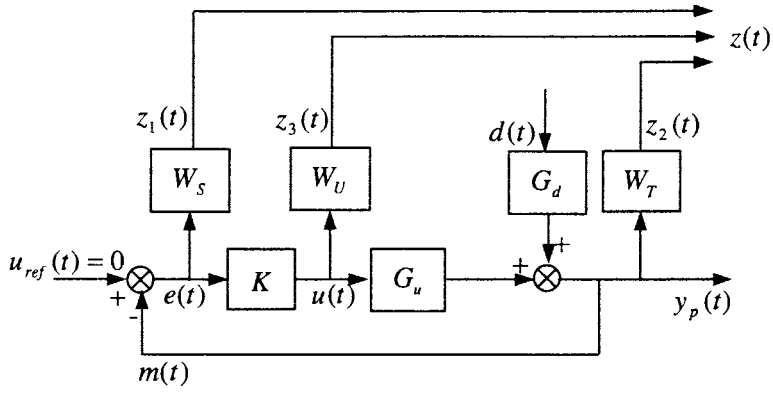

Figure 5.2 Generalized plant configuration

The first step in the $\mathcal{H}_\infty$ controller design is to form the generalized plant, P. In the system of Fig. 5.2, the exogenous input $w(t)$ is the reference signal $u_{ref}(t)$ (here, $d(t)$ is omitted without generality. Since our aim here is shaping the closed-loop transfer function from $d(t)$ to $y_p(t)$, the value of $d(t)$ does not effect). In order to reflect the performance objectives and physical constraints, the regulated outputs were chosen to be the weighted error signal, $Z_1(s) = W_S E(s)$, the weighted control signal, $Z_3(S) = W_U u(S)$, and the weighted measurement output, $Z_2(t) = W_T M(s)$. The transfer function from $w(t)$ to $z_1(t)$ is the weighted sensitivity function, $W_S S$, which characterizes the performance objective for disturbance rejection. The transfer function from $w(t)$ to $z_2(t)$ is the weighted complementary sensitivity function, $W_T T$, which characterizes the rejection of measurement noise (not considered in our case). The transfer function from $w(t)$ to $z_3(t)$ $W_U KS$ is the weighted product of $K(s)$ and $G_u(s)$, which weights the control effort. Also, in robust analysis, the restriction on $W_T T$ and $W_U KS$ translate to the robust stability conditions for input-multiplicative and additive uncertainty, respectively. Also, the bound on $W_U KS$ is used to impose the penalty on control signals. The weighting functions W_S, W_T, and W_U are frequency-dependent to scale the respective transfer functions differently in different frequency regions. The inverse of the weighting functions serves as an upper bound on the transfer functions [59].

Thus, the requirements on the closed loop maps translate into the following conditions:

$$\|W_S S\|_{\mathcal{H}_\infty} \leq 1 \tag{5.2}$$

$$\|W_T T\|_{\mathcal{H}_\infty} \leq 1 \tag{5.3}$$

$$\|W_U K S\|_{\mathcal{H}_\infty} \leq 1 \tag{5.4}$$

Note that the standard $\mathcal{H}_\infty$ algorithm does not solve for controllers that satisfy the above constraints, but it finds the controller which satisfy the stacked constraint

$$\left\| \begin{array}{c} W_S S \\ W_T T \\ W_U K S \end{array} \right\|_{\mathcal{H}_\infty} \leq 1 \tag{5.5}$$

Note that Eq. (5.5) is a more conservative condition than Eq. (5.2, 5.3 and 5.4), since

$$\left\| \begin{array}{c} W_S S \\ W_T T \\ W_U K S \end{array} \right\|_{\mathcal{H}_\infty} = \sup_\omega \sqrt{W_S S^2 + W_T T^2 + W_U K S^2} \tag{5.6}$$

In summary, the regulated outputs are given by

$$z = \begin{bmatrix} z_1 \\ z_2 \\ z_3 \end{bmatrix} = \begin{bmatrix} W_S(u_{ref} - G_u u) \\ W_T G_u u \\ W_U u \end{bmatrix} \tag{5.7}$$

and the generalized plant P is described by

$$\begin{bmatrix} z \\ e \end{bmatrix} = \underbrace{\begin{bmatrix} \begin{bmatrix} W_S & -W_S G_u \\ 0 & W_T G_u \\ 0 & W_U \end{bmatrix} \\ [I - G_u] \end{bmatrix}}_{=P} \begin{bmatrix} u_{ref} \\ u \end{bmatrix} \tag{5.8}$$

In practice, it is computationally efficient to design a suboptimal controller. In particular, for any $\gamma > \gamma_{opt} > 0$, we can find a controller transfer function K such that

$$\left\| \begin{array}{c} W_S S \\ W_T T \\ W_U K S \end{array} \right\|_{\mathcal{H}_\infty} \leq \gamma \tag{5.9}$$

With the framework given above, we can design controllers to satisfy nominal performance and robust stability objectives.

5.2 $\mathcal{H}_\infty$ Controller Design for Nominal Performance

From Eq. (5.1), we can see that, for the nominal plant, if $|S(j\omega_0)| < 1$, then the tonal noise with frequency ω_0 will be reduced. However, due to waterbed effect, $|S(j\omega)|$ can not be restricted below 1, i.e., $|S(j\omega)|$ will be greater than 1 at some frequencies. In our case, we want the noise level at resonant frequencies to be reduced. So $|S(j\omega)|$ can be greater than 1 at frequencies where $G_d(j\omega)$ is relatively small, i.e., we need to shape the sensitivity function S to accommodate the requirements. But, the shaping of S is relatively difficult in the acoustic systems: It has been shown in [60, 61, 62] that the control is seriously compromised in the presence of plants containing right half plane poles and right half plane zeros. Acoustic plants are generally stable and thus possess no right half plane poles. However, right half plane zeros are common, mainly due to the inherent propagation delay of sound. A finite dimensional acoustic system dynamics will always exhibit right half plane (RHP) zeros. The plant with RHP zeros exhibits the following adverse difficulties [34]:

The waterbed effect: the implication of the waterbed effect is that the improvement of sensitivity at certain frequencies deteriorates its behavior at another frequencies. This phenomenon applies only to non-minimum phase plants. It has been shown that the weighting function ,W_S, must be less than unity at the locations of RHP zeros in the

plant or controller. This requires the sensitivity function to be small at these frequencies, but due to the waterbed effect, sensitivity function peaks at some other frequencies. This makes the shaping of the sensitivity function for acoustic systems inherently very difficult.

In this thesis, the weighting function, $W_S(j\omega)$, for the sensitivity function, $S(j\omega)$, is selected such that $W_S(j\omega)$ has a relatively bigger value (bigger than unity) at the resonant frequencies, and has a relatively smaller (less than unity) value at the other frequencies. So if the $\mathcal{H}_\infty$ controller can be found, i.e., if Eq. (5.5) can be satisfied, the noise levels will be reduced at the resonant frequencies. Although the noise levels may increase at other frequencies. Here, $MATLAB$ command *"magfit"* is used to obtain the suitable weighting function, $W_S(j\omega)$. Note that, if there are only one or two resonant frequencies, $W_S(j\omega)$ can be easily designed to have higher values at these frequencies. If the plant has several resonant modes and they are very close to each other; for example, in our case, 3 peaks exist in a frequency range of 50 Hz, although we can shape $W_S(j\omega)$ to be large over the entire frequency range, it decreases the possibility of finding the controller which satisfies Eq. (5.5). In fact, even if we shape $W_S(j\omega)$ very preciously at each resonant in the 50 Hz range, due to the higher level of $W_S(j\omega)$ in the frequency range, it also decrease the possibility of finding the controller. Thus, if the resonant frequencies are nicely separated, the weighting function is easier to shape. Thus, shaping of S for systems with large number of resonance peaks with high modal density is extremely hard. Acoustic systems are one such example. $\mathcal{H}_\infty$ control is very effective for suppressing tonal or narrow band noise.

In our case, our aim is to suppress the peaks at about 100 Hz, 255 Hz and 290 Hz, so the weighting function W_S is chosen as shown in Fig. 5.3. From this figure, we can see that if the controller satisfies Eq. (5.5), the noise level can be reduced in the range of $75-150\ Hz$, and $250-300\ Hz$. In fact, efforts were made to include a wider bandwidth, but unfortunately, the controllers satisfying Eq. (5.5) were difficult to find. $W_u(s)$ is

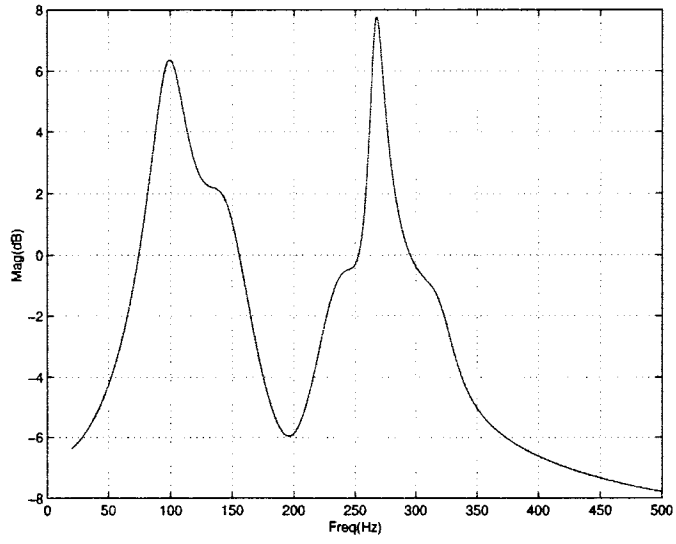

Figure 5.3 Magnitude plot of W_S

chosen such that $W_u(s) = 5e-4$, and $W_T(s)$ is chosen as $W_T(s) = 1$. (This means the measurement noise should not be amplifies.)

With the weighting functions chosen above, MATLAB command *"hinfsyn"* is used to obtain the controller, and the minimal γ value that can be achieved is 1.2264, which is bigger than 1, but still acceptable. Bode plot of $\mathcal{H}_\infty$ controller is given in Fig. 5.4. The simulated and experimental open-loop and closed-loop responses from disturbance to performance output are shown in Figs. 5.5 and 5.6. From these figures, we can see that about 5dB reduction was achieved at 100 Hz, and about 6 dB reduction was achieved at 255 Hz. Although there is an about 2 dB pop-up at 290 Hz, the noise level at 450 Hz was also reduced. To test the controllers result at other sensor locations, the noise reduction at another sensor location was also measured (shown in Fig. 5.7). From Fig. (5.7), we can see that the $\mathcal{H}_\infty$ controller designed for nominal plant cannot guarantee good results at other sensor locations.

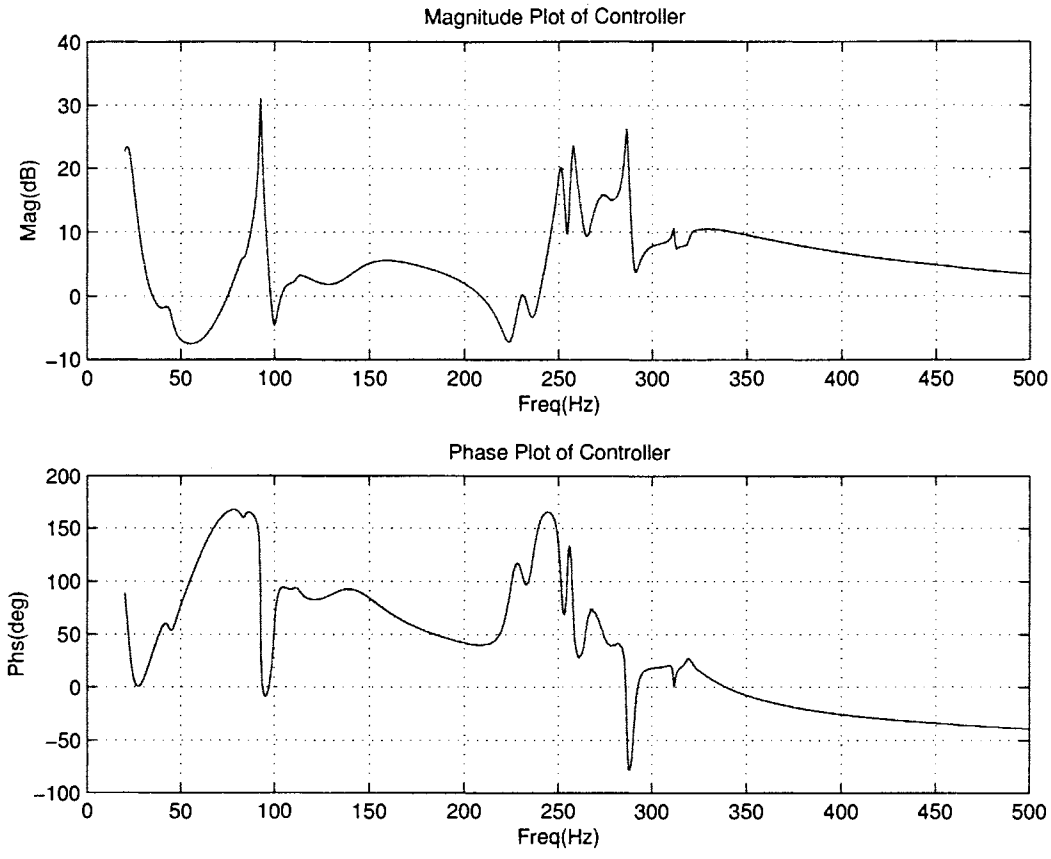

Figure 5.4 Bode plot of $\mathcal{H}_\infty$ controller for nominal performance

5.3 $\mathcal{H}_\infty$ Controller Design and Results for Nominal Performance with Robust Stability

In the previous section, we considered the controller design considering only the nominal plant $G_u(s)$. In this section, we will consider the plant with uncertainty.

Consider a class of plants

$$\Pi := \{G_u(s) + W_A(s)\Delta(s) \quad | \quad \|\Delta\|_{\mathcal{H}_\infty} \leq 1\} \tag{5.10}$$

where $W_A(s)$ is assumed to be a stable, proper rational transfer function. We will denote $L = KG$ and $L_p = KG_p$, and $G_p \in \Pi$. Here, we also assume that the nominal model $G_u(s)$ is such that the unity feedback configuration shown in Fig. 5.8 (with $\Delta = 0$) is stable. Then, we have the following theorem:

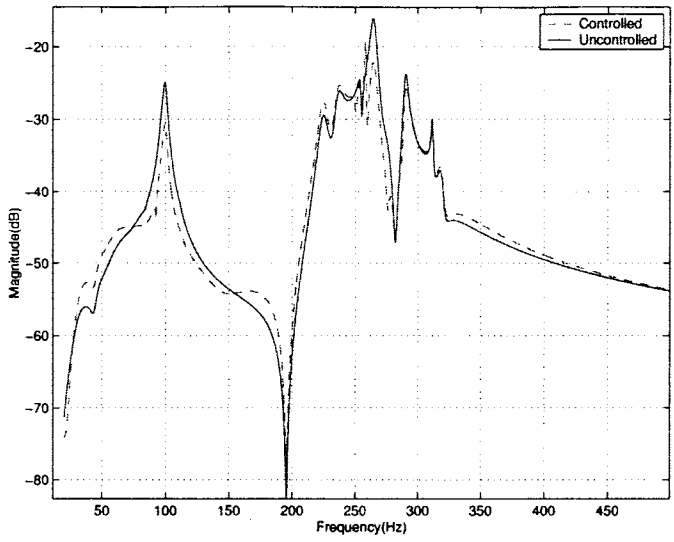

Figure 5.5 Simulated results for $\mathcal{H}_\infty$ controller for nominal performance

Theorem [59]: The closed-loop system shown in Fig. 5.8 is robustly stable (that is for all $G_p \in \Pi$) if and only if

$$\|w_A KS\|_{\mathcal{H}_\infty} \leq 1 \tag{5.11}$$

where $S := (I + L)^{-1}$ is the sensitivity transfer function corresponding to the nominal plant.

Proof:

By assumption, we know that, with $\Delta = 0$, the closed-loop system is stable. Let the number of encirclements of -1 by the Nyquist plot of L be N. Note that Δ and w_A are assumed to be stable. It follows that the number of right half plane poles of any L_p in Π is equal to the right half plane poles of L. Thus, the closed-loop stability is guaranteed if and only if the number of encirclement of $L_p = G_p K$ is equal to N. We are given the number of encirclements by the Nyquist plot of L is N. For the number of encirclements of the perturbed plant to remain unchanged, we need the deviation of L_p from L should not be large enough to touch or include the -1 point. Thus, the distance from L to the point -1 should be greater than the distance between L_p and L. Thus, for the stability with the plant G_p, a necessary and sufficient condition is that $|L_p - L| < |1 + L|$ for all

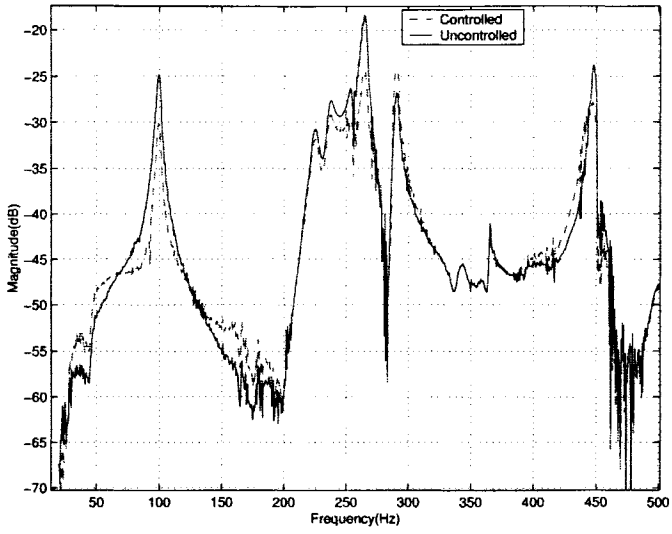

Figure 5.6 Experimental results for $\mathcal{H}_\infty$ controller for nominal performance

ω. This is guaranteed if and only if $|w_A K(I+L)^{-1}\Delta < |I+L|$ for all ω. This, in turn, holds if and only if $\|w_A K(I+L)^{-1}\Delta\|_{\mathcal{H}_\infty} < 1$, thus, if $\|w_A KS\|_{\mathcal{H}_\infty} \leq 1$,

$$\|w_A KS\Delta\|_{\mathcal{H}_\infty} \leq \|w_A KS\|_{\mathcal{H}_\infty}\|\Delta\|_{\mathcal{H}_\infty} \leq \|w_A KS\|_{\mathcal{H}_\infty} < 1 \tag{5.12}$$

This shows that Eq. (5.11) is a sufficient condition for robust stability, it can also be shown that Eq. (5.11) is also a necessary condition.

So, for $\mathcal{H}_\infty$ design, W_u is chosen as the upper bound of the additive uncertainty as shown in Fig. 5.9, which is same as Fig. 2.12. With W_U shown in Fig. 5.9, W_S shown in Fig. 5.3, and $W_T = 1$, *MATLAB* command *"hinfsyn"* is used to find the controller. The minimal γ value that can be achieved is 1.8126, which is bigger than the γ achieved in previous section. The reason being, W_U in this case is bigger than the one used in the previous section. With this controller, the simulated and experimental open-loop and closed-loop responses from disturbance to performance output are shown in Fig. 5.11 and Fig. 5.12. Bode plot of the robust $\mathcal{H}_\infty$ controller is given in Fig. 5.10.

From the experimental results, we can see that about a 3 dB reduction was achieved at 100 Hz, about a 3 dB reduction was achieved at 255 Hz, and small reductions at other peaks. There is a 1.5 dB pop-up at 290 Hz and the noise level at 450 Hz was not reduced.

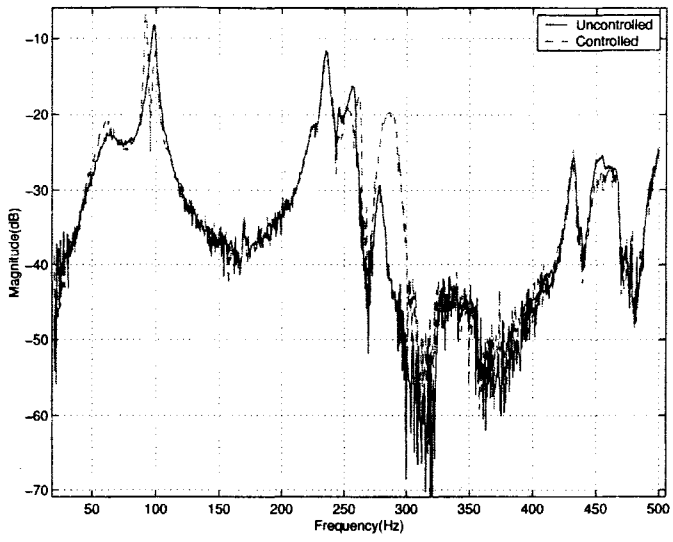

Figure 5.7 Experimental results for the $\mathcal{H}_\infty$ controller for nominal performance at another sensor location

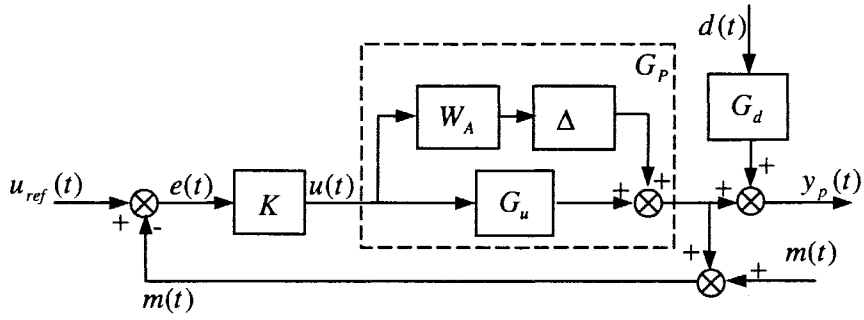

Figure 5.8 Unity feedback configuration with additive uncertainty

To test the controller's performance at other sensor locations the noise reduction level at another sensor location was also measured (shown in Fig. 5.13). Compared with Fig. 5.6, the popup at 290 Hz with the new $\mathcal{H}_\infty$ design is not as bad as the original $\mathcal{H}_\infty$ design. Overall, the performance was sacrificed to guarantee the robust stability.

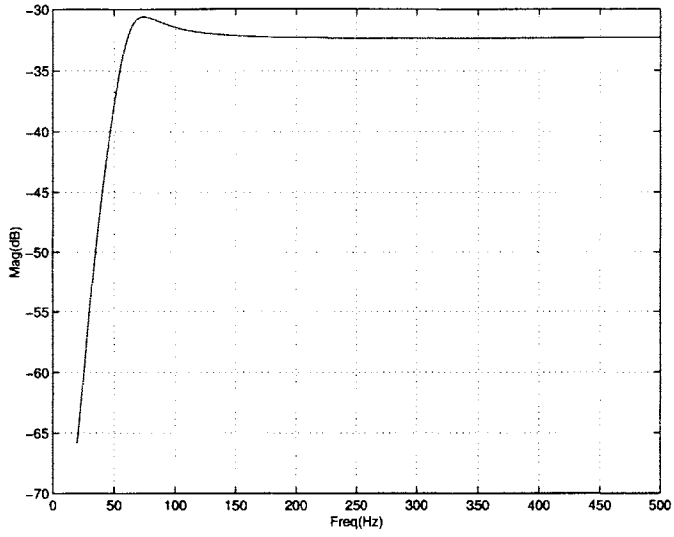

Figure 5.9 Magnitude plot of W_U

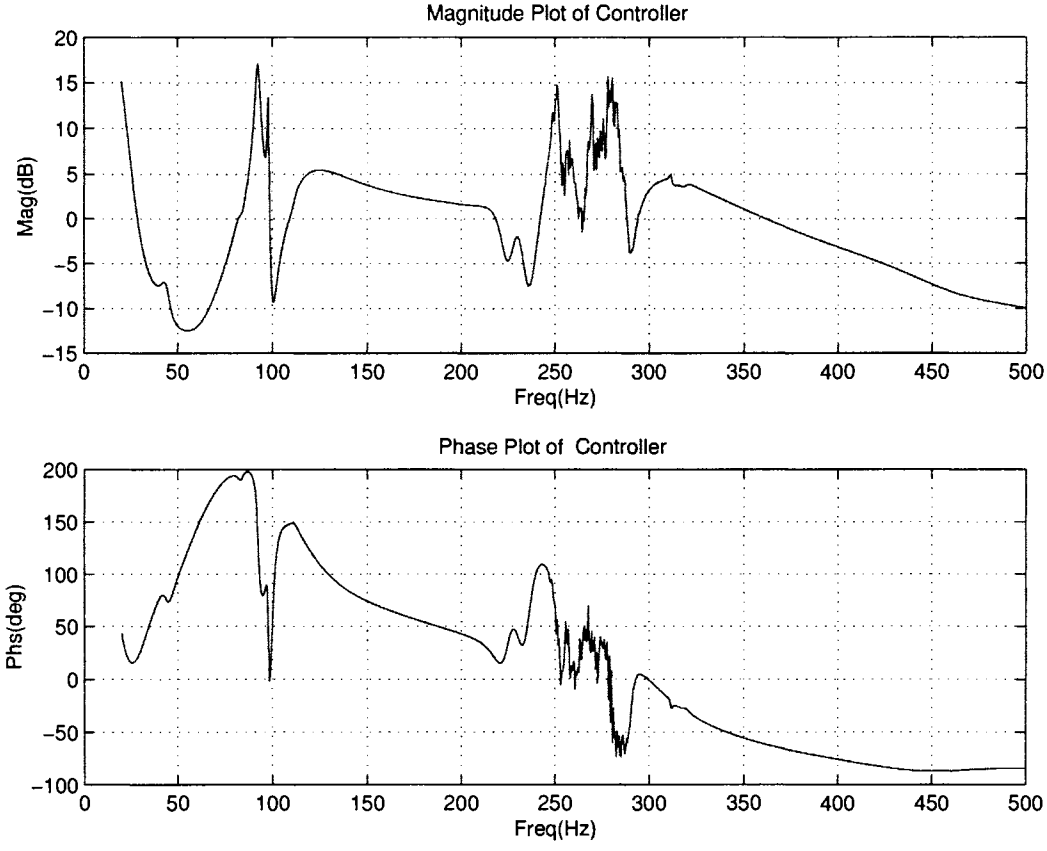

Figure 5.10 Bode plot of robust $\mathcal{H}_\infty$ controller

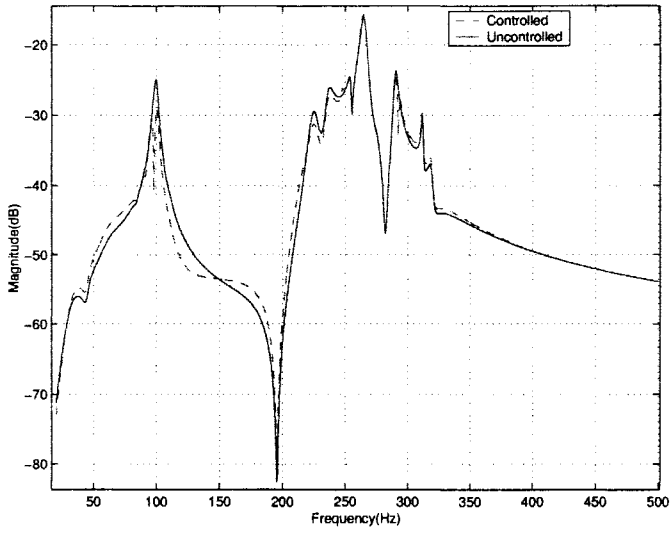

Figure 5.11 Simulated results for robust $\mathcal{H}_\infty$ controller

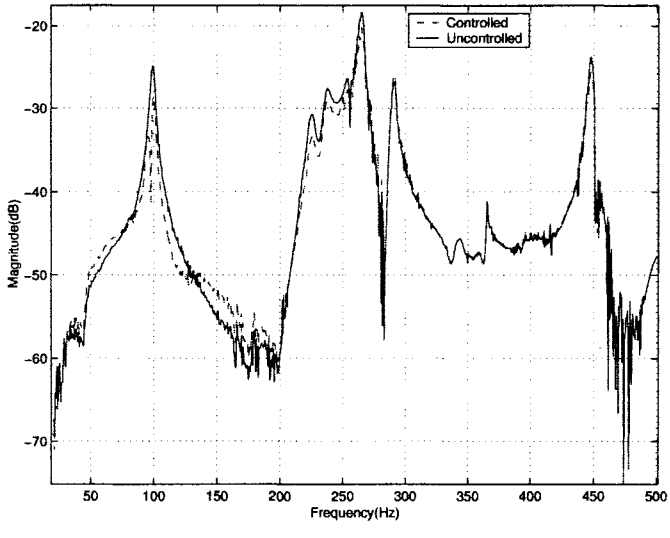

Figure 5.12 Experimental results for robust $\mathcal{H}_\infty$ controller

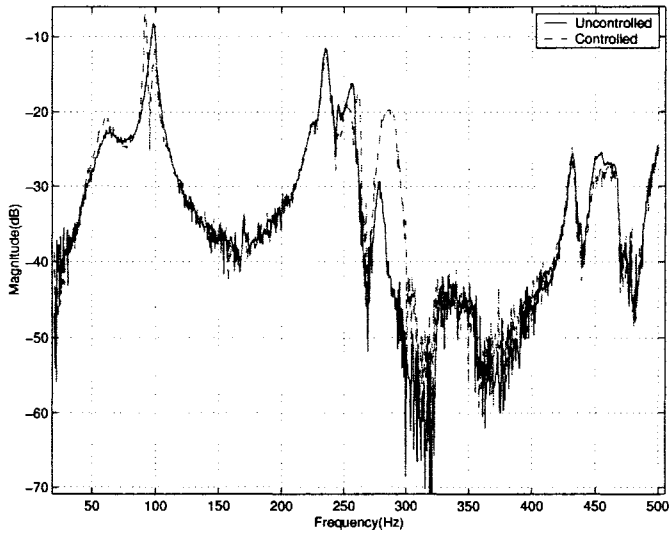

Figure 5.13 Experimental frequency response for new $\mathcal{H}_\infty$ design at another sensor location

6 CONCLUSIONS AND FUTURE WORK

The problem of active feedback control of acoustic noise in 3-D enclosures is addressed in this thesis. The design of 3-D enclosure of interest is such that there exists dynamic interaction between acoustics and structure as one of the boundary surfaces of the enclosure is made of thin aluminum plate. The focus of the research was to investigate the feasibility of the active feedback control methodologies to suppress acoustic noise inside the enclosure and, if feasible, develop controller designs that can achieve robust broadband suppression.

6.1 Concluding Remarks

The work presented includes all aspects of the control system design; for example, modelling, system identification, controller design, and experimental validation. The modelling methods used both analytical as well as system identification-based model development. A finite dimensional analytical model was derived using basic 3-D wave equation and assumed modes method. Due to several uncertainties in the parameter values such as acoustic damping coefficient, dimensions of the box, and imperfect boundary conditions the analytical model is often erroneous and not suitable for controller design. Therefore, the design model was based on a finite-dimensional model obtained using system identification-based method. In particular, the system-id toolbox named SOCIT developed at NASA Langley Research Center was used to obtain state-space model of the system using experimentally obtained frequency response data. Typically, it is ob-

served that for SISO case the model matching is very good for both magnitude as well as the phase plot whereas for MIMO case the model matching is very difficult task. For MIMO case, the order of the system model also increases rapidly with the frequency range as the acoustic systems have high modal densities and no natural roll-off at high frequencies. The inaccuracies in the design model translate into conservative bounds on uncertainties which lead to poor performance of controllers.

Another problem that is observed even with the best controller designs is the local behavior of the control performance. To be specific, it is observed that the controller performance may be desirable at the location of the sensor but deteriorates rapidly away from the sensor location. Similarly, the performance may not be uniform over the entire frequency range of interest. Due to the waterbed effect, if the controller performance is good over certain (small) frequency band it becomes worse over some other frequency band. In short, the challenging problem with the feedback control design is designing the controller that can achieve noise reduction which is "global" not only over frequency but over the space as well.

The acoustic systems pose great difficulty in designing an effective controller even with the state-of-the-art control methodology such as an $\mathcal{H}_\infty$ control. The main problem is the shaping of the sensitivity function for these systems where there is no natural roll-off at high frequencies. This inherent system characteristic together with the fundamental limitation that the sensitivity function has to satisfy the relation $T + S = 1$ imposes significant constraints on shaping the sensitivity function. The only desirable shape for sensitivity function is essentially the one with the flat magnitude response with notches at each resonant peak.

All controllers give satisfactorily performance (see Table. 6.1). The LQG design based on the selection of the state weighting matrix Q which was derived from the energy function of the enclosure performed very well. The reason being the performance function with this Q is a direct measure of the acoustic energy in the system and the

controller designed to minimize it tends to extract the acoustic energy from the system in the closed-loop configuration. This makes the controller performance global and not local. The passivity-based controllers are based on energy-extraction principle and hence are the most desirable candidates for the acoustic noise control systems. Also, the stability robustness of the controller is dependent upon the passivity of the system. Since the passivity property is not inherent to the acoustic systems it is artificially imposed via suitable compensation and therefore, the stability robustness hinges on the robustness of passification. Moreover, since the finite dimensional models of the acoustic systems tend to have non-minimum phase zeros, the passification has to be accomplished via feedforward compensation which inherently limits the overall gain of the system. This tends to limit the performance of the controller. Also, for SISO as well as MIMO systems the suitable method for synthesizing optimal passifier is not available and trial and error design has to be used.

Table 6.1 Comparison of overall noise reduction for different controllers

Controller	Simulation	Controller	Experiment
Robust-LQG	1.337	Robust-LQG	1.053
$PR - C_{fb}$	1.106	$PR - C_{fb}$	1.020
PR-LQG	1.122	PR-LQG	0.993
Nom. $\mathcal{H}_\infty$	1.156	Nom. $\mathcal{H}_\infty$	1.183
Rob. $\mathcal{H}_\infty$	1.032	Rob. $\mathcal{H}_\infty$	1.119

In table 6.1, the performance is compared using the performance index $PI = \int_{20Hz}^{500Hz} M_O(jw)dw / \int_{20Hz}^{500Hz} M_C(jw)dw$, M_O and M_C are magnitudes of open and closed loop transfer functions from disturbance to performance. As seen from the table, for simulation, robust-LQG gives the best overall performance, for experiment, nominal $\mathcal{H}_\infty$ gives the best overall performance. In some cases, the interest could be in the reduction of the highest peak in the frequency response.

6.2 Future Research

The future research in this area has great opportunity for improvement. Several important issues still need to be addressed with regard to the viability of active feedback control methodology for acoustic systems especially from commercialization point of view. The main issues that need thorough investigation are listed below:

1) Under what (analytical) conditions a controller can achieve guaranteed noise reduction that is global in space and frequency and what types of controllers can satisfy such conditions?

2) Can better modelling techniques be devised that can yield reasonable order high fidelity models of the acoustic systems on interests?

3) What are the theoretical limits for active noise control techniques?

4) Are there any better methods to choose weighting functions in $\mathcal{H}_\infty$ design for acoustic systems.

5) Can multiple and optimally placed actuators and sensors give order of magnitude increase in the performance. And if so, how to obtain such optimal placement and optimal number of actuators/sensors needed?

The quest for answers to above questions will keep research in acoustic noise control area very interesting and challenging.

Bibliography

[1] C. R. Fuller, A. H. Von Flotow. Active Control of Sound and Vibration. *IEEE Control Systems Magzine*, vol. 15 (6), pp:9–19, December 1995.

[2] P. Lueg. Process of Silencing Sound Oscillation. *U.S. Patent 2 043 416*, 1936.

[3] G. Guicking, Paul. Lueg. Der Erfinder Der Aktiven Larmbekampfung. *Acustica*, vol. 71, pp: 64–68, 1990.

[4] H. F. Olson, E. G. May. Electronic Sound Absorber. *Journal of Acoustical Society of America*, vol. 25, pp: 1130–1136, 1953.

[5] H. F. Olson. Electronic Control of Noise, Vibration, and Reverberation. *Journal of Acoustical Society of America*, vol. 28 (5), pp: 966–972, 1956.

[6] W. B. Conover. Fighting Noise with Noise. *Noise Control*, vol.2, pp: 78–82, 1956.

[7] K. Kido. Reduction of Noise by Use of Additinal Sound Sources. *Proceedings of Inter-Noise '75*, Seddai, Japan, pp: 647–650, 1977.

[8] C. F. Ross. Active Control of Sound. *Ph.D thesis*, Queen's College, Cambridge, U. K., July 1980.

[9] C. F. Ross. A Demostration of Active Control of Broadband Sound. *Journal of Sound and Vibration*, vol. 74, pp: 411–417, 1981.

[10] P. A. Nelson, S. J. Elliott. Active Control of Sound. *Academic Press*, London, 1992.

[11] G. A. Mangiante. Active Sound Absorption. *Journal of Acoustical Society of America*, vol. 61 (6), pp: 1516–1523, 1977.

[12] C. F. Ross. An Algorithm for Designing a Broadband Active Sound Control System. *Journal of Sound and Vibration*, vol. 80, pp: 373–380, 1982.

[13] A. Roure. Self-adaptive Broadband Active Sound Control System. Journal of Sound and Vibration, vol. 101, pp: 429–441, 1985.

[14] S. J. Elliott. Down with Noise. *IEEE Spectrum*, vol. 36 (6), pp: 51–64, June 1999.

[15] F. Jiang, H. Tsuji, H. Ohmori, and A. Sano. Adaptation for Active Noise Control. *IEEE Control Systems Magzine*, vol.17 (6), pp: 36–47, 1997.

[16] B. Bingham, M. J. Atalla, and N. W. Hagood. Comparison of Structural-Acoustic Control Designs on an Active Composite Panel. *Journal of Sound and Vibration*, vol. 244 (5), pp: 761–778, 2001.

[17] J. S. Hu. Active Sound Attenuation in Finite-Length Ducts Using Close-Form Transfer Function Models. *Juournal of Dynamic Systems, Measurements, and Control- Transaction of the ASME*, vol. 117, pp: 143–154, June 1995.

[18] J. S. Hu, S. H. Yu, and C. S. Hsieh. Application of Model-Matching Techniques to Feedforward Active Noise Control Design. *IEEE Transactions on Control Systems Technology*, vol. 6 (1), pp: 33–42, January 1998.

[19] R. L. Clark. Adaptive Feedforward Modal Space Control. *Journal of the Acoustical Society of America*, vol. 98 (5), pp: 2639–2650, November 1995.

[20] A. J. Hull, C. J. Radcliffe, and S. C. Southward. Global Active Noise Control of a One-Dimensional Acoustic Duct Using Feedback Controller. *Journal of Dynamic*

Systems, Measurements, and Control - Transactions of the ASME, vol. 115, pp: 488–494, September 1993.

[21] J. C. Carmona and V. M. Alvarado. Active Noise Control of a Duct Using Robust Control Theory. *IEEE Trasactions on Control System Technology*, vol. 9, pp: 930–939, November 2000.

[22] J. Hong, J. C. Akers, R. Venugopal, M. N. Lee, A. G. Sparks, P. D. Washabaugh, and D. S. Bernstein. Modeling, Identification, and Feedback Control of Noise in an Acoustic Duct. *IEEE Transactions on Control Systems Technology*, vol. 4(3), pp: 283–291, May 1996.

[23] H. R. Pota and A. G. Kelkar. Modelling and control of acoustic ducts. *ASME Journal of Vibration and Acoustic*, vol. 123, pp: 2–10, January 2001.

[24] Jones, J. D. and Fuller, C. R. Active Control of Structurally-Coupled Sound Fields in Elastic Cylinders by Vibrational Force Inputs. *The International Journal of Analytical and Experimental Modal Analysis*, vol. 5 (3), pp: 123–140, 1990.

[25] H. T. Banks, R. J. Silcox and R. C. Smith. The Modeling and Control of Acoustic/Structure Interaction Problems via Piezoceramic Actuators: 2-D Numerical Examples, *Active Control of Noise and Vibration*, vol. 38, pp: 83–94, 1992.

[26] H. T. Banks, D. E. Brown, R. C. Smith, V. L. Metcalf, Y. Wang, and R. J. Silcox. Noise Control in a 3-D Structural Acoustic System: Numerical and Experimental Implementation of a PDE-Based Methodology. *Proc. 33rd Conference on Decision and Control*, pp: 305–310, Lake Buena Vista, FL, December 1994.

[27] D. E. Cox, G. P. Gibbs, R. L. Clark, and J. S. Vipperman. Experimental Control of Structural Acoustic Radiation. *AIAA Paper*, AIAA-98-2089, pp: 3241–3249, 1998.

[28] H. R. Pota. Acoustical Room Transfer Functions without Using Green's Functions. *Proc. IEEE Conference on Decision and Control* , Orlando, Florida, pp: 2588–2589, Dec. 2001.

[29] H. T. Banks, M. A. Demetriou, and R. C. Smith. An H^{∞}/MinMax periodic control in a two-dimensional structural acoustic model with piezoceramic actuators. *IEEE Transactions on Automataic Control*, vol. 41 (7), pp: 943–959, July 1996.

[30] J. Y. Lin and Z. L. Luo, Internal Model-Based LQG/H_{∞} Design of Robust Active Noise Controllers for an Acoustic Duct System. *IEEE Trans. on Controls Systems Technology*, vol. 8 (5), pp: 864–872, 2000.

[31] I. R. Petersen and H. R. Pota. Experiments in Feedback Control of an Acoustic Duct. *Proc. IEEE International Conference on Control Applications*, Anchorage, Alaska, pp: 261–266, September 2000.

[32] B. Fang, A. G. Kelkar and S. M. Joshi. Modelling and Control of Acoustic-Structure Interaction in 3-D Enclosure. To appear in *Proc. IEEE Conference on Decision and Control* , Las Vegas, Nevada, December, 2002.

[33] J. B. Burl. Linear Optimal Control: H_2 and H_{∞} Methods. *Addison-Wesley Longman*, New York, 1998.

[34] M. O. Brien, P. Pratt. Active Noise Control Using Robust Feedback Techniques. *Acoustics, Speech, and Signal Processing, 2001. IEEE International Conference* , vol. 5, pp: 3209–3212, 2001.

[35] *MATLAB—Control System ToolBox.* Mathworks, Natick, MA, 2000.

[36] *MATLAB—μ Analysis and Synthesis ToolBox.* Mathworks, Natick, MA, 2000.

[37] Sen. M. Kuo, Dennis R. Morgan Active Noise Control Systems. *John Wiley & Sons Inc*, 1996.

[38] G. H. Koopmann and J. B. Fahnline. Designing Quiet Structure–A Sound Power Minimization Approach. *Academic Press*, 1997.

[39] J. N. Juang. Applied System Identification. *Prentice-Hall Inc*, 1994.

[40] C. T. Chen. Linear System Theory and Design. *Oxford Unviersity Press*, 1994.

[41] R. E. Kalman and R. S. Bucy. New Results in Linear Filtering and Prediction Theory. *ASME Journal of Basic Engineering*, Series D, vol. 83, pp: 95–108, 1961.

[42] S. M. Joshi and P. G. Maghami. Robust Dissipative Compensators for Flexible Spacecraft Control. *IEEE Transactions on Aerospace and Electronic Systmes*, vol. 28 No. 3, pp: 768–774, July, 1992.

[43] K. B. Lim, P. G. Maghami and S. M. Joshi. Comparison of Controller Designs for an Experimental Flexible Structure. *IEEE Control Systmes*, pp: 108–118, June, 1992.

[44] A. G. Kelkar, S. M. Joshi and T. E. Alberts. Dynamic Dissipatie Compensators for Multibody Flexible Space Structures. *IEEE Transactions on Aerospace and Electronic Systmes*, vol. 31 (4), pp: 1325–1329, October, 1995.

[45] S. M. Joshi, P. G. Maghami and A. G. Kelkar. Design of Dynamic Dissipative Compensators for Flexible Space Structures. *IEEE Transactions on Aerospace and Electronic Systmes*, vol. 31 (4), pp: 1314–1324, October, 1995.

[46] A. G. Kelkar and S. M. Joshi. Passivity-Based Control of Elastic Systems. *Proc. IEEE Conference on Control Applications*, pp: 724–729, Hartford, CT, October. 1997.

[47] A. G. Kelkar and S. M. Joshi. Robust Control of non-passive systems via passification. *Proceedings of American Control Conference*, vol. 5, pp: 2657–2661, Albuquerque, NM, June 1997.

[48] A. G. Kelkar and H. R. Pota. Robust Broadband Control of Acoustic Duct. *Proceedings of 39th IEEE Conference on Decision and Control*, pp: 4485–4490, Sydney, Australia, December 2000.

[49] S. M. Joshi and A. G. Kelkar. Passivity-Based Robust Control of System with Redndant Sensors and Actuators. *International Journal of Control*, vol. 74 (5), pp: 474–481, March 2001.

[50] A. G. Kelkar, Y. Mao and S. M. Joshi LMI-Based Passification for Control of Non-Passive Systems. *Proceedings of the American Control Conference*, pp: 1271–1275, Chicago, IL, June 2000.

[51] R. Lozano-Leal and S. M. Joshi. On the Design of Dissipative LQG-type Controllers. *Proc. 27th IEEE Conference on Decision and Control* , pp: 1654–1646, Austin, Texas, December. 1988.

[52] S. M. Joshi and S. Gupta. On a Class of Marginally Stable Positive-Real Systems. *IEEE Transactions on Automatic Control*, vol. 41 (1), pp: 152-155, 1996.

[53] A. G. Kelkar and S. M. Joshi. Control of Nonlinear Multibody Flexible Space Structure. *Lecture Notes in Control and Information Sciences*, vol. 221, Springer-Verlag, Albuquerque, NM, 1996.

[54] H. R. Pota, S. O. Reza Moheiman and M. Smith. Resonance Controllers for Flexible Structures. *Proceedings of IEEE International 38th Conference on Decision and Control*, vol. 5, pp: 631–636, Phoenix, AZ, December 1998.

[55] H. R. Pota, S. O. Reza Moheiman and M. Smith. Resonance Controllers for Smart Structures. *Smart Materials and Structures*, vol. 11, pp: 1–8, 2002.

[56] Hassan K. Khalil. Nonlinear Systems. *Prentice-Hall Inc.*, 2002.

[57] G. Zames. Feedback and Optimal Sensitivity: Model ReferenceTransformations, Weighted Seminorms and Approximate Inverses. *Proceedings of 17th Allerton Conference*, pp: 744–752, 1979.

[58] S. Salapaka, A. Sebastian, J. P. Cleveland and M. V. Salapaka. High bandwidth nano-positioner: A robust Control Approach. *Review of Scientific Instruments*, vol. 73, pp: 3232–3241, September 2002.

[59] S. Skogestad and I. Postlethwaite. Multivariable Feedback Control, Analysis and Design. *Addison-Wesley Longman*, New York, 1997.

[60] J. Doyle, B. Francis and A. Tattenbaum. Feedback Control Theory. *Macmillan Publishing Company*, New York, 1992.

[61] M. J. Grimble. Robust Industrial Control–Optimal Design Approach for Polynomial Systems. *Prentice Hall Inc.*, Englewood Cliffs, NJ 1994.

[62] H. Kwakernaak Robust Control and $\mathcal{H}_\infty$-Optimisation –Tutorial Paper. *Automatica*, vol. 29 (2), pp: 255–273, 1993.